EFFECT OF HOFMEISTER IONS ON THERMODYNAMICS OF COMPLEX COACERVATION OF HYALURONIC ACID AND CHITOSAN

by

Gökçe Kantarcı

B.S., Chemistry, Boğaziçi University, 2019

Submitted to the Institute for Graduate Studies in
Science and Engineering in partial fulfillment of
the requirements for the degree of
Master of Science

Graduate Program in Chemistry

Boğaziçi University

2022

ACKNOWLEDGEMENTS

Through the journey of this project, I have had many people around to be appreciative of. First of all, I would like to express my endless and sincere gratitude to my advisor Assoc. Prof. Ayşe Başak Kayıtmazer for her guidance. She was always supportive, and understanding, and pushed me to do my best even when I thought I was not capable and having hard times. The thankfulness for the opportunity to work together with similar perspectives and of learning the ways of scientific research from her will always remain in my heart.

I would like to thank all members of the Kayıtmazer Research Group, but especially: Fatma Akçay Oğur for always guiding with her experiences, İlayda Akbulut for her joyful and lovely convoy and support, Sezin Mamaşoğlu for her talented way of taking over our project and medicinal friendship, Melani Akay for her contributive hard work and geniality during her internship.

I would like to express my deepest gratitude to BUSPIN Research Group. It would not be possible to accomplish some of the experiments without the permission of Prof. Özhan Özatay for using the light microscope in their laboratory. I also would like to thank Dr. Hasan Pişkin for his way of teaching in the laboratory, help in fixing the ITC instrument when it stopped working several times, talent in computational methods that lead us to obtain variable perspectives on the data analysis part of this project, and his valuable friendship that made the coffee breaks during the last two years very much enjoyable.

I would also like to thank Dr. Bilge Gedik Uluocak for Scanning Electron Microscopy analyses.

I gratefully acknowledge the members of my thesis committee: Assist. Prof. Fatma Ahu Akın and Assist. Prof. Erkan Şenses for giving their valuable time in reviewing this thesis and for all the advice.

I have to give my special thanks to my closest friends İpek Azizoğlu and Beyza Yılmaz. They were the best two people on earth for me to share the master's pathway adding hard times lots of laughter and love. I would also like to sincerely thank my friends Furkan Turan and Elvan Korkut for being there for me every step of the way with their unique friendships.

And finally, thanks to my dear family: my father Kayhan Kantarcı, my solid rock that always supported me, my best friend and my forever hero, and my mother Hamiyet Gençalp, supporting me no matter what I do with her love that words fail to describe.

This project was supported by TÜBİTAK Short-Term R&D Funding Program (Project Code: 120Z865). This thesis has been supported by TÜBİTAK National Scholarship Program for MSc Students 2019/2 (BİDEB 2210-E).

ABSTRACT

EFFECT OF HOFMEISTER IONS ON THERMODYNAMICS OF COMPLEX COACERVATION OF HYALURONIC ACID AND CHITOSAN

The Hofmeister series is an ion series that was discovered to have significant effects on the behavior of aqueous protein solutions as a result of Franz Hofmeister's studies in 1888, and its effects on other biomacromolecules have also been investigated. This study aims to examine the effect of this series on the complexation and coacervation of hyaluronic acid (HA) with chitosan (CHI) polyelectrolytes in three different pH values (3.25, 5.25, and 6.25) and two different molecular weights (HA, 1200 kDa & 199 kDa) in terms of thermodynamics. While turbidimetric titration experiments were used to optimize conditions affecting coacervation such as salt type, pH and concentration of buffering agent and polyelectrolyte, images were taken by light microscopy to ensure that the HA/CHI system produces coacervates that could be used in areas such as encapsulation, tissue engineering, and not just precipitate particles. Isothermal titration calorimetry has been found suitable to understand the thermodynamics of coacervation. The results majorly agree with the direct Hofmeister effect for the cations and the reverse Hofmeister effect for the anions. In addition, the salt screening effect can be clearly observed as the interaction between the two polyelectrolytes are most intense in the absence of salt. It was also observed that the interaction between the two macromolecules was greater as the pH increases.

ÖZET

HOFMEISTER SERİSİNİN HİYALÜRONIK ASİT VE KİTOSAN KOASERVASYONUNUN TERMODİNAMİĞİ ÜZERİNDEKİ ETKİSİ

Hofmeister serisi, 1888'de Franz Hofmeister'ın çalışmaları sonucunda proteinlerin su çözeltilerindeki davranışları üzerinde önemli etkileri bulunduğu keşfedilen bir iyon serisi olup, diğer biyomakromoleküller üzerindeki etkileri de araştırılmakta olan bir seridir. Bu çalışmanın amacı, hiyalüronik asit (HA) ve kitosan (CHI) polielektrolitlerinin kompleksleşmesi ve koaservasyonu üzerinde bu serinin etkilerini termodinamik açıdan üç farklı pH değerinde (3.25, 5, 25 ve 6.25) ve iki farklı moleküler ağırlıkta (HA, 1200 kDa & 199 kDa) araştırmaktır. Tuz çeşidi, pH ve tamponlayıcı madde ve polielektrolit konsantrasyonu gibi koaservasyonu etkileyen koşulları optimize etmek için bulanıklık titrasyonu deneylerinden faydalanılırken, HA/CHI sisteminin sadece çökelti parçacıkları oluşturmak yerine enkapsülasyon, doku mühendisliği gibi alanlarda kullanılabilecek koaservatlar oluşturduğundan emin olmak için ışık mikroskobundan görüntüler alınmıştır. Termodinamik araştırma için izotermal titrasyon kalorimetresinin uygun olduğu görülmüştür. Sonuçlar, katyonlar için doğrudan Hofmeister etkisi ve anyonlar için ters Hofmeister etkisi ile büyük ölçüde uyumludur. Ek olarak, iki polielektrolit arasındaki etkileşim, tuzun yokluğunda en yoğun olduğu için, tuz iyonlarının yük perdeleme etkisi açıkça gözlemlenmiştir. Ayrıca iki makromolekül arasındaki etkileşimin pH arttıkça daha fazla olduğu gözlenmiştir.

TABLE OF CONTENTS

ACKNOWLEDGEMENTS iii
ABSTRACT v
ÖZET vi
TABLE OF CONTENTS vii
LIST OF FIGURES ix
LIST OF TABLES xiv
LIST OF SYMBOLS xv
LIST OF ACRONYMS/ABBREVIATIONS xvii
1. INTRODUCTION 1
1.1. Coacervation 1
1.2. Hofmeister Series 3
1.3. Isothermal Titration calorimetry (ITC) 8
2. AIM OF THE STUDY 13
3. METHODOLOGY 15
3.1. Materials 15
3.2. Methods 16
3.2.1. Dialysis for Counterion Exchange 16
3.2.2. Turbidimetric Titration 17
3.2.3. Light Microscopy 18
3.2.4. Isothermal Titration Calorimetry (ITC) Experiments 20
3.2.4.1. Experiments During the Optimization Process 22
3.2.4.2. Experiments with Diafiltration 22
3.2.4.3. Experiments with Dialysis and Stocked-Solution Method 22
3.3. Data Analysis 22

3.3.1. Single Set of Identical Sites (SSIS) Model 23
3.3.2. Two Sets of Individual Sites (TSIS) Model 25
3.3.3. Analysis on Microsoft Excel 26
4. RESULTS AND DISCUSSION 28
4.1. Optimization Studies 28
4.1.1. Selection of Experimental Conditions Based on The Preliminary Study 28
4.1.2. Determination of the Conditions 29
4.1.3. Instrumental Parameters 30
4.1.4. Polyelectrolyte Concentrations 31
4.1.5. Salt Concentrations/Ionic Strength 32
4.1.6. Value of The pH 33
4.1.7. Molecular Weight of The Polyelectrolyte 33
4.2. Adding A Buffer 34
4.2.1. Optimization Experiments for the Buffered System via Turbidimetric Titrations 35
4.2.2. Optimization of the ITC Sample Preparation with Buffering Agent 50
4.2.3. Data Analysis of ITC Results 56
5. CONCLUSION 64
REFERENCES 65
APPENDIX A: PARAMETERS AND RESULTS OF THE EXPERIMENTS BEFORE ADDING BUFFERING AGENT TO THE SYSTEM 78
APPENDIX B: RESULTS OF THE SEM-EDS EXPERIMENTS 110

LIST OF FIGURES

Figure 1.1. Effect of Hofmeister series ions on proteins. [25, 26]..... 4

Figure 1.2. A schematic for a better understanding of the effects of salting in/out by breaking/making hydrogen bonds between the water molecules. 4

Figure 3.1. A processed photograph of particle size analysis done on the image of the sample drop taken from the solution at the end of the turbidimetric titration. This particular image belongs to the experiment done with 0.1 mg/mL CHI & 0.5 mg/mL HA (199 kDa) dissolved in buffered salt solution at pH 5.25 and of I_{total} of 50 mM (1:9 ionic strength ratio of MES:$MgCl_2$)..... 19

Figure 4.1. Scheme describing the inside of the adiabatic jacket in the instrument, covering the cells and keeping the cells at a constant temperature. 35

Figure 4.2. Change of pH with molar ratio of HA to CHI prepared from solutions of initial concentrations of 0.3 mM CHI & 3.0 mM HA dissolved in buffered salt solution at pH of 6.25 ± 0.05, I_{total} of 50 mM (1:9 mole ratio of MES:NaCl). 37

Figure 4.3. Turbidimetric titration plots from solutions of initial concentrations of 0.5 mg/mL CHI & 0.5 mg/mL HA (1200 kDa) dissolved in buffered salt solution of pH of 6.25 ± 0.05. The buffered salt solution is of NaCl with (a) I_{total} of 50 mM, (b) I_{total} of 100 mM, (c) I_{total} of 150 mM, (d) I_{total} of 200 mM. 38

Figure 4.4. Photograph of the precipitate seen in turbidity experiments. Photograph is taken at the end of the turbidimetric titration experiment done with 0.5 mg/mL CHI & 0.5 mg/mL HA dissolved in buffered salt solution at pH = 6.25 ± 0.05

and of I_{total} of 50 mM (1:9 MES:NaCl mole ratio), graphed in Figure 4.3 (a). The same appearance was observed in all cases where precipitate was mentioned. 39

Figure 4.5. Turbidimetric titration plots from solutions of initial concentrations of 0.1 mg/mL CHI & 0.5 mg/mL HA (1200 kDa) dissolved in buffered salt solution of pH of 6.25 ± 0.05. The buffered salt solution is of $MgCl_2$ with (a) I_{total} of 50 mM, (b) I_{total} of 100 mM, (c) I_{total} of 150 mM (d) I_{total} of 200 mM..... 40

Figure 4.6. Turbidimetric titration plot from solutions of initial concentrations of 0.1 mg/mL CHI & 0.5 mg/mL HA (1200 kDa) dissolved in buffered NaCl solution of pH of 5.25 ± 0.05, I_{total} of 100 mM. Experiments were stopped as soon as precipitation occurred. 41

Figure 4.7. Resulting graph of turbidimetric titration experiments for (a) all cations, (b) all anions. Experiments were done with 0.1 mg/mL CHI & 0.5 mg/mL HA (199 kDa) dissolved in MES buffered salt solution of pH of 5.25 ± 0.05, I_{total} of 50 mM. 42

Figure 4.8. Turbidimetric titration experiments of 100 - % T vs. molar ratio of HA to CHI for (a) NaCl condition, (b) $MgCl_2$ condition, (c) $NaNO_3$ condition, (d) No Salt Only Buffer condition. Experiments were done with 0.1 mg/mL CHI & 0.5 mg/mL HA (1200 kDa) dissolved in MES buffered salt solution of pH = 5.25 ± 0.05, I_{total} of 50 mM. 43

Figure 4.9. Resulting graph of turbidimetric titration experiments for (a) all cations, (b) all anions. Experiments were done with 0.1 mg/mL CHI & 0.5 mg/mL HA (1200 kDa) dissolved in MES buffered salt solution of pH = 5.25 ± 0.05, I_{total} of 50 mM. 44

Figure 4.10. Turbidimetric titration experiments for (a) all cations, (b) all anions. Experiments were done with solutions of initial concentrations of 0.1 mg/mL CHI & 0.5 mg/mL HA (1200 kDa) dissolved in citric acid buffered salt solution of pH of 3.25 ± 0.05, I_{total} of 50 mM. 45

Figure 4.11. Turbidity vs. Molar ratio plots at different pHs for (a) NaCl, (b) $MgCl_2$, (c) KCl, (d) $CaCl_2$ salts. All experiments are done using 0.1 mg/mL CHI & 0.5 mg/mL HA dissolved in the buffered salt solutions of I_{total} of 50 mM..... 47

Figure 4.12. Turbidity vs. Molar ratio plots at different pHs for (a) NaCl, (b) $NaNO_3$, (c) No Salt Only MES, (d) NaOAc conditions. All experiments are done using 0.1 mg/mL CHI & 0.5 mg/mL HA dissolved in the buffered salt solutions of I_{total} of 50 mM (No Salt condition only has 5 mM concentrated MES in the medium as solvent.). 48

Figure 4.13. Results of the analysis of the light microscopy images taken at the last data point of turbidimetric titration experiments (at the molar ratio of [HA]/[CHI] = 0.52). Because there was no precipitate for the potassium chloride salt, the "pH = 5.25, 199 kDa HA, precipitates" part of the graph for KCl remained blank. 49

Figure 4.14. Thermograms of the ITC experiments done using 0.1 mg/mL CHI and 0.5 mg/mL HA dissolved in 0.2 M NaCl solution at pH of 6.25 ± 0.05 prepared by the method (a) without dialysis (b) with dialysis. 52

Figure 4.15. Thermograms of ITC experiments: (a) for cations, (b) for anions. All of the dilution experiments (HA into buffer titrations, buffer into CHI titrations, and buffer into buffer titrations) are subtracted from the original experiment (HA into CHI titrations). All experiments were done using 0.1 mg/mL CHI & 0.5 mg/mL HA (1200 kDa) dissolved in MES buffered salt solution of pH of 5.25 ± 0.05, I_{total} of 50 mM. 53

Figure 4.16. Photographs of corrosion on the inner parts of the pipette part of the ITC instrument: (a) lower part of the pipette in use since February 2021; (b) the top part of the pipette in use since February 2021, (c) inside of the top part of the pipette in use before February 2021. 53

Figure 4.17. Turbidity vs. molar ratio curves for (a) all cations, (b) all anions. Experiments were done with 0.1 mg/mL CHI & 0.5 mg/mL HA (199 kDa) dissolved in MES buffered salt solution of pH of 5.25 ± 0.05, I_{total} of 50 mM. 54

Figure 4.18. ITC thermograms for cations: (a) with error bars, (b) closed-up look without error bars for a better understanding. All of the dilution experiments (HiB titrations, BiC titrations and BiB titrations) are subtracted from the original experiment (HiC titrations). All experiments were done using 0.1 mg/mL CHI & 0.5 mg/mL HA (199 kDa) dissolved in MES-buffered salt solution of pH of 5.25 ± 0.05, I_{total} of 50 mM. 55

Figure 4.19. ITC thermograms for anions: (a) with error bars, (b) closed-up look without error bars for a better understanding. All of the dilution experiments (HiC, BiC, and BiB titrations) are subtracted from the original experiment (HiC titrations). All Experiments were done using 0.1 mg/mL CHI & 0.5 mg/mL HA (199 kDa) dissolved in MES-buffered salt solution of pH of 5.25 ± 0.05, I_{total} of 50 mM. 55

Figure 4.20. Resulting graphs of the data analysis done using the Origin for the NaCl condition. Analyses are done using (a) single set of identical sites model, (b) two sets of individual sites model..... 57

Figure 4.21. Resulting graphs of the data analysis done using the Origin for the No Salt condition. Analyses are done using (a) single set of identical sites model, (b) two sets of individual sites model..... 58

LIST OF TABLES

Table 3.1. Concentrations of each salt used in the experiments of different conditions. .. 17

Table 4.1. Coacervation percentages (by number) at the end (the molar ratio of 0.52) of the turbidimetric titration experiments, obtained by analyzing the images taken by the light microscope on the Adobe Photoshop program. 50

Table 4.2. Results of the data analysis done using the two sets of sites model on the Origin. Experiments (three runs of the same condition) were done using 0.1 mg/mL CHI & 0.5 mg/mL HA dissolved in buffered salt solution at pH of 5.25 ± 0.05 and of I_{total} of 50 mM (1:9 MES:NaCl mole ratio). 59

Table 4.3. Results of the data analysis done using the two sets of sites model on the Origin. Experiments (three runs of the same condition) were done using 0.1 mg/mL CHI & 0.5 mg/mL HA dissolved in buffer solution of 5 mM MES at pH of 5.25 ± 0.05. 59

Table 4.4. Average complexation enthalpies and the standard deviation values for each salt. All experiments were done using 0.1 mg/mL CHI & 0.5 mg/mL HA (1200 kDa) dissolved in MES-buffered salt solution of pH of 5.25 ± 0.05, I_{total} of 50 mM. 60

Table 4.5. Average complexation enthalpies and the standard deviation values for each salt. All experiments were done using 0.1 mg/mL CHI & 0.5 mg/mL HA (199 kDa) dissolved in MES-buffered salt solution of pH of 5.25 ± 0.05, I_{total} of 50 mM. 60

LIST OF SYMBOLS

I	Ionic strength
I_{total}	Total ionic strength of the medium
K	Binding coefficient
Molar Ratio	The molar ratio of material from the syringe compared to material in the cell
M_t	Concentration of the titrate in the cell that is diluted after the injection
M_t^0	Concentration of the material in the cell at the beginning of the experiment
n	Reaction stoichiometry
Q	Total heat content
Q_i	Total heat content at the end of the ith injection
T	Temperature (K)
T_c	The critical temperature
V_0	Volume of the cell in the ITC instrument
X_t	Concentration of the titrant that is now in the cell (diluted concentration)
X_t^0	Initial concentration of the titrant
Θ	Fraction of sites occupied by *X*
% T	Transmittance
100 - % T	Turbidity
$\alpha_{pH=6.25}$	Degree of ionization of hyaluronic acid at the pH of 6.25
$\beta_{pH=6.25}$	Degree of ionization of chitosan at the pH of 6.25
ΔG_{PEC}	Gibb's free energy of polyelectrolyte complexation
ΔH	Enthalpy change
ΔH^{atm}	Enthalpy of release of the counterions
$\Delta H_{BiB_{avg}}$	Average enthalpy of the 20 injections of buffer into buffer ITC experiments

$\Delta H_{BiC_{avg}}$	Average enthalpy of the 20 injections of buffer into chitosan ITC experiments
ΔH_c	Enthalpy of complexation
$\Delta H_{HiB_{avg}}$	Average enthalpy of the 20 injections of hyaluronic acid into buffer ITC experiments
$\Delta H_{HiC_{avg}}$	Average enthalpy of the 20 injections of hyaluronic acid into chitosan ITC experiments
ΔH_{pair}	Pairing enthalpy
ΔH_{PEC}	Enthalpy of polyelectrolyte complexation
ΔQ_i	Heat released by the ith injection
ΔS	Entropy change
ΔV	The volume injected into the cell, also representing the overflow volume

LIST OF ACRONYMS/ABBREVIATIONS

BAP	Bilimsel araştırma projeleri (Scientific research projects)
BiB	Buffer into buffer (titration)
BiC	Buffer into chitosan (titration)
BSA	Bovine serum albumin
DDA	Degrees of deacetylation
DLS	Dynamic light scattering
DNA	Deoxyribonucleic acid
DTAB	Dodecyl trimethylammonium bromide
EDAX	Energy dispersive X-ray analysis
EDS	Energy-dispersive X-ray spectroscopy
HiB	Hyaluronic acid into Buffer (titration)
HiC	Hyaluronic acid into chitosan (titration)
IHF	Integration host factor
IPA	Isopropyl alcohol
IR	Infrared
ITC	Isothermal titration Calorimetry
M	Titrate in solution in the sample cell of the ITC instrument
MES	2-(N-morpholino)ethanesulfonic acid hydrate
MOPS	3-(Morpholin-4-yl)propane-1-sulfonic acid
pAA	poly (acrylic acid sodium salt
pAH	poly (allylamine hydrochloride)
PANa-b-PAM	poly(sodium acrylate)-b-poly(acrylamide)
PDADMAC	poly (diallyl dimethylammonium chloride)
PSSNa	poly (styrene sulfonate, sodium salt)
RNA	Ribonucleic acid

SDS	Sodium dodecyl sulfate
SEM	Scanning electron microscope
TÜBİTAK	Türkiye Bilimsel Ve Teknolojik Araştırma Kurumu (The Scientific and Technological Research Institution of Turkey)
UV-VIS	Ultraviolet and visible
X	Titrant in solution in the syringe of the ITC instrument

1. INTRODUCTION

1.1. Coacervation

Complex coacervation is a liquid-liquid phase separation that occurs when two or more oppositely charged macromolecules come together. Of these two liquid phases that are formed, the coacervate phase is a relatively dense and polymer-rich liquid phase, accompanied by a macromolecule-dilute phase that is of a much larger volume called the equilibrium phase or the supernatant phase. The state of the system before it is separated into two liquid phases by low-speed centrifugation is a suspension containing droplets of micron or nano sizes [1 – 3]. Coacervate droplets are easily distinguishable from precipitates or aggregates of polymers of the same content because other structures than coacervates are solid, not liquid. Therefore, they do not show the spherical shape and fluidity properties that coacervate droplets show that are easily observed in light microscopy.

Coacervates in biology have a large variety of examples. Among the macromolecules that make up the complex coacervate, mostly used examples are ionic biomacromolecules such as proteins, ionic polysaccharides, RNA, and DNA [4]. For example, it has been previously observed that the sandcastle worm *Phragmatopoma California* can secrete three highly polar proteins, which can form complex coacervates to adhere exogenous mineral particles together [5]. The electrostatic complex formation has been reported in the cartilage of more advanced organisms, based on the fact that the interaction between lysozyme and glycosaminoglycans is affected by the salt concentration [6]. Perez Sanchez et al. (2006) focused on the formation of a complex between interferon γ (an antiviral, antiproliferative, and immunostimulatory cytokine) and heparin (a type of glycosaminoglycan)[7]. Seyrek et al. (2007) showed that non-specific electrostatic binding occurring in the low ionic strength (10 - 30 mM) range is responsible for the activity of heparin-antithrombin [8].

Regarding the applications, coacervates can be seen as a kind of microencapsulation technique [9] as well as used as a nano-carrier [10]. Bungenberg de Jong's pioneering work focused on biomacromolecular systems such as protein and polysaccharide [11]. Based on this fundamental research, coacervates have also been found useful as additives, emulsifiers, and viscosity modifiers [12]. There are many recent studies focused on the use of coacervates for the encapsulation of small molecules, proteins, RNA, DNA, and other biomaterials [11, 12]. Coacervates have long been used as an encapsulation technique, especially in food and personal care products [13, 14]. Coacervate-containing materials have been found useful in various fields of biomedicine, including cartilage mimics, scaffolds, and adhesives for wet, biological environments [15, 16]. In addition, Messaoud et al.'s study [19] designed, formed, and examined “green coacervates” from bolaform acidic sophorolipid (SL) (a biobased anionic surfactant) and cationic biopolymers (chitosan-oligosaccharide-lactate, poly(L-lysine) and poly(allylamine)). With the understanding that there are coacervates that can be formed in a wide pH range depending on the type of positively charged polyelectrolytes, Messaoud et al.’s study holds promise for microencapsulation as well, especially for use in pollutant and dye removal processes.

It is proven that coacervation is affected by various parameters such as temperature, pH, ionic strength, concentration and molecular mass of polymers, charge density of polyelectrolytes, and stoichiometry of the mixture [20]. Apart from being affected, the coacervation process is driven by the entropy gain resulting from the release of the counterions, following the electrostatic interaction of oppositely charged macromolecules [19 – 21]. The conditions necessary for coacervation are determined by the optimization of the above-mentioned physicochemical parameters which are specific to each macroion pair involved in this process since the observation window is very narrow for coacervation.

The parameters that determine how the phase separation forms, how stable the coacervation is, and what determines the coacervates’ properties are listed above. Another factor that can be added to this list is the Hofmeister series which has been limitedly studied in the literature. This factor can be briefly stated as the specific ion effect.

1.2. Hofmeister Series

The Hofmeister series is an effective, qualitative list of ions based on the hydration of the ions and the proteins and in-solution behaviors of proteins according to their polarity and size (Mazzini and Craig, 2017). Franz Hofmeister, who studied the effects of cations and anions on the solubility of proteins, was the first to examine the changes caused by these ions [24]. Hofmeister discovered several salts that have consistent effects on the solubility of proteins and the stability of their secondary and tertiary structures.

The mechanism of the Hofmeister series' effects is not completely known; they are usually considered in terms of more specific interactions between ions and proteins and between ions and water molecules in direct contact with proteins [21, 23]. When the effects of the salts are observed in the order of series shown in Figure 1.1 (going from left to right in any quantitative manner), it is defined as "the direct Hofmeister series effect" and when the results of the experiments give an order from right to left, it is called "the reverse Hofmeister effect". The order between the ions of the series can vary from protein to protein (from macromolecule to macromolecule) due to ion-specific interactions, so they may differ in sources [26].

The ions of this series, the effects of which are widely researched, are also divided into two classes according to their hydration tendency and their effects on breaking/forming the water structure. These ions tend to affect the solutions by making or breaking the hydrogen bonds between the water molecules and this gives them the power to alter the behaviors of the material inside. They get the names chaotropes for the chaotropic activity of water breaking and kosmotropes for the anti-chaotropic activity of water making [29]. The kosmotropic ions can cause the hydrophobic forces to become dominant and thus the particles to interact more (salting-out effect in Figure 1.2). On the other hand, the chaotropic ions can cause the interaction of the solvent molecules with the particles (biomacromolecules under investigation) to become more favorable thus the increase of the solubility (salting in effect in Figure 1.2).

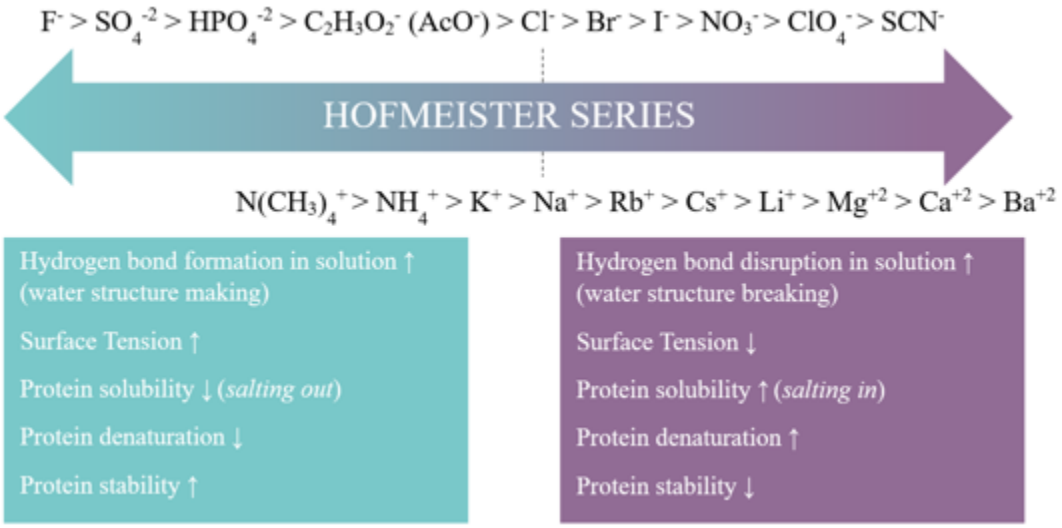

Figure 1.1. Effect of Hofmeister series ions on proteins. [25, 26]

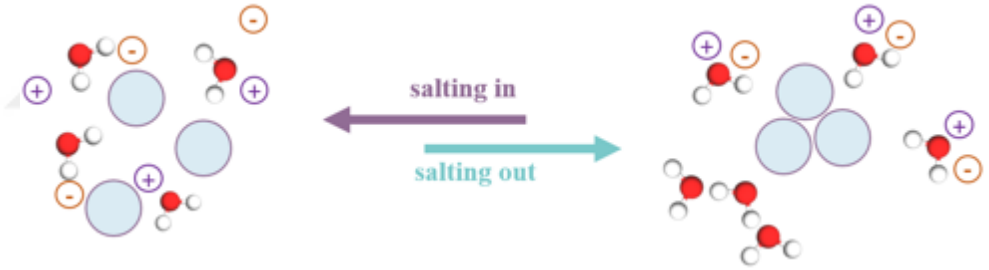

Figure 1.2. A schematic for a better understanding of the effects of salting in/out by breaking/making hydrogen bonds between the water molecules.

The effect of this series is now being investigated not only for proteins but also for other biomacromolecules and natural or synthetic polymers, as can be seen in the following literature examples. Meanwhile, their effects on coacervates are also questioned.

Zhang and Cremer investigated the effect of monovalent anions of the Hofmeister series on lysozyme in chicken egg white [30]. As a result of their research on liquid-liquid phase separation formed by the aggregation of lysozyme, they observed reverse Hofmeister

effect at low salt concentration, and the direct Hofmeister effect at salt concentrations higher than ≈ 200 – 300 mM. Also, they interpreted their observations on the cloud point temperature, which represents the point where phase separation is completed. When the charge screening effects of the ions (in other words, shielding the electrostatic repulsion force) were compared, they explained the obtained reverse Hofmeister effect as that the anions with larger volumes (ClO_4^-, SCN^-) could interact more with the positively charged lysozyme sites due to their less hydration tendency, and they were also more effective in shielding. However, it was noted that highly polarizable anions such as ClO_4^- and SCN^- tend to reduce the protein-water interfacial tension, consistent with their tendency to partition into the hydrophobic phase. As a result, they reported that at low concentrations of chaotropic anions the phase change temperature increases due to ion pairing, reaches a maximum value as the ion concentration increases, and then decreases due to the decrease in surface tension. In conclusion, they stated that the positively charged macromolecules behaving under the reverse Hofmeister effect at low chaotropic anion concentrations could experience the direct effect as the anion concentration was increased.

Mason et al. demonstrated the liquid-liquid phase separation of humanized IgG2 (M_w: ~148 kDa, pI=7.2), a monoclonal antibody, in the presence of three different potassium salts, by selecting two anions from the endpoints of the Hofmeister series and an anion in the middle (F^-: very hydrated, Cl^-: moderately hydrated, SCN^-: slightly hydrated) [31]. In the study where phase separation is visible, UV-Vis spectrophotometer was used to determine the amount of antibodies in the top (protein-poor) and bottom (protein-rich) layers. They conducted their investigations focused on the critical temperature (T_c) which is the temperature at which phase separation begins and is an important measure of intermolecular interactions. The critical temperature is expected to decrease as the intermolecular interaction (antibody-antibody interaction for that study) decreases. The first observed T_c decrease occurs when the concentration is increased for all three salts at pH of 7.1. This pH value is close to the isoelectric point of the protein and therefore the net charge of the protein is close to zero. So, the observation is consistent with the expectation and indicates that the self-association of the antibody decreases as the ionic strength increases. In the study focusing on anion effects, additional three pH values (pH = 5.3, 6.1 & 6.6) were studied as well. At all these pH values, the protein is positively charged since pH is below the pI. In

these solutions that exhibit different behavior in terms of the cloud temperature, as the ionic strength is increased, the highest T_c was mostly observed for KSCN. This behavior in the medium of KSCN is interpreted as the salt could disrupt the antibody-antibody interaction the least. In conclusion of the study which aimed to interpret the data with the Hofmeister series, when the salt concentration in these antibody solutions was increased from 22 mM to further concentrations up to ≈250 mM, the reverse Hofmeister effect was observed before reaching the maximum T_c value, and the direct Hofmeister effect was observed at high concentrations of salts (after reaching the maximum T_c value).

Li et al. examined the coacervation of amphoteric diallyl dimethylammonium chloride and sodium styrene sulfonate copolymer [32]. They questioned the effects of the Hofmeister series and found that sulfate, phosphate, and acetate ions do not block the coacervate formation contrary to expectations arising from belonging to the class of kosmotropes that reduce polymer solubility.

Perry et al. studied coacervation of two vinyl polyelectrolytes (poly (acrylic acid sodium salt) (pAA) and poly (allylamine hydrochloride) (pAH)) by mixing aqueous solutions of the polymers in the presence of salts in the Hofmeister Series [33]. The salts they used were NaCl, KCl, $MgCl_2$, $CaCl_2$, NaBr, NaI, $NaNO_3$, $NaCOOCH_3$, Na_2SO_4, KNO_3, and K_2SO_4, having a total of four cations and six anions. They used turbidimetric titrations while investigating the results through the salts in the Hofmeister series since turbidity can be a qualitative measure of the interaction between the polyelectrolytes resulting in complexation or coacervation. For all salts used in the study, they stated that at salt concentrations less than 75 mM, turbidity of the mixture increased (meaning the amount of coacervation increased) with increasing salt concentration from zero. According to their interpretation, as the salt is introduced to the medium of the polyelectrolytes, it causes a salting-in effect, i.e., increases the solubility of the polyelectrolytes. As the chains become more soluble, they find each other easier in the medium, and interaction between the oppositely charged chains becomes more possible. As a result, the phase separation escalates and the turbidity increases. On the other hand, when a salt concentration higher than 75 mM final concentration was added, turbidity gradually decreased and reached zero, i.e., no phase

separation was observed after this point named the critical salt concentration. They explicated this observation as that the further increase in the solubility of the polyelectrolytes decreases the stability of the phase separation. More importantly, the increase in the salts' concentration greater than 75 mM causes the screening effect on the charges on the monomers. Thus, it prevents the formation of coacervates by inhibiting the electrostatic forces that makes the polyelectrolytes interact in the first place. The main perspective that one should get from the latter observation is that the salt reaching the critical salt concentration at a lower concentration inhibits the coacervation more. When the critical salt concentrations belonging to different kinds of salts were investigated, the ions they examined exhibited relevant behavior with the direct Hofmeister series on the coacervation of pAA and pAH.

Lim et al. conducted a study focused on the Hofmeister effect and interfacial tension on the complex coacervation of mussel sticky proteins (MAP, fp-151) with hyaluronic acid (HA) [34]. According to the Hofmeister series, ions have the ability to increase or decrease the interfacial tension in relation to their hydration force. As a result of turbidity and spectrophotometry experiments, they presented that the coacervate and the protein alone behave roughly in relation to the direct Hofmeister series while HA alone is not affected by ions at all. With dynamic light scattering (DLS), they found that the coacervates (and protein alone) were affected by chaotropic ions, exhibiting higher hydrodynamic radii in the direct Hofmeister order. According to the data obtained from the slope of the hydrodynamic radius *versus* time graphs, the interfacial tension also tends to follow the direct Hofmeister series. When interpreted in terms of hydration, they stated that at salt concentrations below 250 mM, the interaction between the positively charged protein surface and negatively charged ions predominates at the water and protein interface. Highly hydrated ions reduce the number of interacting polymers and cause more water to be present in the coacervate phase. Therefore, in a solution with low hydrated anions, there is a higher interfacial tension between the coacervate phase and the dilute phase, as there is less water in the coacervate phase and the forces between the polymers are stronger. As a result of the gravitational force and contact angle measurements done using a macro-lens camera, ring-type light-emitting diode, and contact point-atomic force microscopy, the reverse Hofmeister effect was observed in the interfacial tension values.

1.3. Isothermal Titration calorimetry (ITC)

Isothermal titration calorimetry (ITC) is a quantitative and thermodynamic technique used especially for the observation of interactions between biochemical molecules [35]. It is the current method of choice for the characterization of biomolecular interactions.

There are three main parts in the instrument: sample cell, reference cell, and syringe. The sample cell usually contains a macromolecule solution; the titration ligand in solution is loaded in the syringe, and the reference cell is filled with the solvent (water or buffer solution). During the experiment, the tip of the syringe containing the ligand solution enters the sample cell, the ligand is titrated into the sample cell automatically (instrument-controlled) at a constant temperature provided by an adiabatic coat surrounding both of the cells. When the ligand is titrated into the solution in the sample cell, the two molecules interact with each other, and heat is released or absorbed in direct proportion to this interaction. The device responds to the release or absorption of heat in the sample cell, keeping the temperatures of the sample and reference cells constant and equal. As the macromolecule within the sample cell becomes saturated with the ligand titrated from the syringe, the heat signal decreases until only the heat of dilution is observed. The heat of dilution can be obtained by titration of the ligand to the solution used as the solvent, and the graph for the solvent-ligand is subtracted from the graph for the macromolecule-ligand before data analysis. [36]

Measuring the heat released or absorbed when molecules interact, ITC allows the determination of binding coefficient (K), reaction stoichiometry (n), enthalpy (ΔH), and entropy (ΔS) values. ITC gives the most direct information in determining the total heat exchange (ΔH) compared to other methods such as ultracentrifugation, spectroscopy, radiolabeling, equilibrium dialysis, and differential scanning calorimetry. [35] In the ITC method, there is no need for labeling as in the case of fluorescence spectrometry. It also does not require surface immobilization as in surface plasmon resonance. Thus, it is widely used in the study of thermodynamics as can be seen in the following literature examples.

Janc et al. investigated the thermodynamic behavior of bovine serum albumin (BSA) in aqueous solutions by ITC experiments [37]. They carried out their experiments below the isoelectric point of BSA (pI) (in the acetate buffer, at the pH at which the protein has a net positive charge), above the pI (in the MOPS buffer, at the pH at which the protein has a net negative charge), and further (in the borate buffer, at the pH at which the protein is more negatively charged). Hofmeister series' salts were used to determine the mixing enthalpy values, and the reverse Hofmeister effect was observed.

Fu and Schlenoff studied complex coacervation of poly (diallyl dimethylammonium chloride) (PDADMAC) and poly (styrene sulfonate, sodium salt) (PSSNa) polyelectrolytes [23]. They focused on the perspectives of the electrostatic model and the ion coupling model regarding associations while examining the effects of the Hofmeister series on the phase separation of these two polyelectrolytes, and carried out their experiments with ITC. According to the electrostatic model, they mentioned the existence of ionic atmospheres surrounding two oppositely charged polyelectrolytes. There are three important enthalpy terms in their studies: i) ΔH_{pair} (pairing enthalpy) is gained when these two polyelectrolytes come together, ii) ΔH^{atm} (enthalpy of release of the counterions) is lost as the counterions around them in the ionic atmosphere move away from the chains, and iii) the net enthalpy value that is named the enthalpy of polyelectrolyte complexation (ΔH_{PEC}). They related the electrostatic model with attractive and repulsive forces, considering the change in entropy caused by ion clouds surrounding polyelectrolytes breaking up and the counterions gaining degrees of freedom. Citing the work of Ou et al., and Elder et al. [19, 36, 37], they indicated that this entropic perspective should not apply since this model is not consistent with many experimental data, and it ignores the effect of the ion type in the self-interaction of polymers. In the study, it is asserted that the ionic coupling model has a chemical specificity and a localized perspective on the chains. The Hofmeister series are analyzed with respect to the degree of hydration of these ions and the effects of ions on the water structure. Since strongly hydrated anions cause greater effects on the structure of water than weakly hydrated ones, they examined whether their energetic changes are proportional to this effect. In their experiments, they exchanged the Cl^- ion, the counterion content in PDADMAC, with different anions (Br^-, NO_3^-, ClO_3^-, Ac^-, F^-) (confirmed the exchange with fluorescence spectroscopy). They observed PDADMA's mixture with PSSNa (coacervation) in the

presence of different anions with ITC, and they observed the coacervates with infrared (IR) spectroscopy. In addition, using Raman spectroscopy experiments, the effects of these ions on the water structure as “in the complex” and “free in water” forms were measured, i.e. water perturbation in different ions is investigated as well. According to the results they got, ions that strengthen the structure of water (kosmotropes) made an endothermic contribution while increasing the effect of hydrogen bonds and lowering the ΔH_{PEC}. They also investigated how chain length affects complex formation and observed that longer chains have greater driving forces in complex formation, according to a previous study [40]. When ΔG_{PEC} and ΔH_{PEC} values were analyzed, they stated that the complexation of these two polyelectrolytes was driven by entropic effect at the rate of 90%-100%.

Vander Meulen et al. examined the binding between 34 bp (base pair) H' DNA and integration host factor (IHF, an E. coli protein that remodels DNA) and provided important thermodynamic data on this binding (coefficient of binding, and enthalpy of binding) from ITC [41]. To see the effect of the Hofmeister series, they carried out their experiments in the presence of KCl (potassium chloride), KF (potassium fluoride), and KGlu (potassium glutamate) salts. They found that at salt concentrations less than 0.05 M, none of these salts affected the thermodynamic data. Further, at salt concentrations higher than 0.05 M, the binding coefficient for IHF-H'DNA interaction in solution containing KCl is higher than that in solutions containing KF or KGlu. They attributed this result to *the favorable enthalpy of binding*, one of the properties of the KCl solution.

Li et al. investigated the coacervates formed by the combination of JR 400, a cationic polyelectrolyte, and SDS (sodium dodecyl sulfate), an anionic surfactant [42]. Their studies, using various methods such as isothermal titration calorimetry, dynamic light scattering, atomic force microscopy, turbidimetry, and cold transmission electron microscopy, aimed to interpret the interaction mechanisms underlying coacervation and/or re-dissolution. As a result of their experiments done by mixing the two ionic substances, a clear solution was obtained when the concentration of SDS was much lower than that of JR 400 (polyelectrolyte-surfactant complexes with a net positive charge). As the SDS concentration was increased, turbid solutions were observed in the region of charge neutralization (near

neutral) where coacervation began. By further addition of SDS, re-dissolution occurred giving clear solutions of single-phase, which is explained by the net negatively charged, dissolved polyelectrolyte-surfactant complexes finally resulting in surfactant micelles. They used the Satake-Yang model to explain the interaction between the polyelectrolyte and the surfactant. Using the ITC data, they stated that the non-cooperative interaction at low surfactant concentration became cooperative when the concentration of SDS was increased. Their definition for non-cooperative binding is that a negatively charged surfactant is attached to a positively charged and available interaction point on the polyelectrolyte. Both ionic and hydrophobic interactions affect this binding. Also, in the final stages of cooperative binding, two or three surfactant molecules bind to each binding site on the polyelectrolyte. Therefore, the limiting factor in the interaction of these two molecules is the amount of available binding points on the polyelectrolyte. The authors mooted that cooperative binding was beyond the stoichiometric point (in the presence of excess SDS) and emerged with the hydrophobic properties of the hydroxy-ethyl groups on the polyelectrolyte. As a result of the addition of excess SDS, many surfactants bound on the polyelectrolyte stabilized the complexes they formed and therefore the coacervate phase was again dissolved because of the net negative charge. At this stage, they stated the driving force for SDS aggregation (micelle formation) as the entropic gain resulting from the release of unfavorably structured water molecules.

Courtois and Berret investigated the complexes formed by poly(sodium acrylate)-b-poly(acrylamide) (PANa-b-PAM, anionic-neutral block copolymer) and dodecyl trimethylammonium bromide (DTAB, quaternary ammonium salt, cationic surfactant) molecules [43]. They used ITC and light scattering and validated the data they received from one by comparing them with those from the other. In line with the data they obtained from ITC, they concluded that the interaction between PANa-b-PAM and DTAB is endothermic. They emphasized the importance of the order of mixing (which molecule is added to the other one). They labeled the order that the surfactant is added to the polymer as the 1st method and the order that the polymer is added to the surfactant as the 2nd method. According to the data obtained from the 1st method, the interaction between these two substances is two-staged. The first step is the formation of single residue surfactant micelles and pairing of these micelles with a polymer before a certain load ratio. The second stage is the re-

arrangement of the micelles after a certain charge ratio and their transformation into large colloidal core-shell complexes. They proved this transformation in the second step by a second endothermic peak in the ITC data. The data obtained from the second method, on the other hand, was interpreted as that there were no two different stages and instead, core-shell complexes were encountered at each charge ratio. In conclusion of these two different results, they stated that the difference in mixing order changes the enthalpy data and proved the importance of the mixing order.

2. AIM OF THE STUDY

As it is suggested by the literature review given in the introduction section, the effect of the Hofmeister series on coacervation was investigated only between protein/protein, protein/polyelectrolyte, and synthetic polyelectrolyte/polyelectrolyte systems. However, there is no study in the literature on the effect of the Hofmeister series on the coacervate formation between two biologically-based oppositely charged polyelectrolytes. Bio-based polyelectrolytes have a relatively high persistence length which corresponds to low chain flexibility, especially when compared to vinyl-based synthetic-based polyelectrolytes. For example, DNA has an intrinsic persistence length of 50 nm [44], while that of polyacrylic acid is 8.7 Angstroms [45].

In a previous study carried out by our research group [20], coacervation conditions between semi-flexible biopolyelectrolytes (anionic hyaluronic acid (HA, persistence length of 4 nm [46]) and cationic chitosan (CHI, persistence length of 6.5 nm [47])) were examined. It was found that the physicochemical parameters affecting HA-CHI coacervation were pH and ionic strength of the medium, molecular weight of the polyelectrolytes, and linear charge densities of the polyelectrolytes. However, only NaCl was used as a salt component in all of the experiments done in the research.

In yet another study [48], HA-CHI coacervation was used to form scaffolds working with both NaCl and $MgCl_2$ salts. This means the number of salt types studied was limited to only two. In our research group's latest project funded by Boğaziçi University Scientific Research Projects (BAP Project no: 15582), the effect of the Hofmeister series on HA-CHI coacervation was investigated by turbidimetric titration, zeta potential, and dynamic light scattering experiments at a constant pH. What is missing is the thermodynamic study of that subject. In another TÜBİTAK project which was completed in 2018 (project no: 116Z096), thermodynamic properties of HA-CHI coacervation were examined only in NaCl solution with ITC. However, a larger variety of salts needs to be studied to understand the effect of the Hofmeister series.

In this study funded by the TÜBİTAK (project number: 120Z865), the main goal is to examine the effect of the Hofmeister series on HA-CHI coacervation in terms of thermodynamics with the ITC method. The information gained from this project will be important not only in terms of polymer physics and colloid science but also in terms of tissue engineering applications since HA and CHI are biocompatible polymers and can be used as tissue scaffolds made of HA-CHI coacervates.

3. METHODOLOGY

3.1. Materials

The high molecular weight sodium salt of hyaluronic acid (HA, molecular weight of 1.2 MDa as determined by viscosity experiments) was kindly given as a gift by Dr. Kazuyuki Miyazawa from Shiseido Co. (Yokohama, Japan). The low molecular weight sodium hyaluronate (HA, molecular weight of 199 kDa as determined by viscosity experiments, Lot Number: 026564) was purchased from Lifecore Biomedical (Chaska, MN, USA). Chitosan HCl (CHI, Molecular weight 396 kDa, determined from gel permeation chromatography, Product Code: 54039) with 83% degree of deacetylation (DDA) was purchased from Heppe Medical Chitosan GmbH (Halle, Germany).

NaCl (Product Code: 106404), KCl (Product Code: 104936), and $NaOAc.3H_2O$ (Product Code: 106267) were purchased from Merck (Darmstadt, Germany). Citric acid (99%, Product Code: C0759) and 2-(N-Morpholino)ethanesulfonic acid hydrate (MES hydrate, >99.5%, Product Code: M8250) were purchased from Sigma Aldrich (Massachusetts, USA).. $NaNO_3$ (Product Code: 481757), $MgCl_2.6H_2O$ (Product Code: 459337), and Na_2SO_4 (Product Code: 483007) were purchased from Carlo Erba (Milano, Italy). Research grade $CaCl_2.2H_2O$ was purchased from VWR Chemicals (Product Code: 22317.260) (Ohio, USA) and ISOLAB Chemicals (Product Code: 909.026) (Wertheim, Germany).

Methanol used for ITC washing (liquid chromatography grade, Product Code: 947.047.2501), research-grade 2.00, 4.00, 7.00, and 10.00 buffer solutions used for pH meter calibration (Product Codes: 908.B02, 908.B04, 908.B07 and 908.B10, respectively) and 1 N and 0.1 N NaOH & HCl solutions used for pH adjustments (Product Codes: 969.20V, 969.22V, 932.13V, and 932.15V, respectively) were purchased from ISOLAB Chemicals (Wertheim, Germany).

All solutions were filtered using 0.45 µm cellulose acetate membrane filters (Product Code: 56133345, 56253345) from Labmarker (Istanbul, Turkey).

The semipermeable membranes, Snakeskin Tubes of 10000 g/mol and 3500 g/mol (product code: 68100 and 680035, respectively) were purchased from Thermo Scientific™ (Massachusetts, USA).

Isopropyl alcohol (Product Code: TK.090250.02501) used for slide and coverslip cleaning was purchased from ISOLAB Chemicals (Wertheim, Germany). Nitrogen gas (99.999% purity) used for the same purpose was purchased from Linde Gaz (Dublin, Ireland).

3.2. Methods

3.2.1. Dialysis for Counterion Exchange

75 mL of polyelectrolyte solutions of 0.5 mg/mL HA or 0.5 mg/mL CHI are prepared in Milli-Q water. The counterions already present in the structure of these polymers are Na^+ and Cl^-, respectively. 0.1 M solutions of the salts containing the desired ions (e.g. KCl if the desired cation for HA is K^+ or NaOAc if the desired anion for CHI is OAc^-) are prepared in Milli-Q water. The polymer solutions are transferred into the semipermeable membranes, and the filled membranes are placed in 5 L solutions of the salt solutions. Polymers are dialyzed sequentially against three batches of the prepared salt solutions for 24 h for each batch, followed by three days of dialysis against Milli-Q water, refreshing the water every 24 h.

The replacement of the counterions was made sure by SEM-EDS experiments (FEI-Philips XL30 Environmental Scanning Electron Microscope with Field Emission Gun

(equipped with EDAX-Energy Dispersive X-ray Analysis Unit)) done in the Advanced Technologies Research and Development Center of Boğaziçi University.

3.2.2. Turbidimetric Titration

First, buffered salt solutions are prepared by dissolving two solids (MES for neutral pH region experiments and citric acid for the acidic region and the corresponding salt to the condition) together in a volumetric flask, and the pH values are adjusted by adding base or acid solutions (1 N or 0.1 N NaOH or 1 N or 0.1 N HCl or Glacial AcOH for NaOAc experiments) to reach the desired pH value for the experiment (6.25 ±0.5, 5.25 ±0.5, or 3.25 ±0.5). Then, HA and CHI polymers are dissolved separately in these salt solutions. 0.5 or 0.1 mg/mL CHI and 0.5 mg/mL HA solutions were prepared by mixing for 2 h in the solutions of the conditions listed in Table 3.1. Total ionic strength (I_{total}) of the medium was ≈50 mM for the salted conditions but differs with respect to the pH value for the "No Salt" condition. I_{total} of the medium for the "No Salt" condition was 3 mM for the experiments done at the pHs of 3.25 and 6.25, but 1 mM for those at the pH of 5.25 while concentration of the buffer was 5 mM for both pHs.

Table 3.1. Concentrations of each salt used in the experiments of different conditions.

Salt Type	**Concentration of salt (mM)**	**I_{total} of the medium with 5 mM concentrated MES or citric acid as the buffering agents**
NaCl	47	50 mM
KCl	47	50 mM
$CaCl_2$	15.67	50 mM
$MgCl_2$	15.67	50 mM
$NaNO_3$	47	50 mM
NaOAc	47	50 mM

The CHI solution is taken into a glass vial to be exactly 10 times the volume used in the experiment performed in the ITC instrument, and the HA solution is titrated by adding 10 times the volume of the ITC experiment with a micropipette (0.02 mL HA solution was titrated into 2.6 mL of CHI solution). The percent transmittance (permeability, % T) of the titrated solution is measured continuously with a colorimeter (PC950, Brinkmann, USA), and then converted to 100 - % T = % Turbidity.

Since the turbidity experiments are replicas of the experiments performed in the ITC instrument, the titration intervals and the total number of droplets in the titration were kept the same as the experiments in the instrument.

3.2.3. Light Microscopy

The turbidimetric titration procedure described above had a total of 20 titration points, drops being titrated every four minutes. During the experiment, the smallest volume of sample that allows image acquisition for the microscope (CTR6000, Leica, USA) is taken at different points of the experiment (at the molar ratios (HA to CHI) of 0.16, 0.35, and 0.52) and the droplets were imaged at the end of the experiments. These images were used to check for the presence of invisible-to-human-eye precipitates and particle size analysis.

Analysis of particle size and type was done using the Adobe Photoshop (22.1.20169.0) program. Firstly, three regions were marked on the images. After doing the pixel-to-mm conversion (10 mm for 39 pixels), each particle’s size was measured using the ruler tool and written on the image. If the particle was spherical (imaging on every angle giving the same size), it was defined as a coacervate. If not, it was defined as a precipitate. An example of the analysis is given in Figure 3.1.

For the particle type analysis, in each image, the number of coacervates and precipitates are counted in each of the three selected areas. Then by using the formula of

$$\%(coacervates) = \frac{(number\ of\ coacervates)}{(number\ of\ coacervates + number\ of\ precipitates)} \times 100,$$

the coacervation percentages by number are calculated and summarized in Tables 4.1 and 4.2.

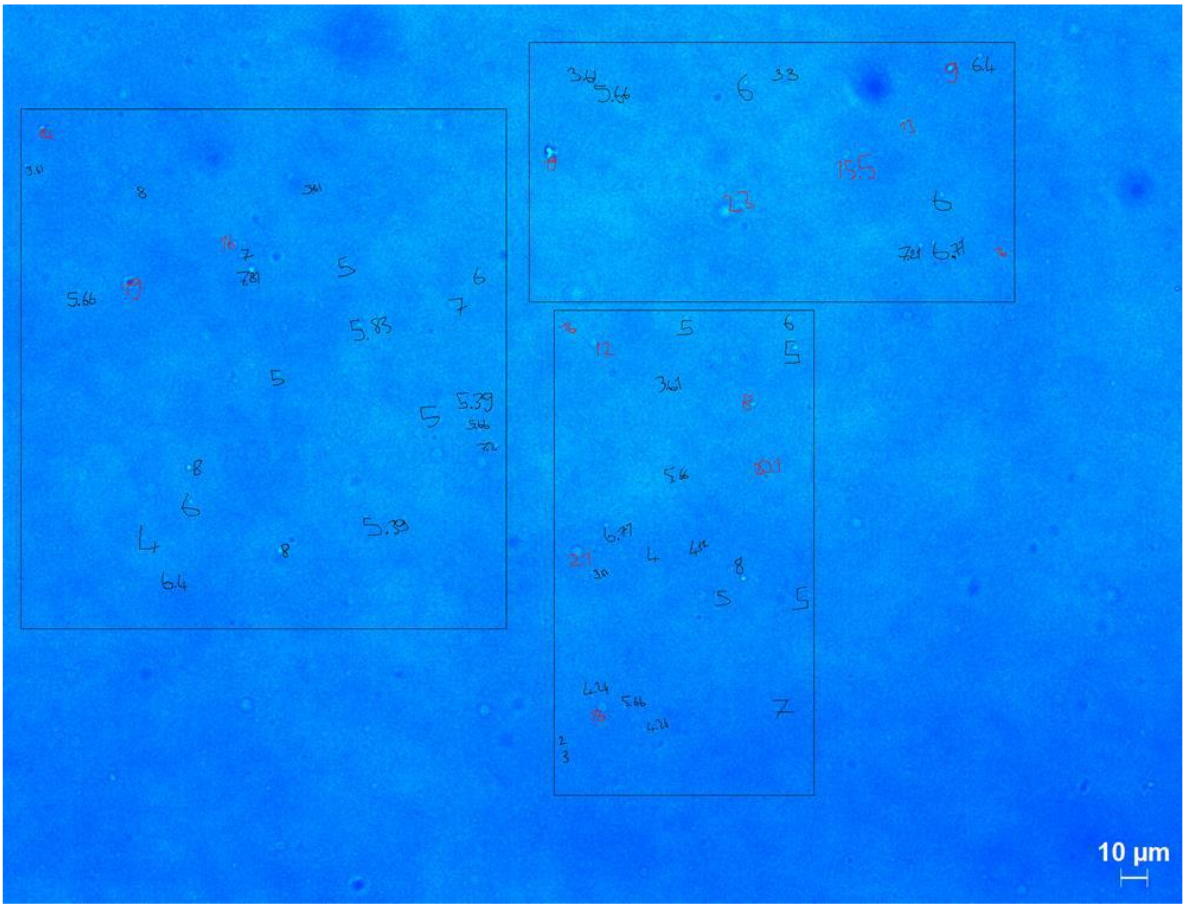

Figure 3.1. A processed photograph of particle size analysis done on the image of the sample drop taken from the solution at the end of the turbidimetric titration. This particular image belongs to the experiment done with 0.1 mg/mL CHI & 0.5 mg/mL HA (199 kDa) dissolved in buffered salt solution at pH 5.25 and of I_{total} of 50 mM (1:9 ionic strength ratio of MES:$MgCl_2$).

3.2.4. Isothermal Titration Calorimetry (ITC) Experiments

ITC200 (Malvern, England) instrument and Thermovac degasser (Malvern, England) were used to determine the thermodynamics of the HA/CHI system in different buffered salt solutions.

3.2.4.1. Experiments During the Optimization Process

0.2 M NaCl solution is prepared by dissolving the weighed solid in a volumetric flask. The pH of the solution is brought to 6.25 ($\pm$ 0.05) by adding 0.1 or 1 N NaOH or HCl. Polymers are dissolved in this salt solution in desired concentrations by mixing for at least 2 h. Every solution is filtered with 0.45 μm cellulose acetate membrane and degassed for 5-10 min prior to the ITC experiment.

3.2.4.2. Experiments with Diafiltration

0.2 M NaCl solution is prepared by dissolving the weighed solid in a volumetric flask. The pH of the solution is brought to 6.25 ($\pm$ 0.05) by adding 0.1 or 1 N NaOH or HCl. CHI is dissolved in this salt solution at the desired concentration. After 2 h of mixing, 5 mL of this CHI solution is transferred into a diafiltration tube (upper part, in the membrane), and 10 mL of the salt solution is added so that the final volume is 15 mL which is the maximum value that the membraned part of the tubes can take. By using a balance tube, centrifugation is done at 5000 rpm for 15 min. When the centrifugation is done, the bottom part that contains only the solvent but not CHI is discarded and another 10 mL of the salt solution that the CHI was dissolved in is added on top. Then a 2nd run of centrifugation is started. This process is kept on until the 5th centrifugation. At the end of the 5th run, the solutions are not discarded but collected in vials. Using the bottom solution as the solvent, HA is prepared in the desired concentration and mixed for at least 2 h. Before the ITC experiment, the solutions are filtered with 0.45 μm cellulose acetate membranes and degassed for at least 5 min.

3.2.4.3. Experiments with Dialysis and Stocked-Solution Method

First, a buffered salt solution is prepared in Milli-Q water by dissolving the two solids (buffering agent and salt) in volumetric flasks and the pH value is adjusted by adding acid or base solutions (1 N NaOH, 0.1 N NaOH, 1 N HCl, or 0.1 N HCl) to reach the desired pH value for the experiment (6.25 ±0.5, 5.25 ±0.5, or 3.25 ±0.5). Then, the individual polymers of hyaluronic acid and chitosan are dissolved in this buffered salt solution at four times the concentration to be used in ITC experiments, a.k.a. 2.0 mg/mL HA and 0.4 mg/mL CHI and mixed for 2 h. Concentrations of all other substances were the same as the ones prepared for the turbidimetric titration experiments.

The prepared polymer solutions are subjected to the dialysis method using semi-permeable membranes with a molecular weight cut-off limit of 10 kDa (Thermo Scientific™ (Massachusetts, USA)) refreshing the buffered salt solutions every 3 hours for a total of five batches. The purpose of this process is to eliminate the heat exchange that is released or absorbed due to the dilution of the ions of the buffered salt solutions caused by the titration of the titrant into the sample cell during titration in ITC (ITC200, Malvern, England) experiments, i.e., to eliminate the differences between the two solutions that are subjected to the titration. In other words, it is to eliminate buffer mismatching. Since the molecular weights of the polymers used are at least 39 times greater than 10 kDa, it is found appropriate to use the molecular cut-off limit of the membranes as 10 kDa.

After dialysis, polyelectrolyte solutions are transferred into vials and diluted to 0.1 mg/mL (CHI) and 0.5 mg/mL (HA) using the final batch of the buffered salt solution and mixed for 2 h. At the end of dilution, all solutions are filtered through cellulose acetate membranes with a pore size of 0.45 μm (Labmarker, Istanbul, Turkey).

Before the ITC experiment, the polyelectrolyte solutions and the buffered salt solutions to be used in the control experiment are degassed under vacuum with the "Thermovac

degasser" instrument, to avoid any errors in the data due to air bubbles that may occur in the ITC sample cell or the syringe.

According to a previous study, precipitation occurred in turbidimetric titration experiments in which CHI solution was added to HA solution [20]. Therefore, in this study, HA solution is titrated into CHI solution. That is, 40 μL HA is loaded into the syringe and 260-290 μL CHI is loaded into the sample cell and the experiment is started with ~280 μL Milli-Q water in the reference cell.

The parameters (mixing speed, reference power, etc.) to be used in ITC experiments were determined as a result of optimization studies. Experiments were carried out at room temperature. All experiments were repeated at least four times.

3.3. Data Analysis

Before presenting the equations of the models that exist in the software of the ITC instrument (Origin) and of the analysis done using Microsoft Excel, first, the variables are presented in the list of symbols section for the reaction of

$$X + M \leftrightarrow XM, \tag{3.1}$$

where *X* stands for the titrant in solution in the syringe and the *M* stands for the titrate in solution in the cell. The cells in the instrument are shaped like lollipops and the straw part is the entrance part (pipe) for either loading the sample or inserting the syringe. The round part is kept at constant temperature and sensed calorimetrically. So, there always is “overflow” volume of solution in the pipe and it is said to be containing the excess volume of solution caused by each injection (titration). The manual [49] proposes the concentrations of the titrant and the titrate in the overflow region in the pipe as the mean value of the diluted concentrations and the initial concentrations of the materials using the expressions of

$$M_t^0 V_0 = M_t V_0 + \frac{1}{2}(M_t + M_t^0)\Delta V, \tag{3.2}$$

$$X_t^0 V_0 = X_t V_0 + \frac{1}{2} X_t \Delta V, \tag{3.3}$$

where X_t^0 and M_t^0 are the initial concentrations of *X* and *M*, respectively, V_0 is the volume of the cell (which is equal to the volume of the solution of *M* inside the cell), ΔV is the overflow volume, and X_t and M_t are the diluted concentrations of *X* and *M*, respectively, after the injection of *X*. Note that the V_0 does not change as *X* is titrated. This is because the titrated amount of the solution (sum of all titrated amount = ΔV) will be excluded from the cell. Then, by only rearranging these equations, X_t and M_t can be expressed as

$$X_t = X_t^0 \left(1 - \frac{\Delta V}{2V_0}\right), \tag{3.4}$$

$$M_t = M_t^0 \left(\frac{1 - \frac{\Delta V}{2V_0}}{1 + \frac{\Delta V}{2V_0}}\right). \tag{3.5}$$

The overflow volume effects that result from each injection are corrected by Origin using the aforementioned formulas for X_t and M_t.

3.3.1. Single Set of Identical Sites (SSIS) Model

This model, based on the Langmuir equation, assumes that all of the binding sites on *M* are identical and have the same enthalpy of interaction between titrant and titrate (*X* and *M*) and the same binding constant. The calculations begin with

$$K = \frac{[MX]}{[X][M]} = \frac{\Theta}{(1 - \Theta)[\mathrm{X}]}, \tag{3.6}$$

where K is the binding constant, Θ is the fraction of sites occupied by *X*, $[MX]$, $[X]$ and $[M]$ are the concentrations of bound *M* and *X*, free *X* in the solution, and free *M* in solution, respectively. The last three are unknowns. Therefore, it is required to eliminate them from

the equations by using the equations below. First, X_t can be expressed in another form than presented as

$$X_t = [X] + n\Theta M_t, \tag{3.7}$$

where n is the number of sites available for binding. Combining the equations 3.6 and 3.7, the following equation can be obtained:

$$\Theta^2 - \Theta\left[1 + \frac{X_t}{nM_t} + \frac{1}{nKM_t}\right] + \frac{X_t}{nM_t} = 0. \tag{3.8}$$

The total heat content (Q) of the solution that is in the sample cell at fractional saturation Θ can be calculated by using

$$Q = n\Theta M_t \Delta H V_0, \tag{3.9}$$

where ΔH is the molar enthalpy of binding *X* to *M*. Solving the equation (3.8) for Θ gives:

$$Q = \frac{nM_t\Delta HV_0}{2}\left[1 + \frac{X_t}{nM_t} + \frac{1}{nKM_t} - \sqrt{\left(1 + \frac{X_t}{nM_t} + \frac{1}{nKM_t}\right)^2 - \frac{4X_t}{nM_t}}\right]. \tag{3.10}$$

At the end of the ith injection, the value of Q in the equation above may be determined (for any defined values of $n, K,$ and ΔH). However, the parameter of importance for experimental comparison is the change in heat content from the end of the (i-1)th injection to the end of the ith injection. Only the liquid contained in volume V_0 is subject to the Q expression in equation (3.10). About half as much heat is produced by the liquid in the overflow volume as it is by an equivalent amount in V_0. The formula used by Origin for the heat released by the ith injection, ΔQ_i, is as follows:

$$\Delta Q_i = Q_i + \frac{dV_i}{V_0}\left(\frac{Q_i + Q_{i-1}}{2}\right) - Q_{i-1}, \tag{3.11}$$

where Q_i is the total heat content at the end of the ith injection.

First estimates of $n, K,$ and ΔH as well as the computation of ΔQ_i for each injection are required in order to fit experimental data. Origin can typically make these initial estimates with sufficient accuracy. Following that, a comparison of these values with the heat observed for the comparable experimental injection should be made. Then, using standard Marquardt procedures, these values should be improved from their starting values of $n, K,$ and ΔH. Until there is no longer a noticeable increase in fit with additional iteration, the aforementioned technique is repeated.

3.3.2. Two Sets of Individual Sites (TSIS) Model

The TSIS model states that the macromolecules have two binding sites, and the binding between them is non-cooperative. In the analyses done using this model, the same definitions of symbols as in section 3.3.1 are used. For each set (1 and 2), the calculation again starts with writing the equations for the binding constants and the diluted concentration of *X* after injection by rewriting the equations as

$$K = \frac{\Theta_1}{(1-\Theta_1)[\mathrm{X}]}, \tag{3.12}$$

$$K = \frac{\Theta_2}{(1-\Theta_2)[\mathrm{X}]}, \tag{3.13}$$

$$X_t = [X] + M_t(n_1\Theta_1 + n_2\Theta_2), \tag{3.14}$$

where the definitions of the variables are the same, but the subscripted numbers represent the belonging to either 1st or the 2nd binding site.

Solving the equations (3.12) and (3.13) and then replacing them in the equation (3.14) gives:

$$X_t = [X] + \frac{n_1 M_t [X] K_1}{1 + [X] K_1} + \frac{n_2 M_t [X] K_2}{1 + [X] K_2}. \quad (3.15)$$

Origin clears the equation (3.15) of fractions and collects them into a cubic equation of the unknown [X], where the coefficients of [X] are in terms of K_1, K_2, n_1, n_2, X_t and M_t. Then it dissolves for [X] numerically by using Newton's Method with assigned K_1, K_2, n_1, and n_2 .

The total heat content (Q) of the solution that is in the sample cell at fractional saturation Θ can be calculated by improving the equation (3.9) for two sites instead of one site as

$$Q = M_t V_0 (n_1 \Theta_1 \Delta H_1 + n_2 \Theta_2 \Delta H_2), \quad (3.16)$$

where the variables are again defined the same as before, but the subscripted numbers represent the belonging to either 1st or the 2nd binding site.

After a similar correction for the overflow volume, the heat released by the ith injection, ΔQ_i is given by the same the formula as given in the SSIS model, proposed in the equation 3.11. This leads into the Marquardt method to obtain values for the fitting parameters.

3.3.3. Analysis on Microsoft Excel

When the analysis done using the Origin program gave very high standard deviations, the method of summing [21, 44, 45] is used to at least obtain the enthalpy of complexation values with lower standard deviation values. In this analysis, the control experiments' energetical values are processed differently. First, for one trial of one condition (one may imagine the 1st trial of the experiment done using 0.1 mg/ mL CHI & 0.5 mg/mL HA (199 kDa) dissolved in the buffered salt solution of NaCl at pH of 5.25 and I_{total} of 50 mM), the average values of the last 15 values of the experiments of 20 titrations were calculated for

the BiB and BiC experiments ($\Delta H_{BiB_{avg}}$ and $\Delta H_{BiC_{avg}}$). Second, the average values of the HiC and the HiB experiments are calculated ($\Delta H_{HiC_{avg}}$ and $\Delta H_{HiB_{avg}}$). Third, these average values of the dilution experiments are subtracted from the original experiment's average value using the expression for the enthalpy of complexation (ΔH_c) as

$$\Delta H_c = \Delta H_{HiC_{avg}} - \left(\Delta H_{HiB_{avg}} + \Delta H_{BiB_{avg}} + \Delta H_{BiC_{avg}}\right). \tag{3.17}$$

Then, this calculation is applied to every trial of every condition's results. The analysis is finalized by calculating the standard deviations of the three trials within every condition.

4. RESULTS AND DISCUSSION

4.1. Optimization Studies

As mentioned above, this project aims to observe the Hofmeister effect on complex formation using different salts in the Hofmeister series. In order to do so, before starting the experiments with different salts in the series, the polymers with the counterions of the salts to be studied should be prepared. For example, if the salt under investigation is NaOAc, the original counterion of CHI (Cl^-) should not be present in the medium. The reason for this is that the interference of any other salt (ion) than the one under investigation may cause misinterpretations. The exchange of the counterions was done by the experiments mentioned in section 3.2.1. The exchange was made sure by SEM-EDS experiments by which one can obtain the percentage of the atoms present in the sample. The results of these experiments are presented in Appendix B. For the ions that contain elements that are originally not in the structures of CHI and HA (Mg^{+2}, $Ca^{+2,}$ and K^+ for HA), seeing whether the exchange occurred or not is easy; i.e. the percentage of original counterions should decrease and the new counterion should be present in the analysis. However, for the counterions whose atoms are already present in the original form of the polyelectrolyte, this part is a little tricky. For NO_3^- and OAc^- (for CHI), the decrease in the percentage of the Cl^- and increase in the percentage of the N atom and the O atom, respectively, are the proofs of exchanging the counterion.

4.1.1. Selection of Experimental Conditions Based on The Preliminary Study

In another study (Bogazici University BAP 15582) which can be presented as a preliminary study of this research, the effects of the Hofmeister series on HA/CHI (hyaluronic acid/chitosan coacervate system) were investigated by turbidity experiments using UV-VIS spectrophotometry. In experiments carried out at pH 6.25 (± 0.05), which is close to the physiological pH value and will not disrupt the system and its content, four different cations (Na^+, K^+, Mg^{+2}, Ca^{+2}) and four different anions (Cl^-, NO_3^-, CH_3COO^-, SO_4^-

^{2}) were used. Since chitosan is known to precipitate at pH values above 6.50 [52], a pH value of 6.25 was used to start with. This study was useful to get information on the conditions such as salt concentration and the polymer concentration that will be appropriate for observing the complexation.

The following points were considered when determining the salts to be used among the salts in the Hofmeister series: 1) Salts that are soluble in water at concentrations in the range of 0-0.8 M should be used, 2) HA-CHI mixture must not cause precipitation (liquid-solid phase separation) in the solution of the salt used, 3) salts should not have the effects that will disrupt the structure of the carbohydrates used or the coacervates that may form. According to the results of the turbidity experiments in which the Hofmeister effect was examined at a variety of salt concentrations (Figure 1.1), the salt concentration that should be used in this study for each salt was determined as the one giving turbid, coacervate-containing solutions. This value was found to be 0.20 M at pH = 6.25. For other pH values that are studied in this research, to keep all the parameters the same but only the pH value different, concentration values are not changed while performing complementary experiments.

The salts used for this research are the same as those in the preliminary study (NaCl, KCl, $CaCl_2$, $MgCl_2$, $NaNO_3$, Na_2SO_4, and NaOAc).

4.1.2. Determination of the Conditions

The ITC experiments at pH 6.25 with chloride salts containing Na^+, K^+, Mg^{+2}, and Ca^{+2} cations were first examined as suggested by the TÜBİTAK project. Therefore, ITC experiments were done with the determined concentration of 0.20 M for the salt.

The experiments' resulting graphs are named numerically in chronological order in Appendix A, going from 1 to 32, and can be seen in the *experiment file naming* in tables 1-

32 that give the conditions of these experiments. In the resulting graphs obtained from the instrument's software, the main goal was to examine a sigmoidal curve. However, the data points seemed to be random rather than bear a meaningful curve. Therefore, different experimental conditions had to be used to obtain interpretable data groups.

4.1.3. Instrumental Parameters

The instrumental parameters defining the experimental design can be listed as the number of injections, volume of the injections, time intervals between the injections, stirring speed, difference power, and the feedback gain. The values of these parameters that are suitable for the system under study (HA/CHI) were determined in the previous studies carried out in our laboratory. Thus, this study took the guidance of the previous studies and began by using the same values. However, when the first experiments' results were not interpretable, optimization was done.

Initially, the experimental design parameters in the instrument have been changed while trying to keep the experimental conditions (pH, concentrations, ionic strength) constant. The alterations in the experimental design parameters in the instrument were on "the number of titration injections" and "the injection intervals". These changes were applied from the perspective of "a higher number of injections" or "longer injection interval". The former is a way of interpreting the energy changes more deeply by obtaining more data points in the peak regions that are considered important in the graphs. The latter is a way of obtaining graphs with flat baselines instead of downward sloped baselines that may be caused by the system finding the time between the titration points inefficient to go back to its stable form. The changes were applied based on what was explained in the troubleshooting section of the manual of the instrument [53]. However, the changes seemed to be ineffective. Thus, subsequently, the concentration of the solution contents and pH values of the samples prepared for the experiment were found important and altered next.

4.1.4. Polyelectrolyte Concentrations

In the decision-making phase for polymer concentrations, the preliminary turbidity experiments mentioned above were taken as the guide. First, the molar ratio of [HA]/[CHI] in the mixture was calculated based on the HA and CHI concentrations used at the points where coacervation was observed in these experiments. Having 0.510 mL of 0.5 mg/mL CHI in a 2.0 mL solution and 0.490 mL of 0.5 mg/mL HA in the same 2.0 mL solution, the concentration of CHI in mM instead of mg/mL was calculated as

$$0.5\frac{mg}{mL} \times 1000\frac{mL}{L} \div 198.5609\frac{g}{mol} = 2.52\ mM, \quad (4.1)$$

where 198.5609 is the molecular weight of the repeating unit of the chitosan with DDA of 83%. Then the final concentration of the CHI in the total of 2 mL of the mixture solution was calculated using the equation of

$$2.52\ mM \times 0.510\ mL \div 2.0\ mL = 0.642\ mM\ CHI\ in\ the\ 2.0\ mL\ solution. \quad (4.2)$$

Subsequently, the same calculations were applied for HA, by starting from converting the mg/mL concentration to molar concentration as

$$0.5\frac{mg}{mL} \times 1000\frac{mL}{L} \div 401.292\frac{g}{mol} = 1.25\ mM, \quad (4.3)$$

where 401.292 is the molecular weight of the repeating unit of hyaluronic acid. Then the final concentration of the HA in the total of 2 mL of the mixture solution was calculated using the equation of

$$1.25\ mM \times 0.490\ mL \div 2.0mL = 0.305\ mM. \quad (4.4)$$

Finally, the molar ratio of the two polyelectrolytes in the final solution was estimated by

$$\frac{[HA]}{[CHI]}(in\ the\ final\ 2.0\ mL\ of\ solution) = \frac{0.305}{0.642} = 0.475. \quad (4.5)$$

Since the mole ratio is located on the x-axis in the ITC results, it was aimed to see lower and higher values than the calculated one on the x-axis to observe the interaction from a broader perspective, and the concentration values were determined accordingly. 0.3 mg/mL HA and 0.6 mg/mL CHI concentrations were chosen to start with, giving the desired range to be observed. Afterward, changes were made either by considering the "concentration ratio of two substances" (in separate solutions before the experiment starts) mentioned in the ITC instrument user manual [53] or by examining the distribution of data points in the heat per mol versus molar ratio graphs. For example, while the concentration ratio of the two polyelectrolytes in mM was [HA]/[CHI]≈1 in experiment #1, it was ≈2.5 in experiment #2, ≈10 in experiment #26, and ≈⅓ in experiment #23. These ratios were used according to the manual [53] leading the experimenter to investigate through high and low ratios. Additionally, as can be seen in Table A.1 and Table A.18, the difference between experiments #1 and #18 is the HA concentration. The reason for switching to a lower concentration in experiment #18 is that the distribution of data points in the heat graphs evokes "saturation". By using a lower concentration of the titrant, it is aimed to observe the interaction before this saturation. However, since the distribution of data points of experiment #18 seems to be not compatible with the least-squares curve (or line) when imagined, different conditions were tried.

4.1.5. Salt Concentrations/Ionic Strength

The salt concentration that should be worked at was determined to be 0.20 M as mentioned above, but the 0.15 M salt concentration was also worked with. The reasons for this change were both the noisy baseline and the imprecise (random-like) data points observed on the heat graph. While ionic strength was reduced from 0.20 M to 0.15 M, it was aimed not to deviate from the agreed condition as explained in the TÜBİTAK project proposal. Therefore, the results of the preliminary study were reviewed and continued with the 0.15 M salt concentration condition, which was the closest condition to physiological conditions with turbidity caused by coacervation. However, as can be seen from the data in

the Appendix A (Figures A.6 – A.11 and A.24), it appeared that a larger reduction in the salt concentration might have been more effective for having more precise results. The reason for this comment is that the small decrease in salt concentration did not affect imprecise data appearance.

4.1.6. Value of The pH

Experiments were carried out by preparing solutions with pH values different than 6.25, i.e., pH 3.00 and 4.00. The reason for this change in pH value was to achieve the desired sigmoidal curves. However, the desired result of obtaining a sigmoidal curve could not be achieved with this change (Figures A.9 – A.11, A.15 – A.17).

4.1.7. Molecular Weight of The Polyelectrolyte

When altering the three important parameters mentioned above did not result as desired, polyelectrolyte molecular weight, which is another factor that can affect the interaction and consequently, the enthalpy, was altered as well. In the experiments numbered 28, 30, 31, and 32, unlike all previous experiments, HA of 199 kDa molecular weight was used instead of 1200 kDa. The reason for this change was the following question: Could 1200 kDa HA cause too strong an interaction with 396 kDa CHI so that results are non-sigmoidal? The concentration of hyaluronic acid, in the titration syringe, was near its overlapping concentration (the concentration at which polymer coils are entangled). While being titrated into the sample cell, the titrant becomes diluted, and HA may be breaking away from its entangled form. However, if four minutes of titration interval was not enough for it to have all the chains free from the entanglement, there would be a chaotic medium where there are entangled coils and free molecules for interaction. As the titration goes on, the free HA chains would interact with CHI chains but at the same time, there would be more free HA chains coming out from the entanglements as the time passes and the duration of titration becomes ‘enough’ for the dilution to be completely effective. In addition, if the entangled chains were still able to interact with the CHI in the medium (not one by one but together), they would cause higher exothermic contributions than free ones since their charge densities

would be higher than their free forms, and molecules with high charge densities release more energy during their interactions [54]. In this way, there would be both small and high amounts of energy coming out from different kinds of HA molecules (entangled and free) during their interactions with CHI molecules. This would be observed in the appearance of heat graphs as random-like.

The overlapping concentration value increases as the molecular weight decreases [55]. So, using 199 kDa HA helped getting away from the overlap concentration when used at similar concentrations with 1200 kDa. The heat graphs of the four experiments done using 199 kDa HA are promising at least in terms of observing a slope, but the imprecision seen as a result of the experiments using 1200 kDa HA is still preserved albeit minorly (Figures A.28, A.30 – A.32).

4.2. Adding A Buffer

After all the alterations, no reproducible or sigmoidal-formed result could be obtained. Thus, more crucial changes were searched for the experimental method. The most important and effective change seemed to be the addition of a buffering agent to the system since there were more studies with buffers [46 – 51] than there are without buffers [20, 52 – 54] done using the ITC instrument. The most important factor in choosing the buffering agent is that it should not interact with other substances in the medium. Good's buffers are used especially in biological systems and are found to be "ideal" for biological research [65]. MES (2-(N-morpholino)ethanesulfonic acid) is a buffer that can be used at the pH value chosen for this study (6.25) since the pK_a is 6.15 at 20 ºC [66]. This buffer is chosen in the following experiments.

4.2.1. Optimization Experiments for the Buffered System via Turbidimetric Titrations

Since all previous experiments, including the preliminary experiments mentioned above, were performed in a not-buffered medium, the conditions such as polyelectrolyte concentrations, salt concentration, and pH value had to be optimized.

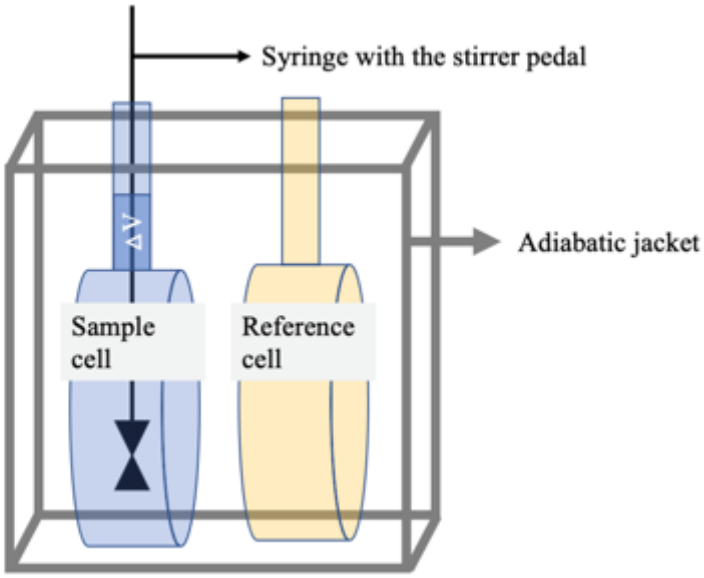

Figure 4.1. Scheme describing the inside of the adiabatic jacket in the instrument, covering the cells and keeping the cells at a constant temperature.

The ITC instrument is highly sensitive. The sample cell is in an adiabatic jacket and therefore cannot be seen from outside (Figure 4.1). This situation makes it necessary to perform the optimization outside the instrument because 1) When precipitation occurs inside the cell, it will not be possible to be sure whether it has been cleaned completely or not, thus, there will be the possibility of damaging the instrument, 2) It will not be possible to observe when the precipitation starts (or ends), so it will not be possible to find valid reasons for the decisions to be taken regarding the polyelectrolyte concentrations for preventing

precipitation. Thus, turbidimetric titration experiments were done to optimize the concentration values. After optimization, ITC experiments were performed.

NaCl was used as the first salt for the optimization experiments and the pH value was adjusted to 6.25 before dissolving the polymer solutions in the buffered salt solution. To ensure that the buffering agent is effective (the pH value remains in the desired range throughout the experiment), change of pH versus mole ratio of HA to CHI was recorded. The concentrations for polyelectrolytes were chosen carefully so that the molar ratio range was large enough to contain any molar ratio to be used in all experiments that will be done during and after the optimization process. As a result of this experiment, it was observed that the pH value remained in the desired range (Figure 4.2).

In the early experiments, initial concentrations of the polyelectrolytes in the preliminary study were used; i.e. 0.5 mg/mL for both polyelectrolytes.

To see the effect of total ionic strength, turbidimetric titration experiments were done in 200, 150, 100, and 50 mM buffered salt solutions. Because the salt ions (NaCl and MES ions) are monovalent, the ionic strength is the same as the salt concentration. 9:1 Salt: Buffering Agent molar ratio was kept constant for all solutions to minimize the energetical effects that could arise from the buffering agent’s dilution.

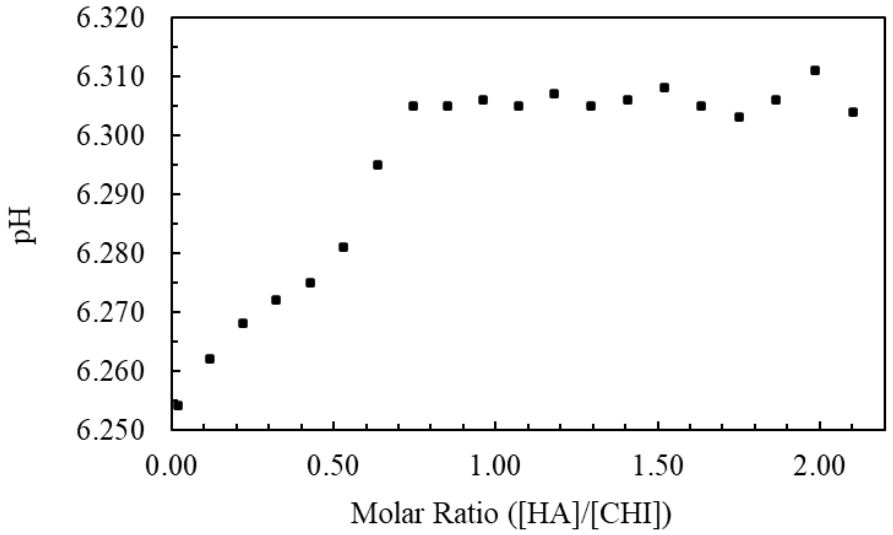

Figure 4.2. Change of pH with molar ratio of HA to CHI prepared from solutions of initial concentrations of 0.3 mM CHI & 3.0 mM HA dissolved in buffered salt solution at pH of 6.25 ± 0.05, I_{total} of 50 mM (1:9 mole ratio of MES:NaCl).

In Figure 4.3, the areas where precipitation was observed during the first series of titration experiments are presented, and in Figure 4.4, the appearance of the precipitation can be seen. In these experiments, the effect of the charge ratio ([-]/[+]) on the saturation point was considered when precipitation was observed. The last data points collected with polymer solutions of initial concentrations of 0.5 mg/mL, had a charge ratio of 0.142. This ratio was higher in the preliminary UV-VIS experiments mentioned in Section 4.1.1. Therefore, it was concluded that either by increasing the HA concentration or by decreasing the CHI concentration, this ratio should be increased to approach coacervation. However, increasing polymer concentration is not desirable for ITC experiments since high concentration values can magnify and even saturate the peaks. For these reasons, the CHI concentration value was reduced to 0.1 mg/mL and the charge ratio for the final data point was increased to 0.712. The charge ratios of the polyelectrolytes in solution were calculated using the equation of

$$\frac{[-]}{[+]} = \frac{\left[\frac{(mass\ of\ HA\ in\ solution)}{(repeating\ unit\ weight\ of\ HA)}\right] \times \alpha_{\mathrm{pH=6.25}}}{\left[\frac{(mass\ of\ CHI\ in\ solution)}{(repeating\ unit\ weight\ of\ CHI)}\right] \times \beta_{\mathrm{pH=6.25}} \times (degree\ of\ deacetylation\ of\ CHI)}, \quad (4.6)$$

where $\alpha_{pH=6.25}$ and $\beta_{pH=6.25}$ are the degree of ionization of HA and CHI at pH = 6.25, respectively.

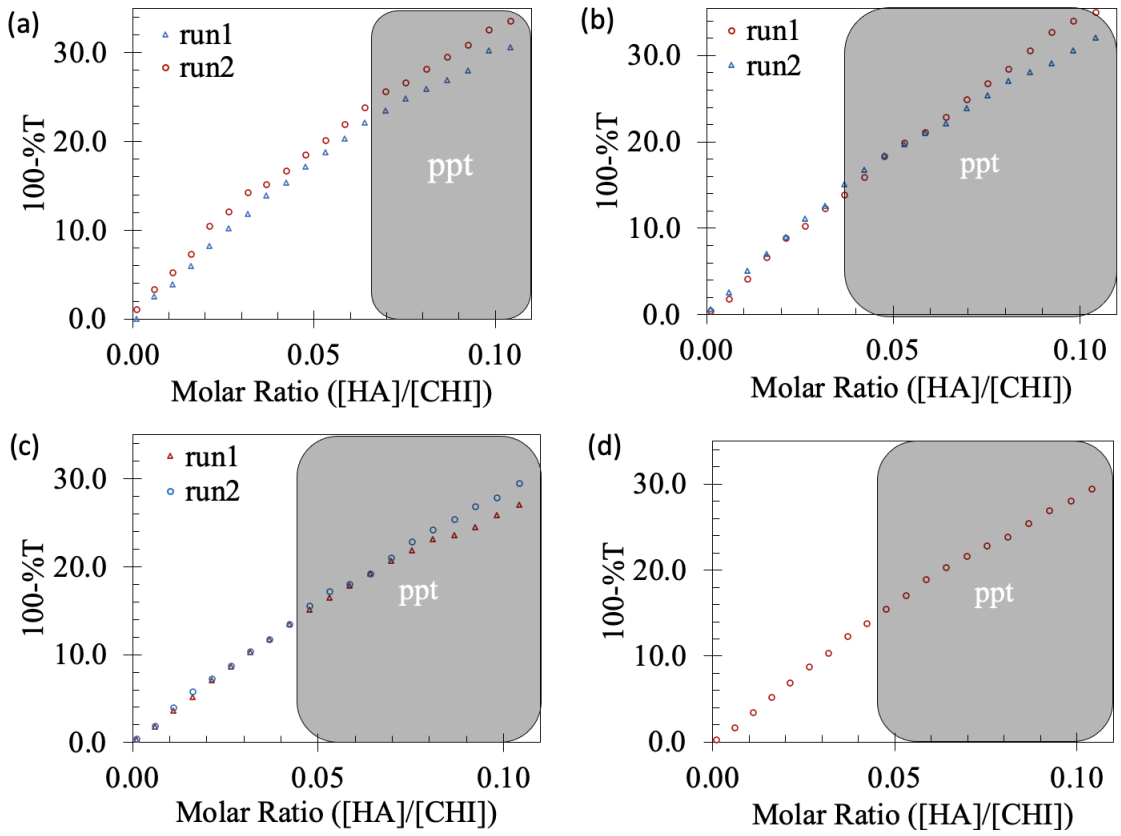

Figure 4.3. Turbidimetric titration plots from solutions of initial concentrations of 0.5 mg/mL CHI & 0.5 mg/mL HA (1200 kDa) dissolved in buffered salt solution of pH of 6.25 ± 0.05. The buffered salt solution is of NaCl with (a) I_{total} of 50 mM, (b) I_{total} of 100 mM, (c) I_{total} of 150 mM, (d) I_{total} of 200 mM.

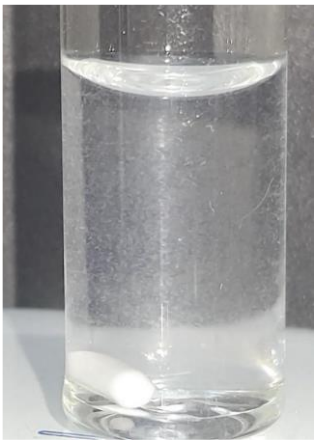

Figure 4.4. Photograph of the precipitate seen in turbidity experiments. Photograph is taken at the end of the turbidimetric titration experiment done with 0.5 mg/mL CHI & 0.5 mg/mL HA dissolved in buffered salt solution at pH = 6.25 ± 0.05 and of I_{total} of 50 mM (1:9 MES:NaCl mole ratio), graphed in Figure 4.3 (a). The same appearance was observed in all cases where precipitate was mentioned.

In the second series of experiments done with 0.1 mg/mL CHI (instead of 0.5 mg/mL as in the first series) and 0.5 mg/mL HA, precipitation was again observed but only under conditions of 150 and 200 mM total concentrations of buffered salt solution. Optimization experiments with turbidimetry were also repeated with a divalent salt rather than NaCl. Here, $MgCl_2$ is chosen with MES buffer at total ionic strengths of 50, 100, 150, and 200 mM. In experiments with $MgCl_2$, precipitation was observed in experiments of 100 mM total ionic strength (Figure 4.5) as well as experiments with 150 and 200 mM total ionic strength. At this stage, the 100 mM total ionic strength condition was seen as risky in terms of reaching precipitation for the NaCl salt as well, and this risk was tested by an additional turbidity experiment. This experiment aimed to see if precipitation would be observed by increasing the molar ratio value at the last point of the titration from 0.5 to a higher value, i.e. molar ratio = 0.6 (Figure 4.6). As soon as the molar ratio of 0.57 was passed, precipitation occurred. Since precipitation was observed with both monovalent and divalent salts for 100 mM total ionic strength, this experimental condition was eliminated, and it was decided to continue the experiments in 50 mM total ionic strength.

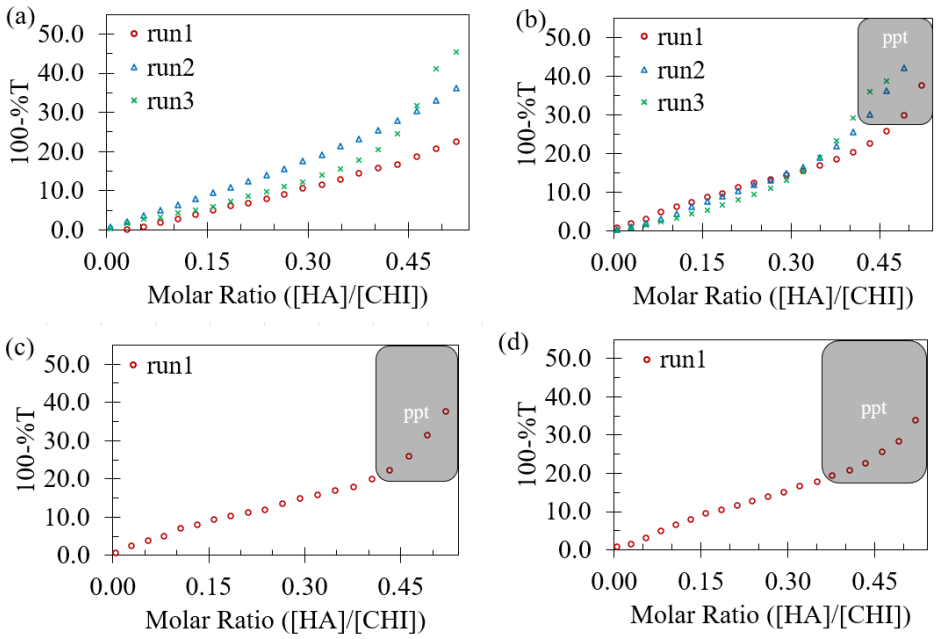

Figure 4.5. Turbidimetric titration plots from solutions of initial concentrations of 0.1 mg/mL CHI & 0.5 mg/mL HA (1200 kDa) dissolved in buffered salt solution of pH of 6.25 ± 0.05. The buffered salt solution is of $MgCl_2$ with (a) I_{total} of 50 mM, (b) I_{total} of 100 mM, (c) I_{total} of 150 mM (d) I_{total} of 200 mM.

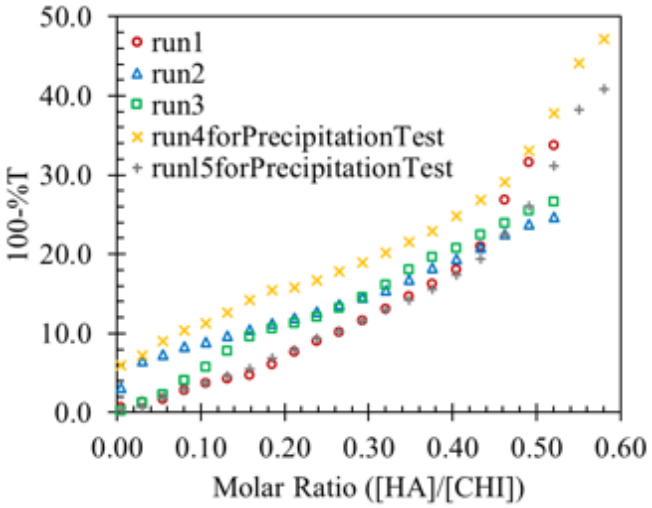

Figure 4.6. Turbidimetric titration plot from solutions of initial concentrations of 0.1 mg/mL CHI & 0.5 mg/mL HA (1200 kDa) dissolved in buffered NaCl solution of pH of 5.25 ± 0.05, I_{total} of 100 mM. Experiments were stopped as soon as precipitation occurred.

Here, it should be explained why it was preferred to switch from the "concentration" concept to the "ionic strength" one. As mentioned above, the tests done for the divalent salt were done for e.g. 50 mM "ionic strength". It must be kept in mind that 50 mM ionic strength for multivalent salts means concentration values lower than 50 mM; i.e. 15.67 mM for divalent salts. This can be reminded by the expression of the ionic strength as

$$I = \frac{1}{2}\sum_{i=1}^{i=n}(c_i Z_i^2)\,, \tag{4.7}$$

where c_i represents the concentration of the ion and Z_i^2 represents the square of the charge of the ion in the medium. Since we had observed precipitation at high concentrations of NaCl experiments (Figure 4.3), we had speculated that high ionic strength inhibited coacervation and promoted precipitation. With $MgCl_2$ instead of NaCl, as even the 100 mM total ionic strength promoted precipitation, it is taken that 100 mM $MgCl_2$ would cause higher amounts of precipitation. A study in the literature for two vinyl polyelectrolytes [33] also claimed that high salt concentrations caused coacervation to not occur after a critical salt concentration. In conclusion, all the proceeding experiments were carried out at 50 mM total ionic strength with a 9:1 molar ratio between the buffering agent and the salt, salt being higher in concentration.

Counting on the results of the optimization process done with the two cations, the turbidimetric titration experiments with different cations of Cl^- were completed as well. The results are given in the graph represented in Figure 4.7. Although there are quite minor differences between the turbidity values for salts with different cations of Cl^-, it can be seen that turbidity values are highest for $CaCl_2$ throughout the experiment, but at the last point, it becomes the highest for $MgCl_2$. All salts except $CaCl_2$ had very similar turbidities up to the molar ratio of 0.35, and a variation started after that point. At the end of titration, the order

of the turbidity values for the cations was $Mg^{+2}>Ca^{+2}>K^{+}>Na^{+}$. This indicates that the coacervation amount was also in this order because as complexation increases, the turbidity increases. This matches the direct Hofmeister series effect not perfectly but majorly. Thus, we can conclude that the coacervation of HA/CHI system for the cations at pH of 6.25 and I_{total} of 50 mM follows the direct Hofmeister effect.

Then, optimization experiments for anions were started. Since the dissolution of the CHI solution was not observed for all anions, the pH value was changed for the rest of the experiments, and the pH value of 5.25 was chosen, which is within the region where the buffering agent MES is effective, to stay close to the neutral region while decreasing the pH value as much as possible. Experiments could be performed at pH 5.25 for nitrate and acetate anions. However, since CHI did not dissolve at any pH value in MES buffer with Na_2SO_4, experiments with sulfate ions could not be done.

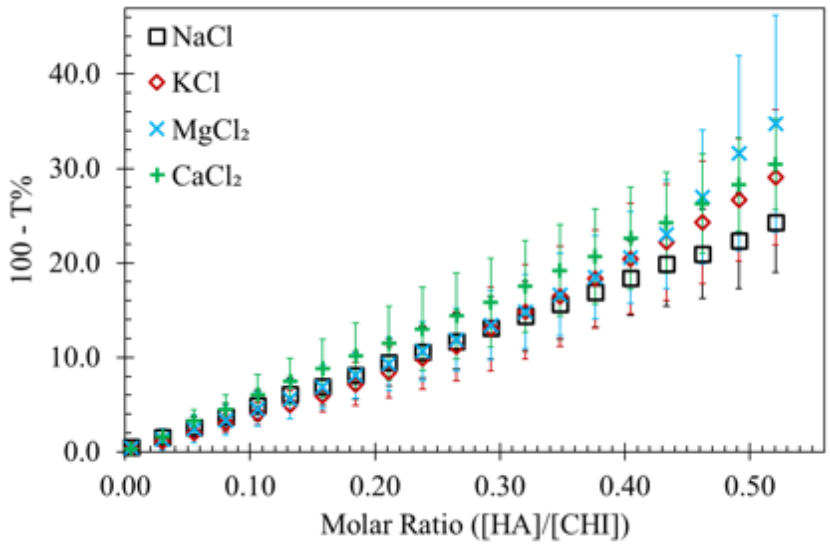

Figure 4.7. Resulting graph of turbidimetric titration experiments for (a) all cations, (b) all anions. Experiments were done with 0.1 mg/mL CHI & 0.5 mg/mL HA (199 kDa) dissolved in MES buffered salt solution of pH of 5.25 ± 0.05, I_{total} of 50 mM.

To be consistent with the buffered salt solution experiments with anions at pH of 5.25, turbidimetric titration experiments were carried also out with the cations at this pH value. In Figure 4.8, turbidimetric titration results of different runs of experiments for NaCl, $MgCl_2$, $NaNO_3$, and under the condition of absence of salt ions are given. All the experiments were reproducible results within 1.4 % and are presented in the Figure 4.9.

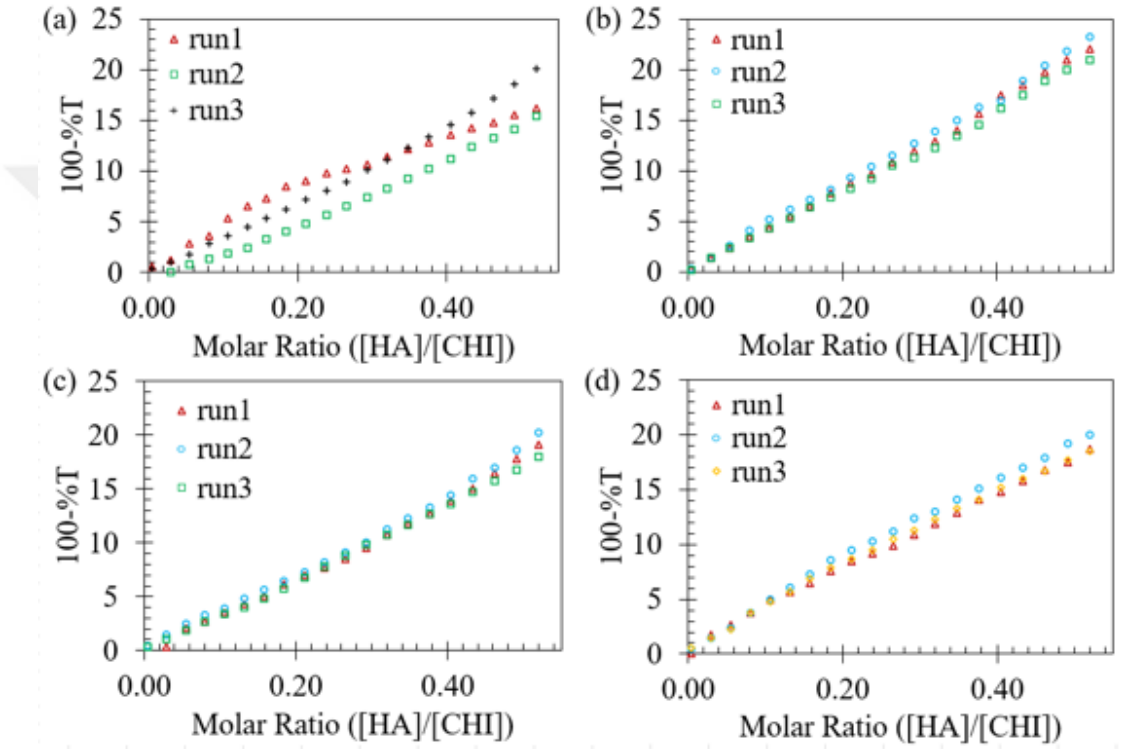

Figure 4.8. Turbidimetric titration experiments of 100 - % T vs. molar ratio of HA to CHI for (a) NaCl condition, (b) $MgCl_2$ condition, (c) $NaNO_3$ condition, (d) No Salt Only Buffer condition. Experiments were done with 0.1 mg/mL CHI & 0.5 mg/mL HA (1200 kDa) dissolved in MES buffered salt solution of pH = 5.25 ± 0.05, I_{total} of 50 mM.

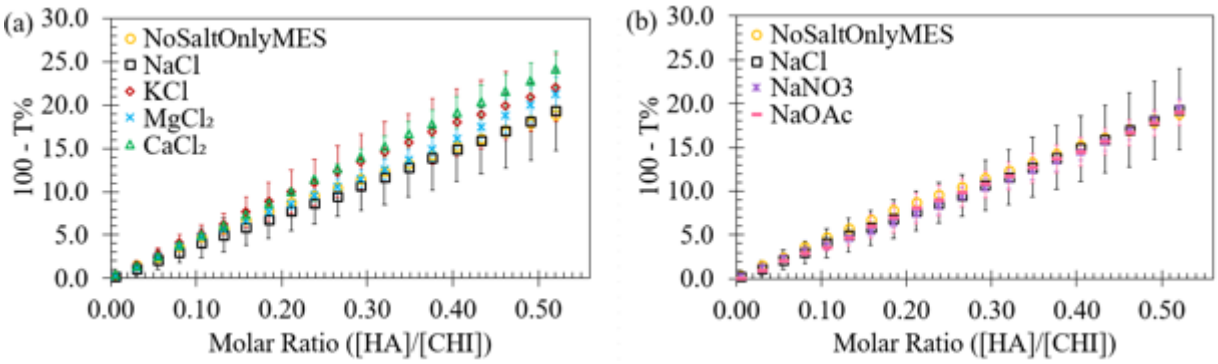

Figure 4.9. Resulting graph of turbidimetric titration experiments for (a) all cations, (b) all anions. Experiments were done with 0.1 mg/mL CHI & 0.5 mg/mL HA (1200 kDa) dissolved in MES buffered salt solution of pH = 5.25 ± 0.05, I_{total} of 50 mM.

For the experiments at acidic pH, a buffering agent was needed again due to the reasons mentioned above. Considering all the salts and polyelectrolytes used, citric acid was considered suitable for this purpose since it does not interact with any molecule that plays an important role in the experiments (pK_{a1} is 3.1 for citric acid buffer [67]). pH of 3.25 was regarded as safe enough to stay within the buffering region. It was judged appropriate to keep all the conditions (buffer:salt mole ratio, total ionic strength, salt type, HA and CHI concentrations) constant except the pH. No precipitation was observed during the experiments with all cations and anions. Hence, all the experiments are successfully completed. Results of these experiments can be seen in Figure 4.10.

When the data of turbidimetric titration experiments (done with 1200 kDa HA and 396 kDa CHI) are examined, it should be noted that no result obeyed the Hofmeister series (except at the pH of 6.25), as the ions were ordered differently under each condition, as can be seen in Figures 4.7, 4.9, and 4.10, considering three different pH values. For example, when the results are compared: (a) In Figure 4.7, the maximum turbidity order for cations is $Na^{+}<K^{+}<Ca^{+2}<Mg^{+2}$ (pH = 6.25), while (b) in Figure 4.9, the maximum turbidity order for cations is $Na^{+}<Mg^{+2}<K^{+}<Ca^{+2}$ (pH = 5.25) and (c) the maximum turbidity order for cations in Figure 4.10 is $Mg^{+2}<(K^{+}$ & $Ca^{+2})<Na^{+}$ (pH = 3.25). The lower the pH, the more complex the order becomes.

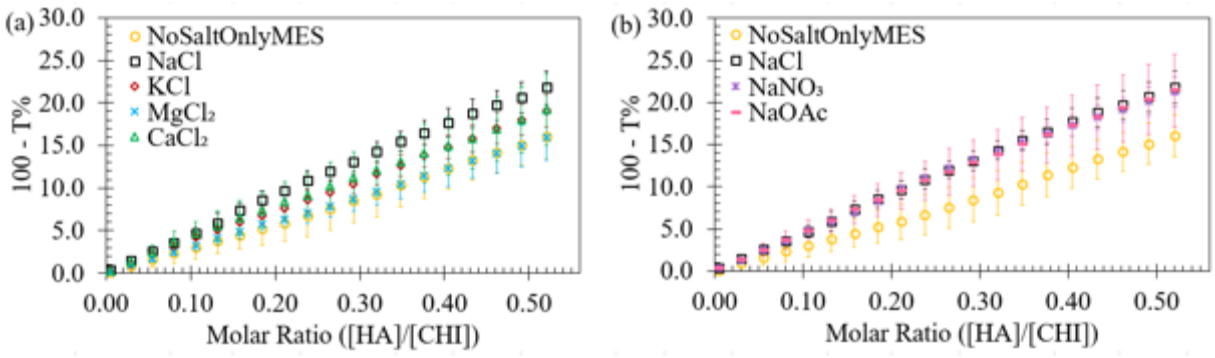

Figure 4.10. Turbidimetric titration experiments for (a) all cations, (b) all anions. Experiments were done with solutions of initial concentrations of 0.1 mg/mL CHI & 0.5 mg/mL HA (1200 kDa) dissolved in citric acid buffered salt solution of pH of 3.25 ± 0.05, I_{total} of 50 mM.

Effect of salt type on HA/CHI coacervation at different pH values can also be interpreted in a different perspective than Hofmeister Series. For cations at pH = 6.25 (Figure 4.5), an increase in turbidity is observed when switching from monovalent to divalent ions. This increase indicates that divalent ions promote polyelectrolyte complexation and coacervation. The results at 50 mM total ionic strength are in agreement with Perry et al. [33], who observed that at high ionic strength values of 2000 mM for pH 6.5, divalent ions had an inhibiting role in polyelectrolyte complexation compared to monovalent ions. On the contrary, when turbidity results at lower ionic strength values of 75-750 mM were examined, divalent ions were in a supportive position of complexation compared to monovalent ions, just like in this study ([33], "Figure 6"). However, when it comes to the two other pH values (see Figure 4.9 for pH = 5.25 and Figure 4.10 for pH = 3.25), such an observation cannot be made. Thus, the results suggest that this situation occurs when approaching the neutral region on the pH scale.

As can be seen in Figure 4.11, for all cations, the turbidity value increases as the pH value approaches the neutral region, i.e. as the pH value increases. For anions, this trend is in the opposite direction: as the pH value decreases from pH 5.25 to 3.25, turbidity values increase for all three anions (NO_3^-, Cl^-, OAc^-, Figure 4.12). For OAc^- condition, the reason

for this increase can be explained by the basicity of the anion. In the introduction section, it was mentioned that coacervation occurs with the increase in the entropy that comes with the counterion release. The acidity of the medium (where interaction between the polyelectrolytes takes place) increases the tendency of the weakly basic anions to be released from the surface of the polyelectrolyte to the environment. This can be explained by the fact that the basic anions tend to combine with H^+ in the environment. Likewise, in the potentiometric titration graph presented in Figure 4.2, the pH value of the environment approaches neutral values as the interaction takes place. Although the ion in the potentiometric titration experiment was Cl^-, which is not a basic anion, it showed a similar characteristic with the OAc^- in this manner.

In addition, as it is seen the Figures 4.9 and 4.10, all anions had the same turbidities at constant pH. This indicates that they did not have an effect on the coacervation amount of the HA/CHI system at pHs of 5.25 and 3.25 and at I_{total} of 50 mM. However, the particle amount analysis results are different (Table 4.1). It should be noted here that the particle amount (percentage) analysis done on the images by using Adobe Photoshop program may be insufficient for the exact results, but it proposes an understanding. Although there is no correlation to the Hofmeister series in the results of the microscopic analysis, it can be seen that the coacervation amount is not the same for all anions.

In experiments with NaCl salt, another behavior of the system, different from other salts, is that the standard deviation values are higher. This behavior can be observed in turbidimetric titration experiments (Figures 4.7, 4.9 - 4.10, and 4.17), and in microscopic particle size analysis (Figure 4.13).

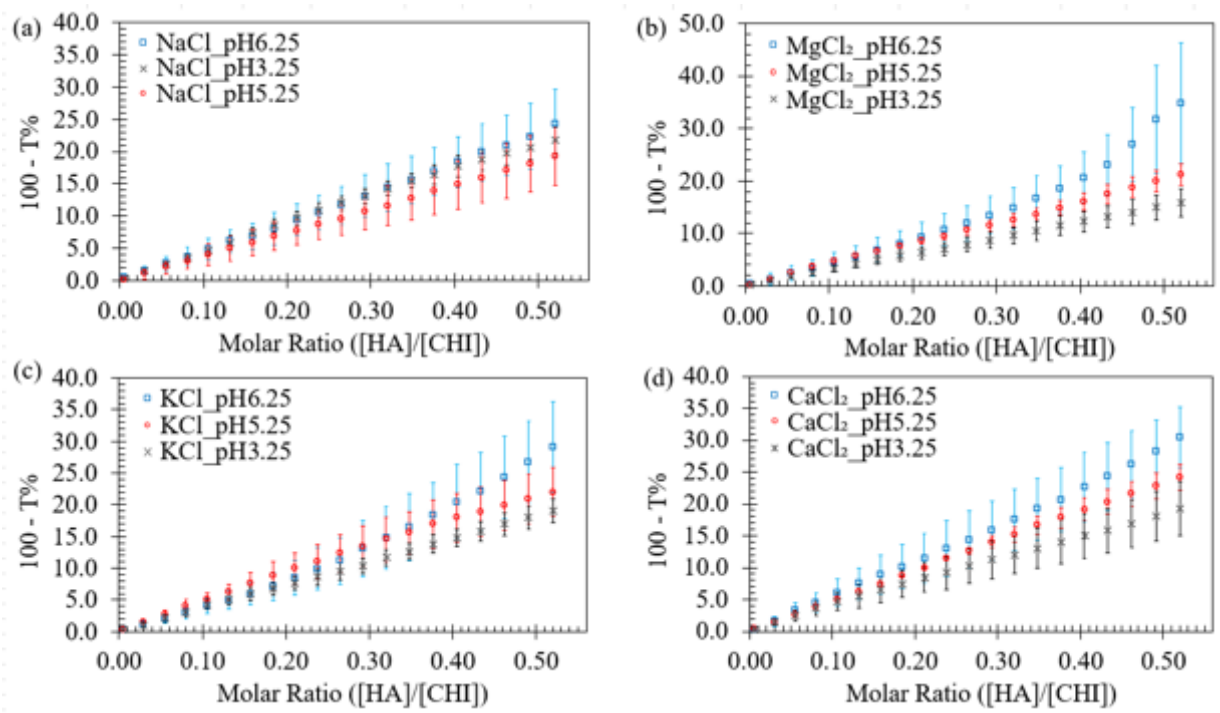

Figure 4.11. Turbidity vs. Molar ratio plots at different pHs for (a) NaCl, (b) $MgCl_2$, (c) KCl, (d) $CaCl_2$ salts. All experiments are done using 0.1 mg/mL CHI & 0.5 mg/mL HA dissolved in the buffered salt solutions of I_{total} of 50 mM.

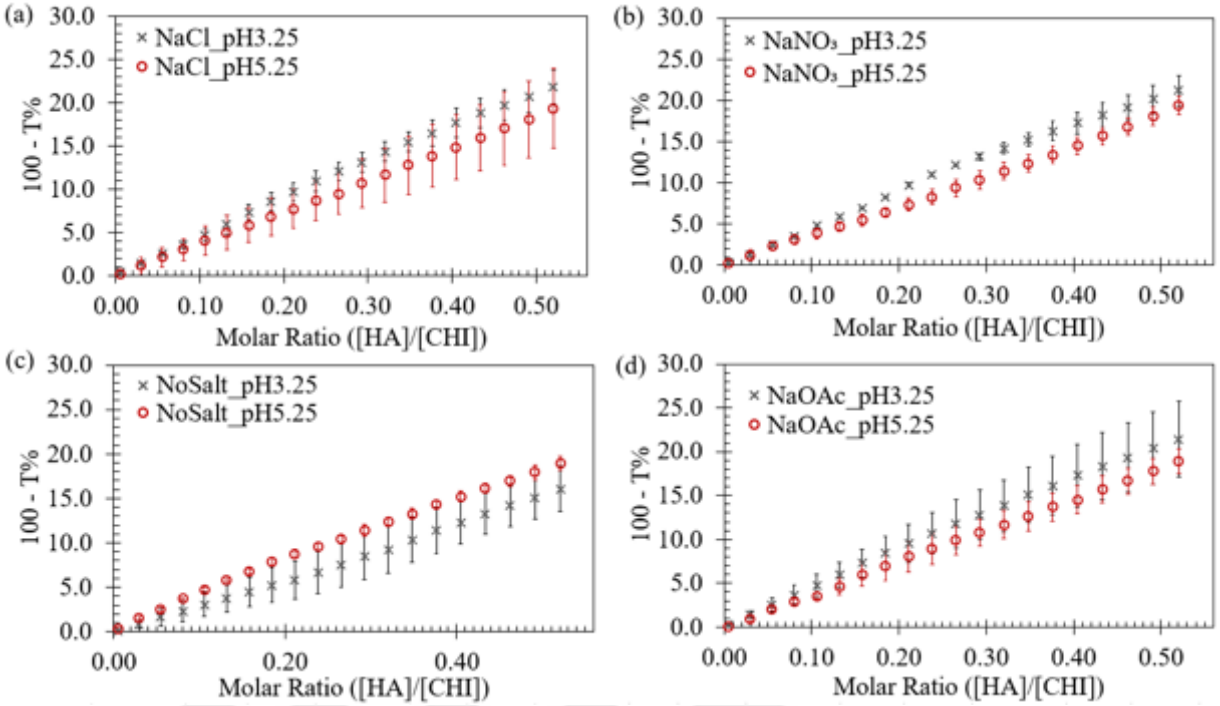

Figure 4.12. Turbidity vs. Molar ratio plots at different pHs for (a) NaCl, (b) $NaNO_3$, (c) No Salt Only MES, (d) NaOAc conditions. All experiments are done using 0.1 mg/mL CHI & 0.5 mg/mL HA dissolved in the buffered salt solutions of I_{total} of 50 mM (No Salt condition only has 5 mM concentrated MES in the medium as solvent.).

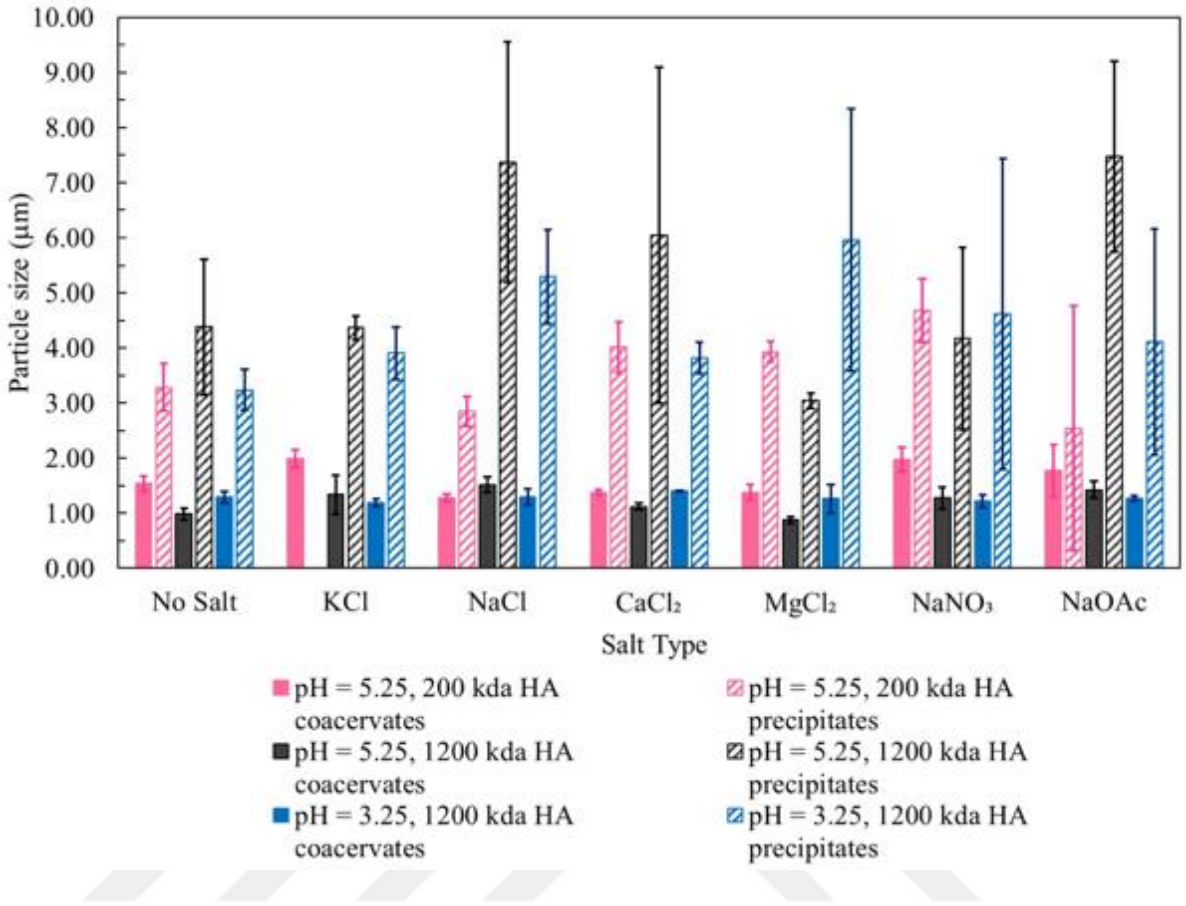

Figure 4.13. Results of the analysis of the light microscopy images taken at the last data point of turbidimetric titration experiments (at the molar ratio of [HA]/[CHI] = 0.52). Because there was no precipitate for the potassium chloride salt, the "pH = 5.25, 199 kDa HA, precipitates" part of the graph for KCl remained blank.

Table 4.1. Coacervation percentages (by number) at the end (the molar ratio of 0.52) of the turbidimetric titration experiments, obtained by analyzing the images taken by the light microscope on the Adobe Photoshop program.

Type of Salt	**pH = 5.25, 199 kDa HA**	**pH = 5.25, 1200 kDa HA**	**pH = 3.25, 1200 kDa HA**
No Salt	85.80	57.54	55.51
$NaNO_3$	92.22	51.01	63.46
NaCl	90.68	68.73	66.94
NaOAc	74.27	61.18	63.29
KCl	100	65.20	76.49
$CaCl_2$	75.59	78.87	67.36
$MgCl_2$	74.17	84.27	87.88

4.2.2. Optimization of the ITC Sample Preparation with Buffering Agent

It should be noted here that since optimization studies of turbidimetric titrations and ITC experiments were done simultaneously, the pH value of 6.25 was still in use. When started the ITC experiments under the conditions optimized by turbidimetric titration experiments, reproducible data were obtained in contrast to the nonreproducible ones in the unbuffered condition. However, to observe a better overlap between trials performed under the same conditions, diafiltration method was used, which is a way of eliminating the buffer mismatch. According to the literature, the buffer mismatch could be eliminated by the "stock solution" method which could also be useful for data reproducibility [17, 20, 60, 64, 29, 30, 38 – 40, 49, 58, 59]. In this "stock solution" method, experiments are performed after diluting the stocked solutions and using the diluted materials. Nonetheless, the diafiltration method does not provide the necessary amount of solutions for performing the dilution of the stocked materials. Since dialysis is also a method of eliminating the buffer mismatch, it was decided

to use both the stock solution and the dialysis method at the same time. This means the preparation of the solutions for ITC experiments were done by the method presented in the section 3.2.4.3.

As a result of the experiments carried out for the development of this dialysis-stock method, reproducible data were obtained. The difference between pre-(dialysis and stock)-method and post-(dialysis and stock)-method experiment results can be seen in by examining the peak points in the heat versus molar ratio graphs (Figure 4.14). It was observed that the peak point before dialysis was located at different molar ratios in different trials of the same condition, while the peak point after dialysis was fixed at approximately 0.37 in molar ratio.

To be able to compare our ITC results with the turbidimetric titration experiments, the solutions prepared for ITC experiments of both cations and anions were prepared and dialyzed by having the I_{total} of 0.05 M and the pH value of 5.25. Thermograms of these experiments can be seen in Figure 4.15.

Although ITC experiments at pH = 3.25 and I_{total} = 0.05 M were planned to be carried out within the scope of this study, two major troubles in succession made these experiments impossible: (1) the pipette of the ITC instrument became inoperable as a result of corrosion (Figure 4.16), (2) the 1200 kDa HA fell to the ground and became contaminated. The glass bottle was broken, the polymer was scattered on the ground, and the parts that had as little contact with the ground as possible were collected with the help of a paper. Since there was not enough budget to buy 1200 kDa HA again in the TÜBİTAK project, to compensate for this contamination, purification procedures that may be appropriate with the materials available in the laboratory have been investigated. Currently, the purification process, which takes an article in the literature [75] as a guide, is still in development.

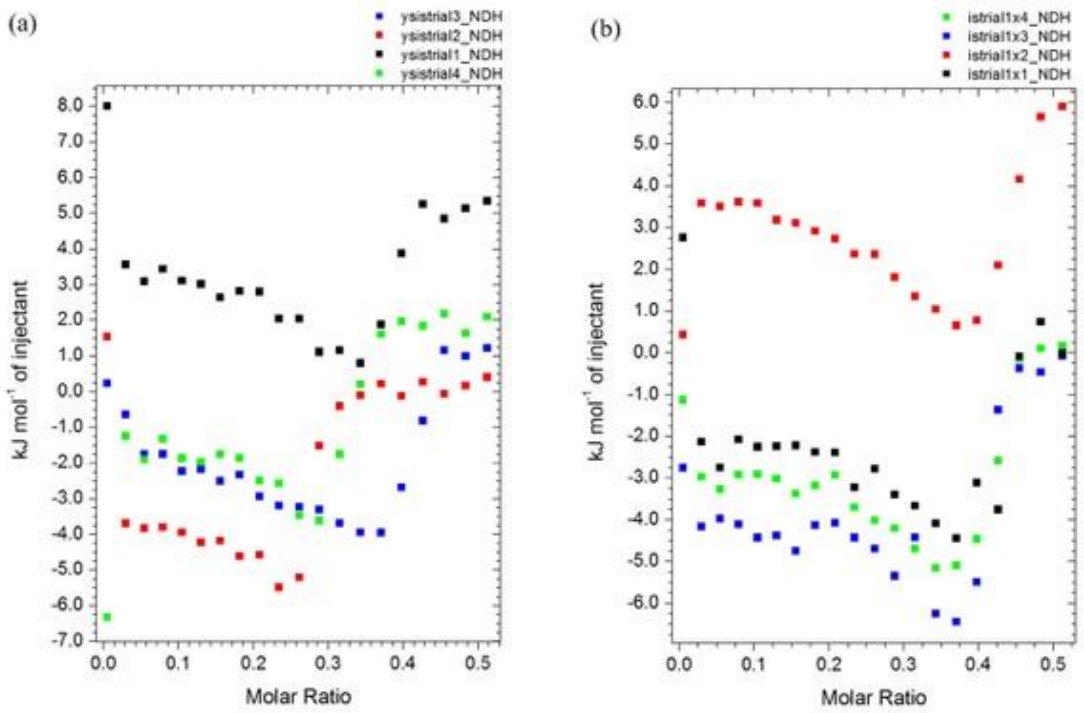

Figure 4.14. Thermograms of the ITC experiments done using 0.1 mg/mL CHI and 0.5 mg/mL HA dissolved in 0.2 M NaCl solution at pH of 6.25 ± 0.05 prepared by the method (a) without dialysis (b) with dialysis.

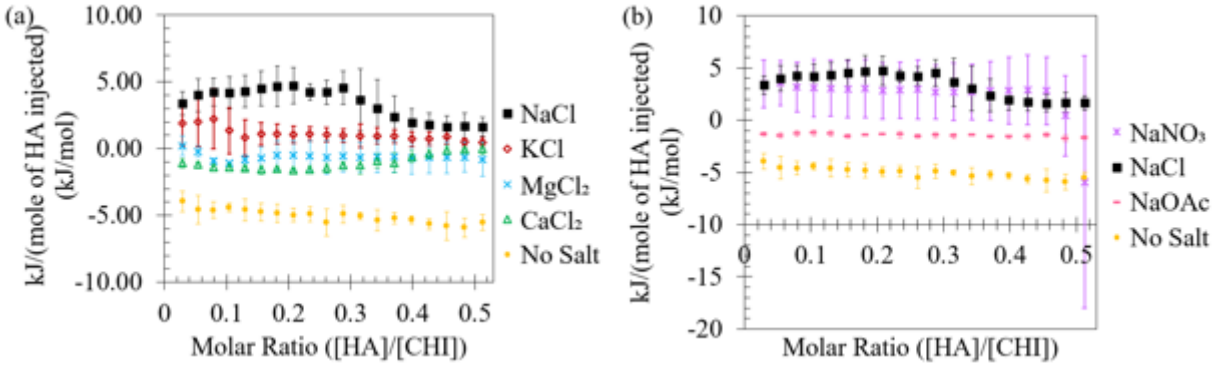

Figure 4.15. Thermograms of ITC experiments: (a) for cations, (b) for anions. All of the dilution experiments (HA into buffer titrations, buffer into CHI titrations, and buffer into buffer titrations) are subtracted from the original experiment (HA into CHI titrations). All experiments were done using 0.1 mg/mL CHI & 0.5 mg/mL HA (1200 kDa) dissolved in MES buffered salt solution of pH of 5.25 ± 0.05, I_{total} of 50 mM.

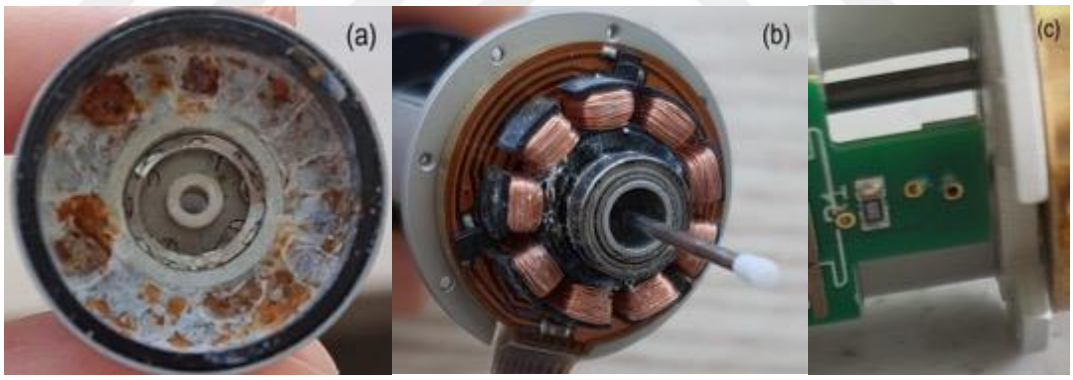

Figure 4.16. Photographs of corrosion on the inner parts of the pipette part of the ITC instrument: (a) lower part of the pipette in use since February 2021; (b) the top part of the pipette in use since February 2021, (c) inside of the top part of the pipette in use before February 2021.

For the replacement of missing experiments, additional data had to be presented. Remembering the consideration in section 4.1.7, a lower molecular weight of HA (199 kDa) that was available in the laboratory was brought to use. For experiments with this new

material, optimized conditions (polyelectrolyte, salt, and buffering agent concentrations) are used for both the turbidimetric titrations and the ITC experiments. Since there was no data for the acidic medium ITC experiments to compare with, the pH of 5.25 is chosen to carry on with. Results of the turbidimetric titrations can be seen in Figures 4.17 and the results of the ITC experiments can be seen in Figures 4.18 – 4.19.

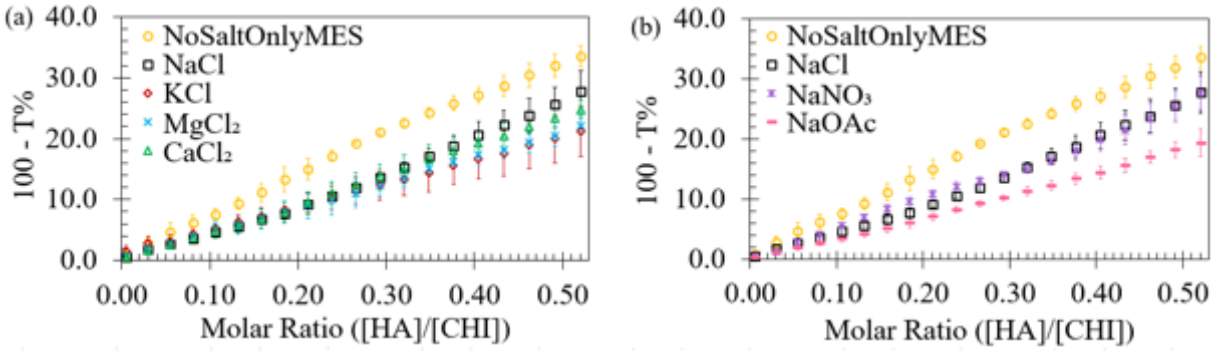

Figure 4.17. Turbidity vs. molar ratio curves for (a) all cations, (b) all anions. Experiments were done with 0.1 mg/mL CHI & 0.5 mg/mL HA (199 kDa) dissolved in MES buffered salt solution of pH of 5.25 ± 0.05, I_{total} of 50 mM.

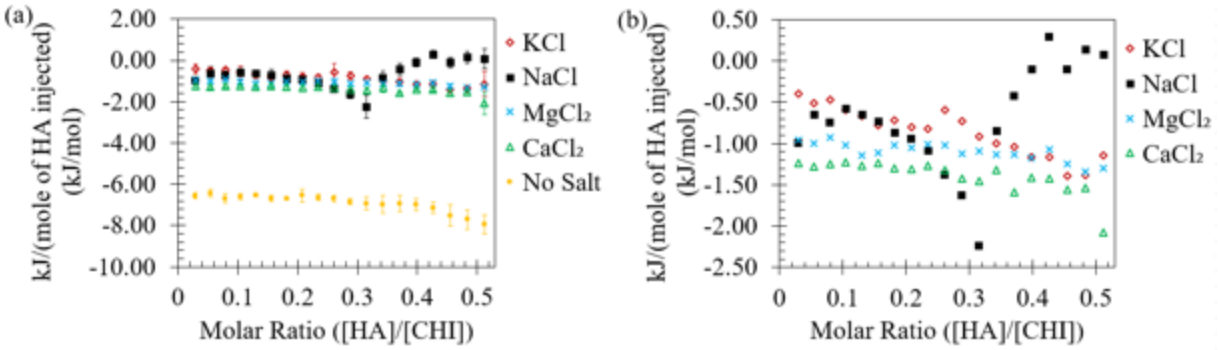

Figure 4.18. ITC thermograms for cations: (a) with error bars, (b) closed-up look without error bars for a better understanding. All of the dilution experiments (HiB titrations, BiC titrations and BiB titrations) are subtracted from the original experiment (HiC titrations). All experiments were done using 0.1 mg/mL CHI & 0.5 mg/mL HA (199 kDa) dissolved in MES-buffered salt solution of pH of 5.25 ± 0.05, I_{total} of 50 mM.

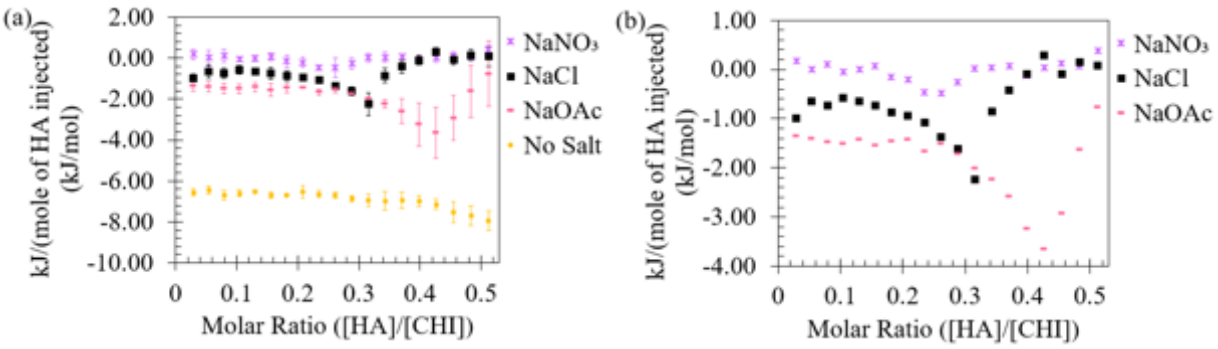

Figure 4.19. ITC thermograms for anions: (a) with error bars, (b) closed-up look without error bars for a better understanding. All of the dilution experiments (HiC, BiC, and BiB titrations) are subtracted from the original experiment (HiC titrations). All Experiments were done using 0.1 mg/mL CHI & 0.5 mg/mL HA (199 kDa) dissolved in MES-buffered salt solution of pH of 5.25 ± 0.05, I_{total} of 50 mM.

4.2.3. Data Analysis of ITC Results

ITC data analysis was first carried out with the software (Origin) of MicroCal ITC200. In the analysis done with the assumption of a “single set of sites” in this software, although more than 100 simplex iterations were made, the curve fit with the least-squares method was not compatible with the data (Figures 4.20 and 4.21). On the other hand, in the analysis done with the assumption of “two sets of sites” in the software, the compatibility between the curve and the data was better. This difference can be attributed to the fact that the distance between charged units of HA (1.3 nm, [20]) is higher than that of CHI (0.6 nm, [20]). When two CHI charges fit in the distance from one HA charge to another HA charge, it is possible that the two positively charged points on the CHI interact with the negative charge together. This behavior indicates “two sets of sites”. On the other hand, when the obtained thermodynamic values were analyzed statistically, this data analysis method done with the Origin software was insufficient since the standard deviation values were very high (Tables 4.2 and 4.3). Therefore, ΔH_c (enthalpy of complexation) values were obtained with another method, which was described in section 3.3.3, and these values for cations are presented in Tables 4.4 and 4.5 with their standard deviation values. The results of the ITC experiments which gave the most consistent results with each other for every condition are used for the data analysis.

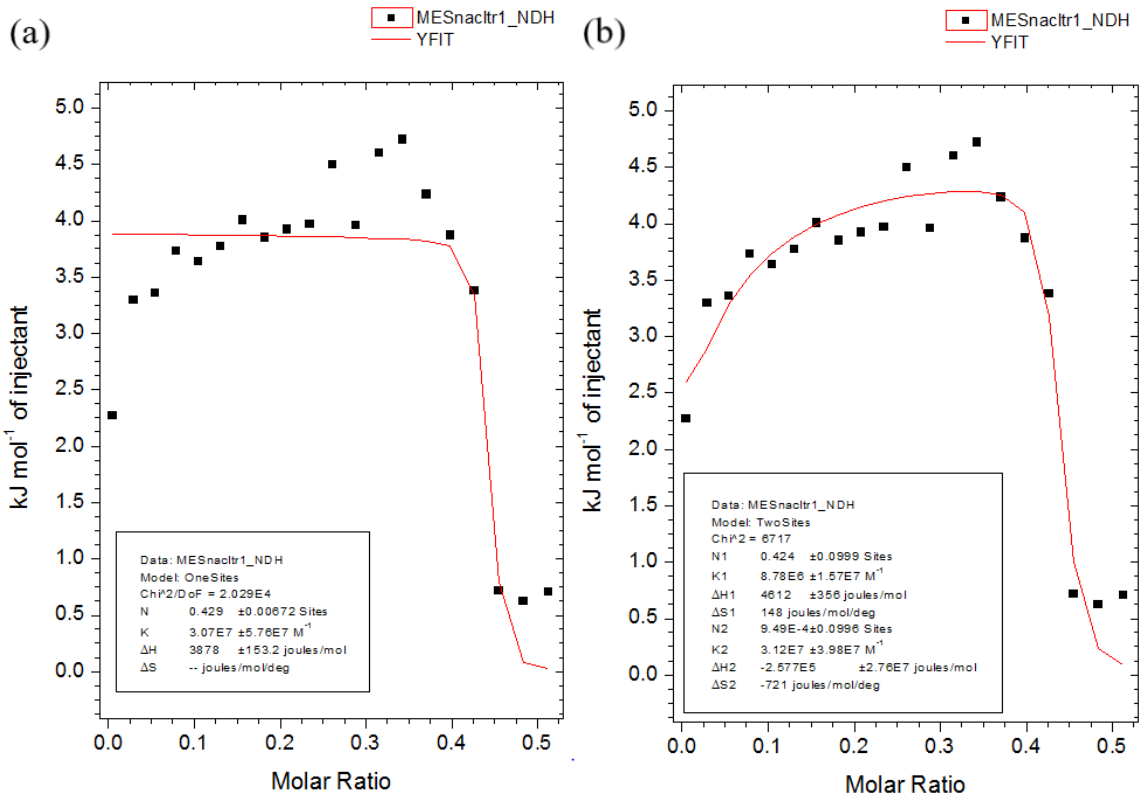

Figure 4.20. Resulting graphs of the data analysis done using the Origin for the NaCl condition. Analyses are done using (a) single set of identical sites model, (b) two sets of individual sites model.

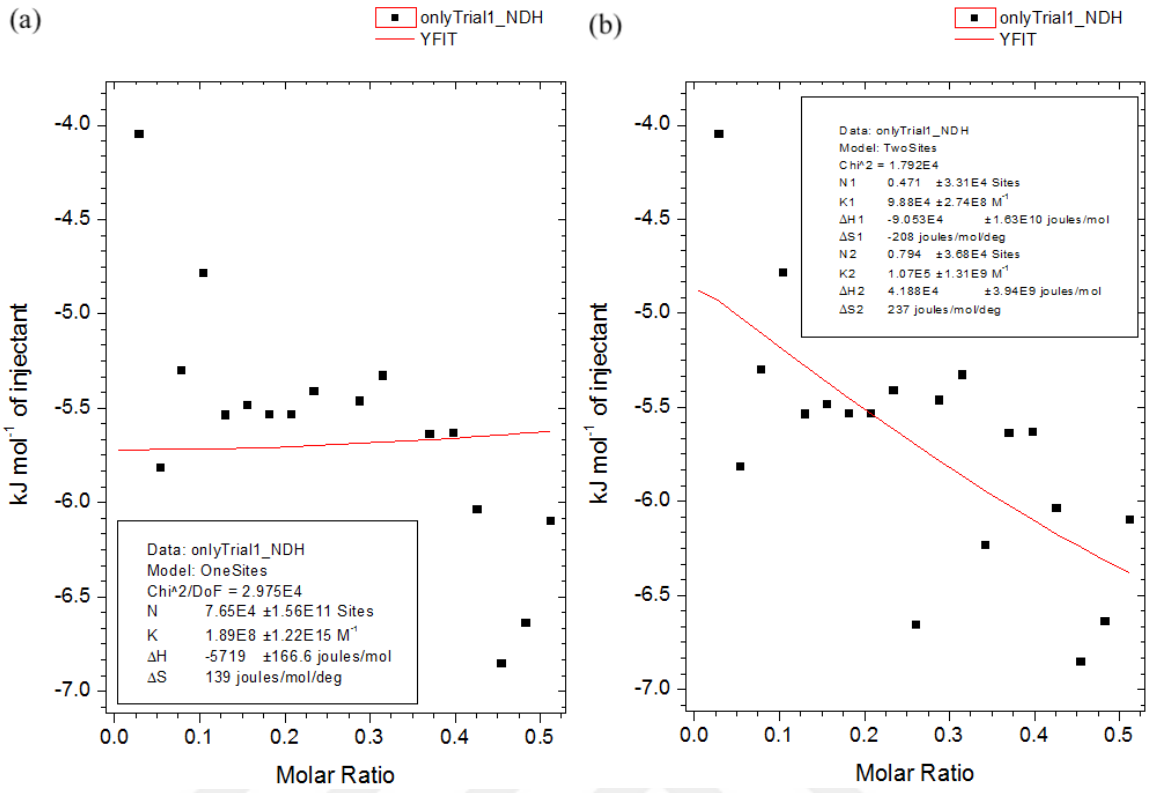

Figure 4.21. Resulting graphs of the data analysis done using the Origin for the No Salt condition. Analyses are done using (a) single set of identical sites model, (b) two sets of individual sites model.

Table 4.2. Results of the data analysis done using the two sets of sites model on the Origin. Experiments (three runs of the same condition) were done using 0.1 mg/mL CHI & 0.5 mg/mL HA dissolved in buffered salt solution at pH of 5.25 ± 0.05 and of I_{total} of 50 mM (1:9 MES:NaCl mole ratio).

NaCl		
Parameter	**Average Value**	**Standard Deviation**
$(Chi)^2$	8.66E+03	3.36E+03
N_1	1.41E-01	2.45E-01
K_1 (M^{-1})	4.42E+06	6.17E+06
ΔH_1 (K/mol)	6.63E+06	6.76E+06
ΔS_1 (J mol^{-1} C^{-1})	1.08E+04	1.50E+04
N_2	1.82E-01	1.57E-01
K_2 (M^{-1})	1.22E+07	1.65E+07
ΔH_2 (J/mol)	-8.34E+04	1.51E+05
ΔS_2 (J mol^{-1} C^{-1})	-2.92E+02	6.07E+02

Table 4.3. Results of the data analysis done using the two sets of sites model on the Origin. Experiments (three runs of the same condition) were done using 0.1 mg/mL CHI & 0.5 mg/mL HA dissolved in buffer solution of 5 mM MES at pH of 5.25 ± 0.05.

No Salt Only MES		
Parameter	**Average Value**	**Standard Deviation**
$(Chi)^2$	9.04E+03	7.75E+03
N_1	8.42E-01	5.63E-01
K_1 (M^{-1})	1.82E+05	2.22E+05
ΔH_1 (K/mol)	-1.09E+05	5.70E+04
ΔS_1 (J mol^{-1} C^{-1})	-2.70E+02	1.78E+02
N_2	1.12E+00	7.94E-01
K_2 (M^{-1})	1.95E+05	2.35E+05
ΔH_2 (J/mol)	6.66E+04	4.00E+04
ΔS_2 (J mol^{-1} C^{-1})	3.19E+02	1.46E+02

Table 4.4. Average complexation enthalpies and the standard deviation values for each salt. All experiments were done using 0.1 mg/mL CHI & 0.5 mg/mL HA (1200 kDa) dissolved in MES-buffered salt solution of pH of 5.25 ± 0.05, I_{total} of 50 mM.

Salt	**Average ΔH_c (kJ/mol)**	**Standard Deviation (kJ/mol)**
NaCl	3.20	1.04
KCl	1.12	0.88
$MgCl_2$	-0.23	0.82
$CaCl_2$	-1.10	0.14
$NaNO_3$	2.49	1.90
NaOAc	-1.21	0.14
No Salt	-4.84	0.58

Table 4.5. Average complexation enthalpies and the standard deviation values for each salt. All experiments were done using 0.1 mg/mL CHI & 0.5 mg/mL HA (199 kDa) dissolved in MES-buffered salt solution of pH of 5.25 ± 0.05, I_{total} of 50 mM.

Salt	**Average ΔH_c (kJ/mol)**	**Standard Deviation (kJ/mol)**
NaCl	-0.93	0.11
KCl	-0.84	0.13
$MgCl_2$	-0.73	0.03
$CaCl_2$	-1.45	0.03
$NaNO_3$	0.09	0.18
NaOAc	-1.63	0.08
No Salt	-6.70	0.21

It should also be noted that at molar ratio of 0.52, which is the last data point of ITC experiments and corresponds to charge ratio of $[-]/[+]$ = 0.712, we still observe coacervation although this charge ratio is far from the stoichiometric ratio of 1:1. In an earlier work from our group [20], one of the reasons for this complete disproportion was attributed to that fact that the distance between the charges of HA and the charges of CHI differ; i.e. they have different charge spacings.

The commonly accepted hydration order of the cations used in this study is $Mg^{+2}>Ca^{+2}>Na^{+}>K^{+}$ [74 – 77], and the same of anions used in this study is $OAc^{-}>Cl^{-}>NO_3^{-}$ [28, 71, 73 – 75]. It is expected of Hofmeister Series to follow this order for their effects as well because hydrations of the ions have a significant effect on the interactions between polyelectrolytes [83]. However, as mentioned before, the order of these ions in the series may differ in the literature. For example, in some other studies, the order of the Mg^{+2} and Ca^{+2} ions are presented in reverse order to the one presented at the beginning of this paragraph ($Ca^{+2}>Mg^{+2}$) [31, 82, 83]. In another study, the hydration numbers of these divalent ions are found equal [86]. In addition, the original order of the monovalent cations is different in the very first work of Hofmeister and many others ($Na^{+}=K^{+}$ [22, 85], $K^{+}>Na^{+}$ [26, 86, 87]).

The results of this study are in agreement with the divergent orders giving $Ca^{+2}>Mg^{+2}>K^{+}>Na^{+}$. Accepting this order as the true one, the ITC results that can be seen in Tables 4.4 and 4.5 make sense. Since more hydrated ions tend to be expelled from the polyelectrolyte interaction region more easily [23], the complexation thus the coacervation would be more favorable in the presence of these ions, and the ΔH_c values of these ions would be expected to be more exothermic. The experiments done with 1200 kDa HA present the direct Hofmeister Series effect (Table 4.4). On the other hand, when the molecular weight of HA decreases (Table 4.5), the observation is that the experiments done with K^{+} and Mg^{+2} gave the most endothermic ΔH_c. This means that the K^{+} and Mg^{+2} ions had an inhibiting effect on coacervation as opposed to the expectations.

When it comes to the anions, there are findings in the literature that give different orders as well. For example, some studies propose that the effects of Cl^- and NO_3^- are quite similar as they would appear in the order as $Cl^- = NO_3^-$ [33]. In another example, the ion NO_3^- is given on the side of kosmotropes, meaning they propose the order between the two as $Cl^- > NO_3^-$ [30].

The results of this study for the anions are in agreement with the commonly accepted reverse order as the ΔH_c becomes more negative through the order of $OAc^- > Cl^- > NO_3^-$ (Table 4.4 and 4.5).

The series also affects the solubility of the polymers. Chaotropic ions, being more hydrated, tend to break the hydrogen bonds between the water molecules. As a result, water molecules become more available for the polyelectrolytes when solute-solvent interactions are considered once the solute-solute interactions are weakened. In this way, the solubility of the polyelectrolytes increases. This increase in the solubility may tend to decrease the amount of interaction between the polyelectrolytes thus inhibit the complexation and/ or coacervation. This phenomenon supports the easier expulsion of more hydrated ions. Moreover, either chaotrope or kosmotrope (weakly or strongly hydrated), all ions have the effect of "screening" the charge of the polyelectrolytes. The study by Perry et al. [33] suggests that the ions start inhibiting the coacervation of pAA and pAH after the concentration of 75 mM. In this study, the salt screening effect can be observed both in ITC and turbidity experiments. In the results of ITC, the "No Salt" condition has the most negative ΔH_c value for both of the experiment groups (experiments done with HA of 199 kDa and 1200 kDa, Tables 4.4 and 4.3). In addition, in the results of turbidity experiments done with 199 kDa HA, it can be seen in Figure 4.17 that the condition of "No Salt" gave the maximum values of turbidity, meaning the interaction between the polymers was more effective than the salted solutions. This shows the interaction between the polyelectrolytes is the most enhanced without the presence of any salt.

When compared to the literature values of the enthalpy of complexation of CHI with different molecules (ovalbumin [90], heparin [91], chondroitin sulfate [91], DNA [91], and

xanthan [92]), ΔH_c of the HA/CHI interaction is quite small (closer to zero). On the other hand, when compared to the literature values of the enthalpy of complexation of HA with different molecules, there are different results. For example, the enthalpy value for the bovine serum albumin/HA and β-lactoglobulin/HA coacervation [93] is much higher than the ΔH_c of the HA/CHI system. In contrast, the enthalpy of reaction between pAH, pLL (poly-L-lysine), and PDADMAC [38] are much smaller than ΔH_c of the HA/CHI system. Although the molecular weights of HA and CHI vary in these studies, the values may propose an understanding. For instance, the interaction enthalpies of both HA and CHI with proteins are much higher than the ΔH_c values found in this research. This may be because of the relatively lower charge densities of the polysaccharides compared to the proteins [91].

As mentioned in the introduction part (Section 1.3), Fu and Schlenoff's work [23] has proven that entropic contributions to the reaction energy have very significant effect on polyelectrolyte complexation as being the driving factor. It was expected to obtain a similar interpretation in this research. However, the data analysis method used for this research is not able to provide any information on the Gibbs free energy or the entropy values. Thus, by either finding a better data analysis method or using additional experimental data, it is aimed to provide the necessary information on this concept in the future works.

5. CONCLUSION

In this research, the interaction between the positively charged CHI and the negatively charged HA is examined. The main goal was to find relevancy between the Hofmeister Series and the effects of the salts on the thermodynamics of the coacervation between CHI and HA. In the optimization process of the turbidimetric titration experiments and the light microscopy image acquisitions, no relation to the Hofmeister series is observed, neither in the direct direction nor in the reverse direction, except for the pH of 6.25 experiments with cations (Mg^{+2}, Ca^{+2}, K^{+}, and Na^{+}). At the pH of 6.25 in the solutions of I_{total} of 50 mM, the salts affect the coacervation of CHI and HA by the direct Hofmeister effect, not in the same way but in a majorly similar way.

The results of the ITC experiments propose that the coacervation of the HA/CHI system follows the direct Hofmeister effect through the cations but the reverse Hofmeister effect through the anions. For the cations, as chaotropic ions increase the solubilities of the polyelectrolytes, they increase the abilities of the polyelectrolytes to find each other in the solution and form coacervates. Thus, the ΔH_c values of the chaotropic conditions are more negative than the kosmotropic conditions.

In addition, the ions' effect of salt screening can be observed both in the turbidimetric titration results and in the ITC experiment results. Under the condition of "No Salt Only the Buffering Agent", the turbidity values are the highest, and the ΔH_c values are the most negative, indicating that the interaction between the polyelectrolytes was more effective for coacervation to take place.

REFERENCES

1. Irache, J. M., L. Bergougnoux, I. Ezpeleta, J. Gueguen and A. M. Orecchioni, "Optimization and In Vitro Stability of Legumin Nanoparticles Obtained by a Coacervation Method", *International Journal of Pharmaceutics*, Vol. 126, No. 1–2, pp. 103–109, Dec. 1995.

2. Stuart, M. A. C., N. A. M. Besseling and R. G. Fokkink, "Formation of Micelles with Complex Coacervate Cores", *Langmuir*, Vol. 14, No. 24, pp. 6846–6849, 1998.

3. Lemetter, C. Y. G., F. M. Meeuse and N. J. Zuidam, "Control of the Morphology and the Size of Complex Coacervate Microcapsules During Scale-up", *American Institute of Chemical Engineer*s, Vol. 55, No. 6, pp. 1487–1496, 2009.

4. Aumiller, W. M., B. W. Davis and C. D. Keating, "Phase Separation as a Possible Means of Nuclear Compartmentalization", in *International Review of Cell and Molecular Biology*, Vol. 307, Elsevier Inc., Amsterdam, 2014, pp. 109–149.

5. Zhao, H., C. Sun, R. J. Stewart and J. H. Waite, "Cement Proteins of the Tube-Building Polychaete Phragmatopoma Californica", *Journal of Biological Chemistry*, Vol. 280, No. 52, pp. 42938–42944, 2005.

6. Moss, J. M., M. P. I. Van Damme, W. H. Murphy and B. N. Preston, "Dependence of Salt Concentration on Glycosaminoglycan-Lysozyme Interactions in Cartilage", *Archives of Biochemistry and Biophysics*, Vol. 348, No. 1, pp. 49–55, 1997.

7. Sanchez, H. P., Tatarenko, M. Nigen, G. Pavlov, A. Imberty, H. Lortat-Jacob, J. G. De La Torre and C. Ebel, "Organization of Human Interferon Γ-Heparin Complexes from

Solution Properties and Hydrodynamics", *Biochemistry*, Vol. 45, No. 44, pp. 13227–13238, 2006.

8. Seyrek, E., P. L. Dubin and J. Henriksen, "Nonspecific Electrostatic Binding Characteristics of the Heparin-Antithrombin Interaction", *Biopolymers*, Vol. 86, No. 3, pp. 249–259, 2007.

9. Timilsena, Y. P., T. O. Akanbi, N. Khalid, B. Adhikari and C. J. Barrow, "Complex Coacervation: Principles, Mechanisms and Applications in Microencapsulation", *International Journal of Biological Macromolecules*, Vol. 121, pp. 1276–1286, 2019.

10. Bayraktar, O., I. Erdogan, M. D. Köse and G. Kalmaz, "Nanocarriers for Plant-Derived Natural Compounds", in *Nanostructures for Antimicrobial Therapy*, Elsevier Inc., Amsterdam, 2017, pp. 395–412.

11. Holleman, L. W. J., H. G. Bungenberg de Jong and R. S. Tjaden Modderman, "XXI . M i t t e i l u n g . Uber Koazervation I : Einfache", *Kolloid-Beihefte*, Vol. 39, No. 8, pp. 334–420, 1934.

12. Turgeon, S. L., C. Schmitt and C. Sanchez, "Protein-Polysaccharide Complexes and Coacervates", *Current Opinion in Colloid and Interface Science*, Vol. 12, No. 4–5, pp. 166–178, 2007.

13. Devi, N., C. Deka, P. Nath and D. K. Kakati, "Encapsulation of Theophylline in Gelatin A–Pectin Complex Coacervates", in *Advances in Experimental Medicine and Biology*, Vol. 1052, Springer, Singapore, 2018, pp. 63–74.

14. Zhao, M. and N. S. Zacharia, "Protein Encapsulation via Polyelectrolyte Complex Coacervation: Protection Against Protein Denaturation", *Journal of Chemical Physics*, Vol. 149, No. 16, 2018.

15. Nori, M. P., C. S. Favaro-Trindade , S. Matias de Alencar, M. Thomazini, J. C. de Camargo Balieiro and C. J. Contreras Castillo, "Microencapsulation of Propolis Extract by Complex Coacervation", *LWT - Food Science and Technology*, Vol. 44, No. 2, pp. 429–435, 2011.

16. Jain, A., D. Thakur, G. Ghoshal, O. P. Katare and U. S. Shivhare, "Microencapsulation by Complex Coacervation Using Whey Protein Isolates and Gum Acacia: An Approach to Preserve the Functionality and Controlled Release of β-Carotene", *Food Bioprocess Technology*, Vol. 8, No. 8, pp. 1635–1644, 2015.

17. Blocher, W. C. and S. L. Perry, "Complex Coacervate-Based Materials for Biomedicine", *Wiley Interdisciplinary Reviews: Nanomedicine and Nanobiotechnology*, Vol. 9, No. 4, 2017.

18. Karabıyık Acar, Ö., S. Bedir, A. B. Kayıtmazer and G. T. Köse, "Chondro-Inductive Hyaluronic Acid/Chitosan Coacervate-Based Scaffolds for Cartilage Tissue Engineering", *International Journal of Biological Macromolecules*, Vol. 188, No. July, pp. 300–312, 2021.

19. Ben Messaoud, G., L. Promeneur, M. Brennich, S. L. K. W. Roelants, P. Le Griel and N. Baccile, "Complex Coacervation of Natural Sophorolipid Bolaamphiphile Micelles with Cationic Polyelectrolytes", *Green Chemistry*, Vol. 20, No. 14, pp. 3371–3385, 2018.

20. Kayıtmazer, A. B., A. F. Köksal and E. Kılıç İyilik, "Complex Coacervation of Hyaluronic Acid and Chitosan: Effects of pH, Ionic Strength, Charge Density, Chain Length and the Charge Ratio", *Soft Matter*, Vol. 11, No. 44, pp. 8605–8612, 2015.

21. Ou, Z. and M. Muthukumar, "Entropy and Enthalpy of Polyelectrolyte Complexation: Langevin Dynamics Simulations", *Journal of Chemical Physics*, Vol. 124, No. 15,

2006.

22. Priftis, D., N. Laugel and M. Tirrell, “Thermodynamic Characterization of Polypeptide Complex Coacervation”, *Langmuir*, Vol. 28, No. 45, pp. 15947–15957, 2012.

23. Fu, J. and J. B. Schlenoff, “Driving Forces for Oppositely Charged Polyion Association in Aqueous Solutions: Enthalpic, Entropic, but Not Electrostatic”, *Journal of the American Chemical Society*, Vol. 138, No. 3, pp. 980–990, 2016.

24. Hofmeister, F., “Zur Lehre von der Wirkung der Salze - Dritte Mittheilung”, *Archiv für Experimentelle Pathologie und Pharmakologie*, Vol. 25, No. 1, pp. 1–30, 1888.

25. Zhang, Y. and P. S. Cremer, “Interactions Between Macromolecules and Ions: the Hofmeister Series”, *Current Opinion in Chemical Biology*, Vol. 10, No. 6, pp. 658–663, 2006.

26. Collins, K. and M. Washabaugh, “The Hofmeister Effect and the Behaviour of Water at Interfaces”, *Quarterly Reviews of Biophysics*, Vol. 18, No. 4, pp. 323–422, 1985.

27. Mazzini, V. and V. S. J. Craig, “What Is the Fundamental Ion-Specific Series for Anions and Cations? Ion Specificity in Standard Partial Molar Volumes of Electrolytes and Electrostriction in Water and Non-Aqueous Solvents”, *Chemical Science*, Vol. 8, No. 10, pp. 7052–7065, 2017.

28. Patel, R., M. Kumari and A. B. Khan, “Recent Advances in the Applications of Ionic Liquids in Protein Stability and Activity: a Review”, *Applied Biochemistry and Biotechnology*, Vol. 172, No. 8, pp. 3701–3720, 2014.

29. Moelbert, S., B. Normand and P. De Los Rios, “Kosmotropes and Chaotropes:

Modelling Preferential Exclusion, Binding and Aggregate Stability", *Biophysical Chemistry*, Vol. 112, No. 1, pp. 45–57, Dec. 2004.

30. Zhang, Y. and P. S. Cremer, "The inverse and Direct Hofmeister Series for Lysozyme", *Proceedings of the National Academy of Sciences of the United States of America*, Vol. 106, No. 36, pp. 15249–15253, 2009.

31. Mason, B. D., J. Zhang-Van Enk, L. Zhang, R. L. Remmele and J. Zhang, "Liquid-Liquid Phase Separation of a Monoclonal Antibody and Nonmonotonic Influence of Hofmeister Anions", *Biophysical Journal*, Vol. 99, No. 11, pp. 3792–3800, 2010.

32. Li, Y., S. Fang, X. Wang, L. Zhai, K. Chen and M. Duan, "Coacervation of Copolymer of Diallyldimethylammonium Chloride and Sodium Styrenesulfonate Aqueous Solution", *Journal of Macromolecular Science, Part A: Pure and Applied Chemistry*, Vol. 55, No. 2, pp. 154–160, 2018.

33. Perry, S. L., Y. Li, D. Priftis, L. Leon and M. Tirrell, "The effect of Salt on the Complex Coacervation of Vinyl Polyelectrolytes", *Polymers*, Vol. 6, No. 6, pp. 1756–1772, 2014.

34. Lim, S., D. Moon, H. J. Kim, J. H. Seo, I. S. Kang and H. J. Cha, "Interfacial Tension of Complex Coacervated Mussel Adhesive Protein According to the Hofmeister Series", *Langmuir*, Vol. 30, No. 4, pp. 1108–1115, 2014.

35. Pierce, M. M., C. S. Raman and B. T. Nall, "Isothermal Titration Calorimetry of Protein-Protein Interactions", *Methods: A Companion to Methods in Enzymology*, Vol. 19, No. 2, pp. 213–221, 1999.

36. Srivastava, V. K. and R. Yadav, *Isothermal Titration Calorimetry*. , Elsevier Inc., Amsterdam, 2019.

37. Janc, T., V. Vlachy and M. Lukšič, “Calorimetric Studies of Interactions Between Low Molecular Weight Salts and Bovine Serum Albumin in Water at pH Values Below and Above the Isoionic Point”, *Journal of Molecular Liquids*, Vol. 270, pp. 74–80, 2018.

38. Laugel, N., C. Betscha, M. Winterhalter, J. C. Voegel, P. Schaaf and V. Ball, “Relationship Between the Growth Regime of Polyelectrolyte Multilayers and the Polyanion/Polycation Complexation Enthalpy”, *Journal of Physical Chemistry B*, Vol. 110, No. 39, pp. 19443–19449, 2006.

39. Elder, R. M., T. Emrick and A. Jayaraman, “Understanding the Effect of Polylysine Architecture on DNA Binding Using Molecular Dynamics Simulations”, *Biomacromolecules*, Vol. 12, No. 11, pp. 3870–3879, 2011.

40. Karibyants, N. and H. Dautzenberg, “Preferential Binding With Regard to Chain Length and Chemical Structure in the Reactions of Formation of Quasi-Soluble Polyelectrolyte Complexes”, *Langmuir*, Vol. 14, No. 16, pp. 4427–4434, 1998.

41. Vander Meulen, K. A., R. M. Saecker and M. T. Record, “Formation of a Wrapped DNA–Protein Interface: Experimental Characterization and Analysis of the Large Contributions of Ions and Water to the Thermodynamics of Binding IHF to H′ DNA”, *Journal of Molecular Biology*, Vol. 377, No. 1, pp. 9–27, Mar. 2008.

42. Li, D., M. S. Kelkar and N. J. Wagner, “Phase Behavior and Molecular Thermodynamics of Coacervation in Oppositely Charged Polyelectrolyte/Surfactant Systems: a Cationic Polymer JR 400 and Anionic Surfactant SDS Mixture”, *Langmuir*, Vol. 28, No. 28, pp. 10348–10362, 2012.

43. Courtois, J. and J. F. Berret, “Probing Oppositely Charged Surfactant and Copolymer Interactions by Isothermal Titration Microcalorimetry”, *Langmuir*, Vol. 26, No. 14, pp. 11750–11758, 2010.

44. Manning, G. S., “The Persistence Length of DNA Is Reached from the Persistence Length of Its Null Isomer through an Internal Electrostatic Stretching Force”, *Biophysical Journal*, Vol. 91, No. 10, pp. 3607–3616, Nov. 2006.

45. Reed, C. E. and W. F. Reed, “Monte Carlo Electrostatic Persistence Lengths Compared with Experiment and Theory”, *The Journal of Chemical Physics*, Vol. 94, No. 12, pp. 8479–8486, 1991.

46. Hayashi, K., K. Tsutsumi, F. Nakajima, T. Norisuye and A. Teramoto, “Chain-Stiffness and Excluded-Volume Effects in Solutions of Sodium Hyaluronate at High Ionic Strength”, *Macromolecules*, Vol. 28, No. 11, pp. 3824–3830, 1995.

47. Harding, S. E., “Analysis of Polysaccharides by Ultracentrifugation. Size, Conformation and Interactions in Solution”, in *Advances in Polymer Science*, Vol. 186, Springer, Berlin, 2002.

48. Karabıyık Acar, Ö., A. B. Kayıtmazer and G. Torun Köse, “Hyaluronic Acid/Chitosan Coacervate-Based Scaffolds”, *Biomacromolecules*, Vol. 19, No. 4, pp. 1198–1211, 2018.

49. ITC Data Analysis in Origin®, 7th ed. Microcal, Northhampton, MA, January. 2004. pp. 105–115.

50. Akkaoui, K., M. Yang, Z. A. Digby and J. B. Schlenoff, “Ultraviscosity in Entangled Polyelectrolyte Complexes and Coacervates”, *Macromolecules*, Vol. 53, No. 11, pp. 4234–4246, 2020.

51. Niskanen, J., A. J. Peltekoff, J. R. Bullet, B. H. Lessard and F. M. Winnik, “Enthalpy of the Complexation in Electrolyte Solutions of Polycations and Polyzwitterions of Different Structures and Topologies”, *Macromolecules*, Vol. 54, No. 14, pp. 6678–6690, 2021.

52. Qin, C., H. Li, Q. Xiao, Y. Liu, J. Zhu and Y. Du, "Water-Solubility of Chitosan and Its Antimicrobial Activity", *Carbohydrate Polymers*, Vol. 63, No. 3, pp. 367–374, Mar. 2006.

53. MicroCal iTC 200 System User Manual, Microcal, Worcestershire.

54. Kayıtmazer, A. B., "Thermodynamics of Complex Coacervation", *Advances in Colloid and Interface Science*, Vol. 239, pp. 169–177, 2017.

55. Snetkov, P., K. Zakharova, S. Morozkina, R. Olekhnovich and M. Uspenskaya, "Hyaluronic acid: The influence of Molecular Weight on Structural, Physical, Physico-Chemical, and Degradable Properties of Biopolymer", *Polymers*, Vol. 12, No. 8, 2020.

56. Maity, P., B. Saha, G. Suresh Kumar and S. Karmakar, "Effect of Zwitterionic Phospholipid on the Interaction of Cationic Membranes with Monovalent Sodium Salts", *Langmuir*, Vol. 34, No. 33, pp. 9810–9817, 2018.

57. Jelesarov, I. and H. R. Bosshard, "Isothermal Titration Calorimetry and Differential Scanning Calorimetry as Complementary Tools to Investigate the Energetics of Biomolecular Recognition", *Journal of Molecular Recognition*, Vol. 12, No. 1, pp. 3–18, 1999.

58. Water, J. J., M. M. Schack, A. Velazquez-Campoy, M. J. Maltesen, M. Van De Weert and L. Jorgensen, "Complex Coacervates of Hyaluronic Acid and Lysozyme: Effect on Protein Structure and Physical Stability", *European Journal of Pharmaceutics and Biopharmaceutics*, Vol. 88, No. 2, pp. 325–331, Oct. 2014.

59. Pei, L. M., M. Lavertu, F. M. Winnik and M. D. Buschmann, "New Insights into Chitosan-DNA Interactions Using Isothermal Titration Microcalorimetry", *Biomacromolecules*, Vol. 10, No. 6, pp. 1490–1499, 2009.

60. Harnsilawat, T., R. Pongsawatmanit and D. J. McClements, "Characterization of β-lactoglobulin-sodium Alginate Interactions in Aqueous Solutions: a Calorimetry, Light Scattering, Electrophoretic Mobility and Solubility Study", *Food Hydrocolloids,* Vol. 20, No. 5, pp. 577–585, 2006.

61. Walkowiak, J., Y. Lu, M. Gradzielski, S. Zauscher and M. Ballauff, "Thermodynamic Analysis of the Uptake of a Protein in a Spherical Polyelectrolyte Brush", *Macromolecular Rapid Communications,* Vol. 41, No. 1, pp. 1–8, 2020.

62. Flanagan, S. E., A. J. Malanowski, E. Kızılay, D. Seeman, P. L. Dubin, L. Donato-Capel, L. Bovetto and C. Schmitt, "Complex Equilibria, Speciation, and Heteroprotein Coacervation of Lactoferrin and β-lactoglobulin", *Langmuir*, Vol. 31, No. 5, pp. 1776–1783, 2015.

63. Łudzik, K., A. Kacperska, K. Kustrzepa and R. Dychto, "Interactions Between Sodium Dodecylsulphate and Didodecyldimethylammonium Bromides Vesicles in Aqueous Solutions", *Journal of Molecular Liquids*, Vol. 240, pp. 273–279, 2017.

64. Wang, H. Q., W. N. Cheng, L. Y. Zhu and X. G. Hu, "Enthalpic Pairwise Self-Association of L-Carnitine in Aqueous Solutions of Some Alkali Halides at T = 298.15 K", *Journal of Chemical Thermodynamics*, Vol. 95, pp. 111–115, 2016.

65. Taha, M., F. A. E. Silva, M. V. Quental, S. P. M. Ventura, M. G. Freire and J. A. P. Coutinho, "Good's Buffers as a Basis for Developing Self-Buffering and Biocompatible Ionic Liquids for Biological Research", *Green Chemistry*, Vol. 16, No. 6, pp. 3149–3159, 2014.

66. Good, N. E., G. D. Winget, W. Winter, T. N. Connolly, S. Izawa and R. M. Singh, "Hydrogen Ion Buffers for Biological Research", No. 2, pp. 467–477, 1966.

67. Trujillo-Reyes, J., A. R. Vilchis-Nestor, S. Majumdar, J. R. Peralta-Videa and J. L. Gardea-Torresdey, “Citric Acid Modifies Surface Properties of Commercial CeO_2 Nanoparticles Reducing Their Toxicity and Cerium Uptake in Radish (Raphanus Sativus) Seedlings”, *Journal of Hazardous Materials*, Vol. 263, pp. 677–684, Dec. 2013.

68. Czeslik, C., R. Jansen, M. Ballauff, A. Wittemann, C. A. Royer, E. Gratton and T. Hazlett, “Mechanism of Protein Binding to Spherical Polyelectrolyte Brushes Studied in Situ Using Two-Photon Excitation Fluorescence Fluctuation Spectroscopy”, *Physical Review E - Statistical, Nonlinear, and Soft Matter Physics*, Vol. 69, No. 2 1, pp. 1–9, 2004.

69. Sarmento, B., Ribeiro, A., Veiga, F., Sampaio, P., Neufeld, R. and D. Ferreira, “Alginate/Chitosan Nanoparticles Are Effective for Oral Insulin Delivery”, *Pharmaceutical Research*, Vol. 24, No. 12, pp. 2198–2206, 2007.

70. Silletti, E., M. H. Vingerhoeds, W. Norde and G. A. van Aken, “Complex Formation in Mixtures of Lysozyme-Stabilized Emulsions and Human Saliva”, *Journal of Colloid and Interface Science*, Vol. 313, No. 2, pp. 485–493, 2007.

71. Vitorazi, L., N. Ould-Moussa, S. Sekar, J. Fresnais, W. Loh, J. P. Chapel and J. F. Berret, “Evidence of a Two-Step Process and Pathway Dependency in the Thermodynamics of Poly(Diallyldimethylammonium Chloride)/Poly(Sodium Acrylate) Complexation”, *Soft Matter*, Vol. 10, No. 47, pp. 9496–9505, 2014.

72. Weinbreck, F., R. de Vries, P. Schrooyen and C. G. de Kruif, “Complex Coacervation of Whey Proteins and Gum Arabic”, *Biomacromolecules*, Vol. 4, No. 2, pp. 293–303, 2003.

73. Alatorre-Meda, M., P. Taboada, B. Krajewska, M. Willemeit, A. Deml, R. Klösel and J. R. Rodríguez, “DNA−Poly(diallyldimethylammonium Chloride) Complexation and Transfection Efficiency”, *The Journal of Physical Chemistry B*, Vol. 114, No. 29, pp. 9356–9366, Jul. 2010.

74. Bharadwaj, S., R. Montazeri and D. T. Haynie, “Complexation and Implications Thereof for Electrostatic”, *Langmuir*, Vol. 22, No. 18, pp. 6093–6101, 2006.

75. Reddy, K. J. and K. T. Karunakaran, “Purification and Characterization of Hyaluronic Acid Produced by Streptococcus Zooepidemicus”, *J. BioSci. Biotech*, Vol. 2, No. 3, pp. 173–179, 2013.

76. Bockris, J. O. M. and P. P. S. Saluja, “Ionic Solvation Numbers from Compressibilities and Ionic Vibration Potentials Measurements”, *Journal of Physical Chemistry*, Vol. 76, No. 15, pp. 2140–2151, 1972.

77. Sadeghi, R. and F. Jahani, “Salting-In and Salting-Out of Water-Soluble Polymers in Aqueous Salt Solutions”, *The Journal of Physical Chemistry B*, Vol. 116, No. 17, pp. 5234–5241, Apr. 2012.

78. Bončina, M., J. Lah, J. Reščič and V. Vlachy, “Thermodynamics of the Lysozyme-Salt Interaction from Calorimetric Titrations”, *Journal of Physical Chemistry B*, Vol. 114, No. 12, pp. 4313–4319, 2010.

79. Kang, B., H. Tang, Z. Zhao and S. Song, “Hofmeister Series: Insights of Ion Specificity from Amphiphilic Assembly and Interface Property”, *ACS Omega*, Vol. 5, No. 12, pp. 6229–6239, 2020.

80. Garajová, K., A. Balogová, E. Dušeková, D. Sedláková, E. Sedlák and R. Varhač, “Correlation of Lysozyme Activity and Stability in the Presence of Hofmeister Series

Anions", *Biochimica et Biophysica Acta - Proteins and Proteomics*, Vol. 1865, No. 3, pp. 281–288, 2017.

81. Sullivan, M. R., W. Yao, D. Tang, H. S. Ashbaugh and B. C. Gibb, "The Thermodynamics of Anion Complexation to Nonpolar Pockets", *Journal of Physical Chemistry B*, Vol. 122, No. 5, pp. 1702–1713, 2018.

82. Marcus, Y., "Effect of Ions on the Structure of Water", *Pure and Applied Chemistry*, Vol. 82, No. 10, pp. 1889–1899, 2010.

83. Schlenoff, J. B., A. H. Rmaile and C. B. Bucur, "Hydration Contributions to Association in Polyelectrolyte Multilayers and Complexes: Visualizing Hydrophobicity", *Journal of the American Chemical Society*, Vol. 130, No. 41, pp. 13589–13597, 2008.

84. Cacace, M. G. E. M. Landau and J. J. Ramsden, "The Hofmeister Series: Salt and Solvent Effects on Interfacial Phenomena", *Quarterly Reviews of Biophysics*, Vol. 30, No. 3, pp. 241–277, 1997.

85. Okur, H. I., J. Hladílková, K. B. Rembert, Y. Cho, J. Heyda, J. Dzubiella, P. S. Cremer and P. Jungwirth, "Beyond the Hofmeister Series: Ion-Specific Effects on Proteins and Their Biological Functions", *Journal of Physical Chemistry B*, Vol. 121, No. 9, pp. 1997–2014, 2017.

86. Israelachvili, J. N., "Interactions Involving Polar Molecules", *Intermolecular and Surface Forces*, Third edition. Elsevier Inc., Amsterdam, pp. 71–90, 2011.

87. Pegram, L. M. and M. T. Record, "Hofmeister Salt Effects on Surface Tension Arise from Partitioning of Anions and Cations Between Bulk Water and the Air-Water Interface", *Journal of Physical Chemistry B*, Vol. 111, No. 19, pp. 5411–5417, 2007.

88. Mohanakumar, S. and S. Wiegand, “Towards Understanding Specific Ion Effects in Aqueous Media Using Thermodiffusion”, *European Physical Journal E*, Vol. 45, No. 2, pp. 1–9, 2022.

89. Musilová, L., A. Mráček, V. Kašpárková, A. Minařík, A. J. M. Valente, E. F. G. Azevedo, L. M. P. Veríssimo, M. M. Rodrigo, M. A. Esteso and A. C. F. Ribeiro, “Effect of Hofmeister Ions on Transport Properties of Aqueous Solutions of Sodium Hyaluronate”, *International Journal of Molecular Sciences*, Vol. 22, No. 4, pp. 1–13, 2021.

90. Xiong, W., C. Ren, M. Tian, X. Yang, J. Li and B. Li, “Complex Coacervation of Ovalbumin-Carboxymethylcellulose Assessed by Isothermal Titration Calorimeter and Rheology: Effect of Ionic Strength and Charge Density of Polysaccharide”, *Food Hydrocolloids*, Vol. 73, pp. 41–50, 2017.

91. Ma, P. L., M. Lavertu, F. M. Winnik and M. D. Buschmann, “Stability and Binding Affinity of DNA/Chitosan Complexes by Polyanion Competition”, *Carbohydrate Polymers*, Vol. 176, pp. 167–176, 2017.

92. Maurstad, G., S. Kitamura and B. T. Stokke, “Isothermal Titration Calorimetry Study of the Polyelectrolyte Complexation of Xanthan and Chitosan Samples of Different Degree of Polymerization”, *Biopolymers*, Vol. 97, No. 1, pp. 1–10, 2012.

93. Du, X., P. L. Dubin, D. A. Hoagland and L. Sun, “Protein-Selective Coacervation with Hyaluronic Acid”, *Biomacromolecules*, Vol. 15, No. 3, pp. 726–734, 2014.

APPENDIX A: PARAMETERS AND RESULTS OF THE EXPERIMENTS BEFORE ADDING BUFFERING AGENT TO THE SYSTEM

Table A.1. Parameters of experiment #1 done using the ITC instrument.

Name of the experiment's file	HAtoCHIgktrial1
Concentration of CHI (mM)	0.3
Concentration of HA (mM)	0.6
pH value	6.25 ± 0.05
Concentration of NaCl (M)	0.2

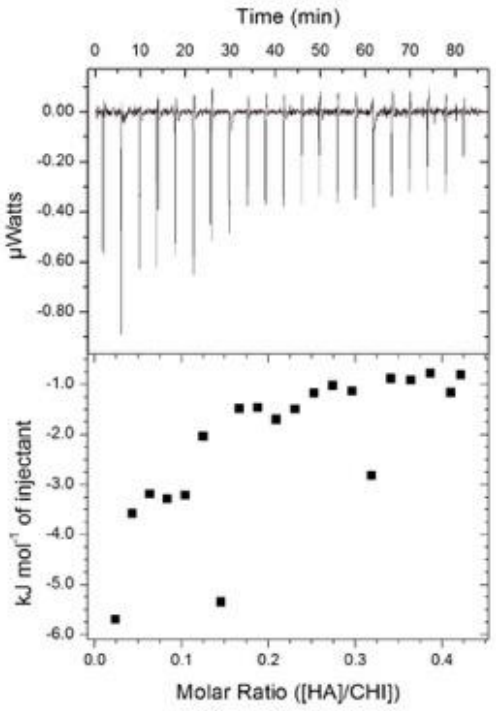

Figure A.1. Final figure of experiment #1 (top: graph of the power difference between cells versus time (i.e. raw data), bottom: graph of the energy change per mole of injectant (HA) versus on mole ratio (i.e., thermogram)).

Table A.2. Parameters of experiment #2 done using the ITC instrument.

Name of the experiment's file	HAtoCHIgktrial2
Concentration of CHI (mM)	0.03
Concentration of HA (mM)	0.15
pH value	6.25 ± 0.05
Concentration of NaCl (M)	0.2

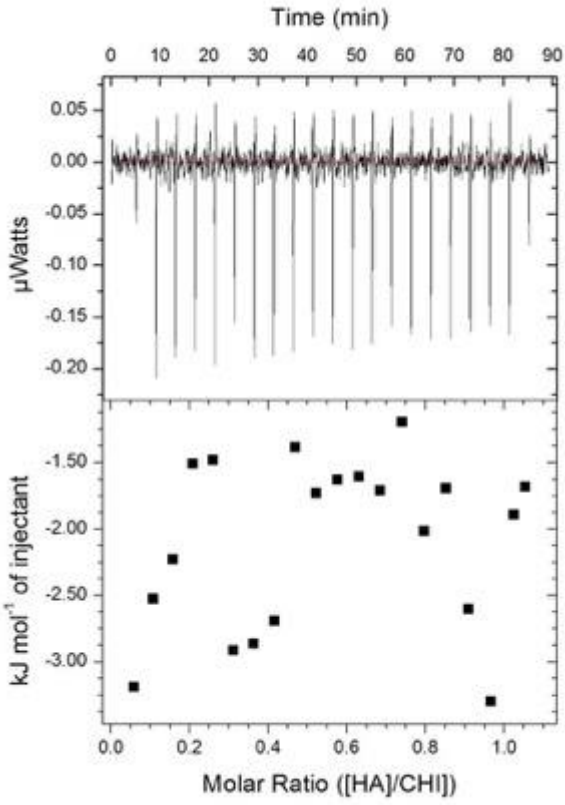

Figure A.2. Final figure of experiment #2 (top: graph of the power difference between cells versus time (i.e. raw data), bottom: graph of the energy change per mole of injectant (HA) versus on mole ratio (i.e., thermogram)).

Table A.3. Parameters of experiment #3 done using the ITC instrument.

Name of the experiment's file	HAtoCHIgktrial3
Concentration of CHI (mM)	0.3
Concentration of HA (mM)	0.1125
pH value	6.25 ± 0.05
Concentration of NaCl (M)	0.2

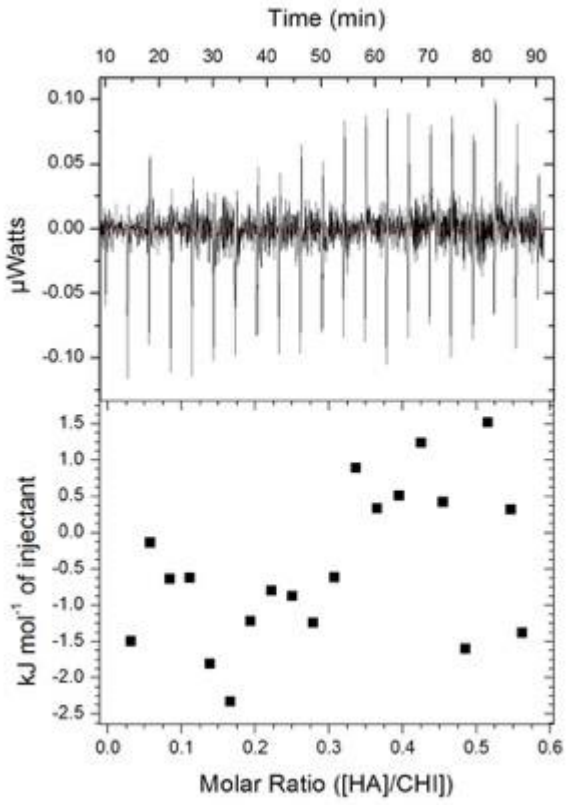

Figure A.3. Final figure of experiment #3 (top: graph of the power difference between cells versus time (i.e. raw data), bottom: graph of the energy change per mole of injectant (HA) versus on mole ratio (i.e., thermogram)).

Table A.4. Parameters of experiment #4 done using the ITC instrument.

Name of the experiment's file	HAtoCHIgktrial4
Concentration of CHI (mM)	0.3
Concentration of HA (mM)	0.7
pH value	6.25 ± 0.05
Concentration of NaCl (M)	0.2

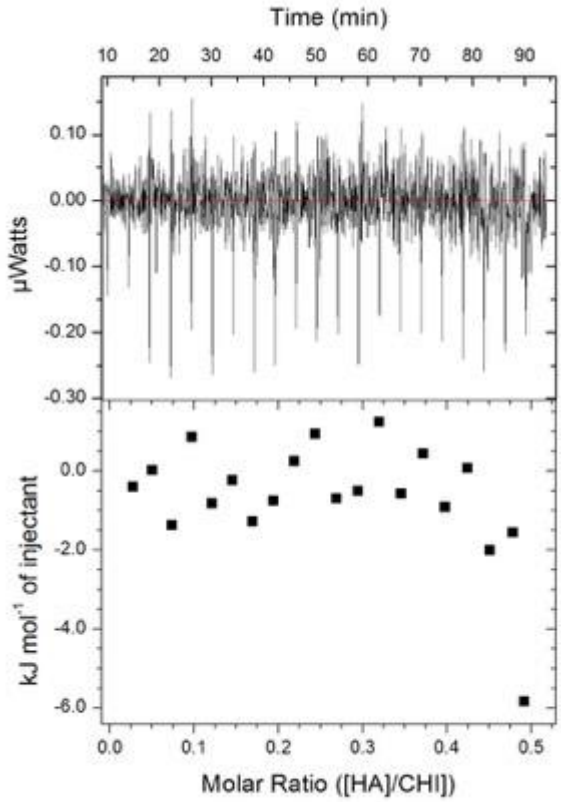

Figure A.4. Final figure of experiment #4 (top: graph of the power difference between cells versus time (i.e. raw data), bottom: graph of the energy change per mole of injectant (HA) versus on mole ratio (i.e., thermogram)).

Table A.5. Parameters of experiment #5 done using the ITC instrument.

Name of the experiment's file	HAtoCHIgktrial5
Concentration of CHI (mM)	0.3
Concentration of HA (mM)	1.5
pH value	6.25 ± 0.05
Concentration of NaCl (M)	0.2

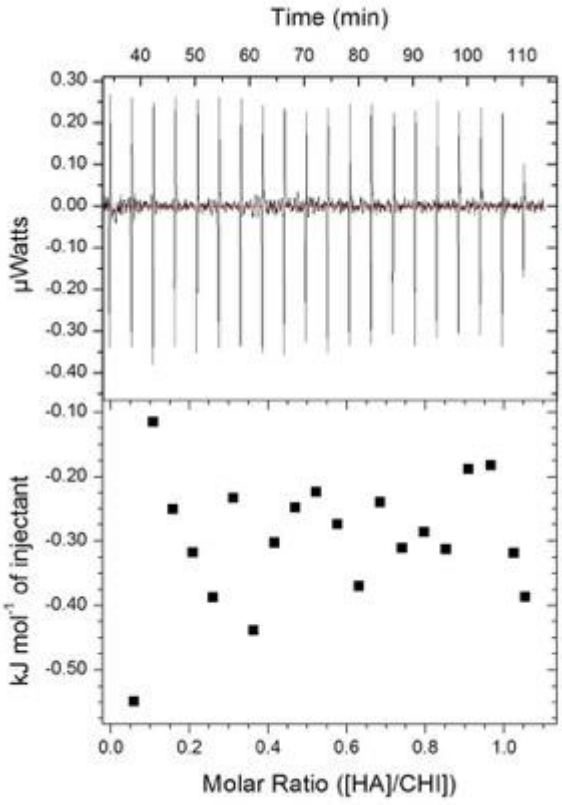

Figure A.5. Final figure of experiment #5 (top: graph of the power difference between cells versus time (i.e. raw data), bottom: graph of the energy change per mole of injectant (HA) versus on mole ratio (i.e., thermogram)).

Table A.6. Parameters of experiment #6 done using the ITC instrument.

Name of the experiment's file	HAtoCHIgktrial6
Concentration of CHI (mM)	0.3
Concentration of HA (mM)	1.0
pH value	6.25 ± 0.05
Concentration of NaCl (M)	0.15

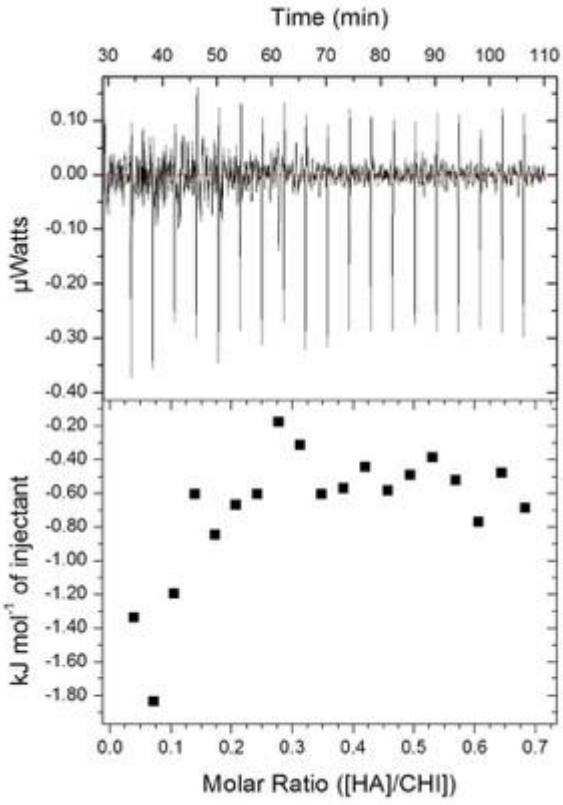

Figure A.6. Final figure of experiment #6 (top: graph of the power difference between cells versus time (i.e. raw data), bottom: graph of the energy change per mole of injectant (HA) versus on mole ratio (i.e., thermogram)).

Table A.7. Parameters of experiment #7 done using the ITC instrument.

Name of the experiment's file	HAtoCHIgktrial7
Concentration of CHI (mM)	0.6
Concentration of HA (mM)	1.0
pH value	6.25 ± 0.05
Concentration of NaCl (M)	0.15

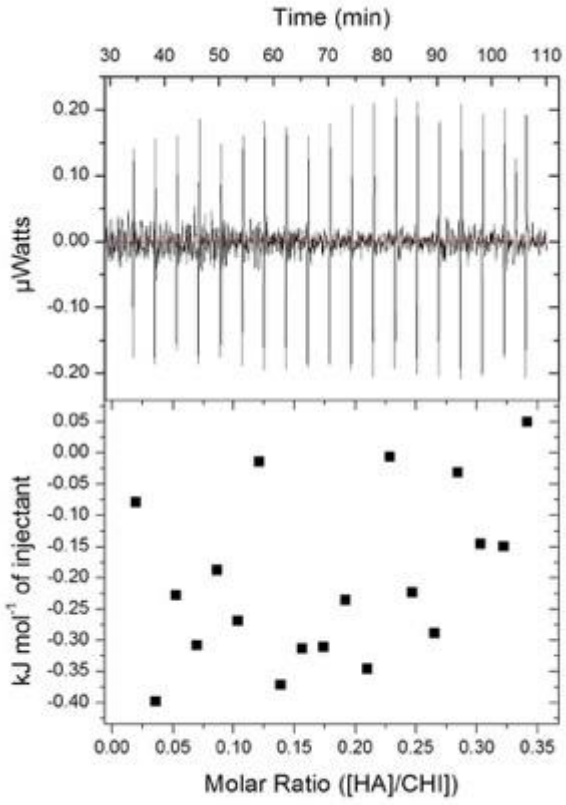

Figure A.7. Final figure of experiment #7 (top: graph of the power difference between cells versus time (i.e. raw data), bottom: graph of the energy change per mole of injectant (HA) versus on mole ratio (i.e., thermogram)).

Table A.8. Parameters of experiment #8 done using the ITC instrument.

Name of the experiment's file	HAtoCHIgktrial8
Concentration of CHI (mM)	0.6
Concentration of HA (mM)	1.5
pH value	6.25 ± 0.05
Concentration of NaCl (M)	0.15

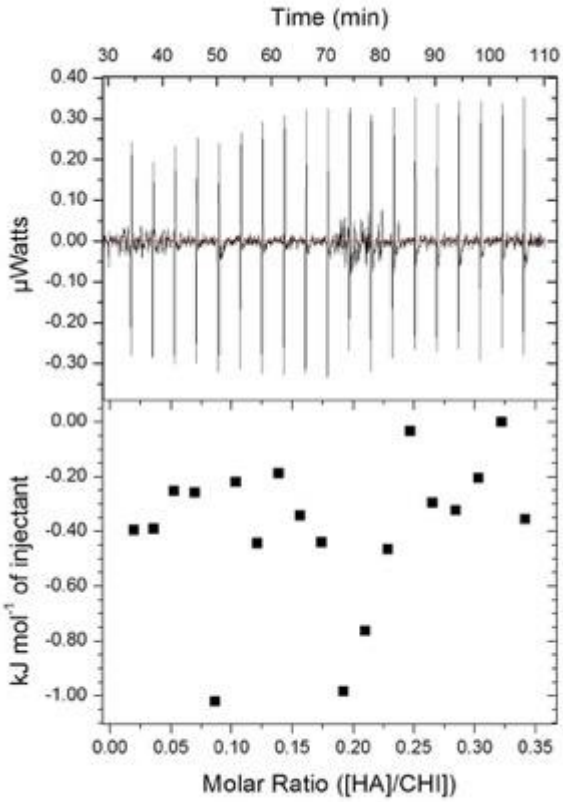

Figure A.8. Final figure of experiment #8 (top: graph of the power difference between cells versus time (i.e. raw data), bottom: graph of the energy change per mole of injectant (HA) versus on mole ratio (i.e., thermogram)).

Table A.9. Parameters of experiment #9 done using the ITC instrument.

Name of the experiment's file	HAtoCHIgktrial9
Concentration of CHI (mM)	0.3
Concentration of HA (mM)	1.0
pH value	4.00 ± 0.05
Concentration of NaCl (M)	0.15

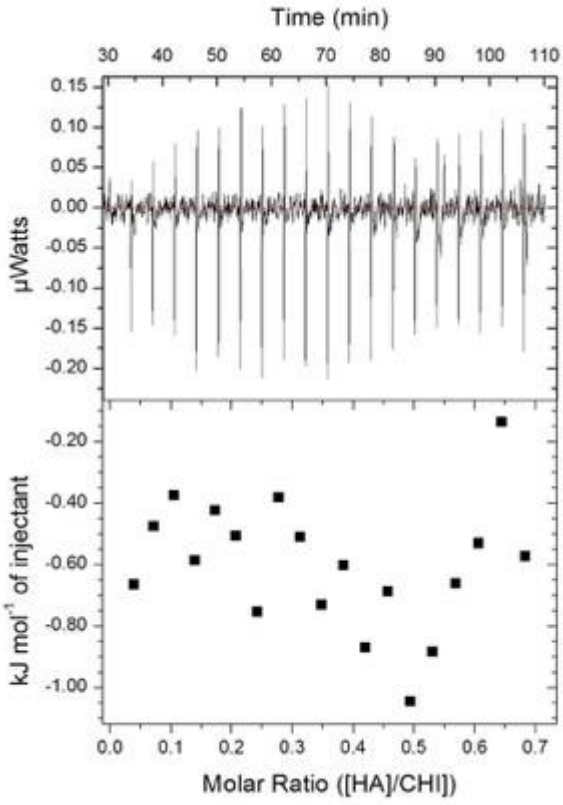

Figure A.9. Final figure of experiment #9 (top: graph of the power difference between cells versus time (i.e. raw data), bottom: graph of the energy change per mole of injectant (HA) versus on mole ratio (i.e., thermogram)).

Table A.10. Parameters of experiment #10 done using the ITC instrument.

Name of the experiment's file	HAtoCHIgktrial10
Concentration of CHI (mM)	0.3
Concentration of HA (mM)	1.0
pH value	3.00 ± 0.05
Concentration of NaCl (M)	0.15

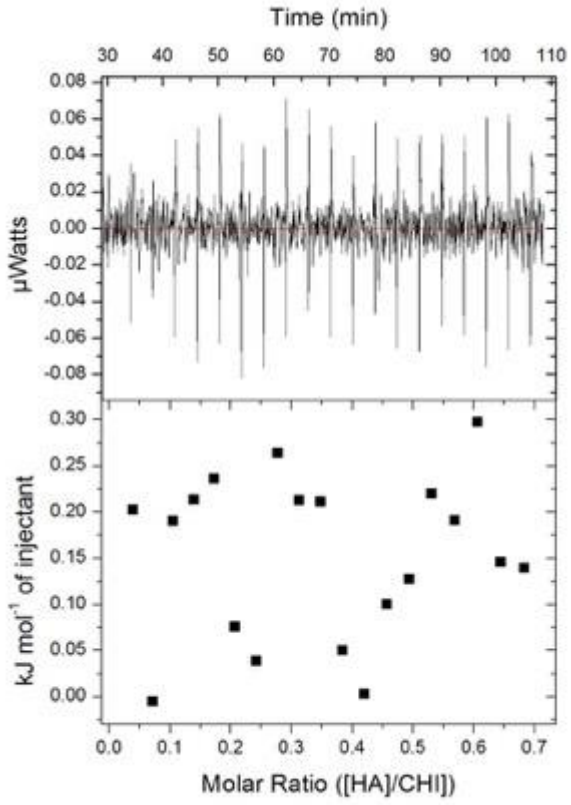

Figure A.10. Final figure of experiment #10 (top: graph of the power difference between cells versus time (i.e. raw data), bottom: graph of the energy change per mole of injectant (HA) versus on mole ratio (i.e., thermogram)).

Table A.11. Parameters of experiment #11 done using the ITC instrument.

Name of the experiment's file	HAtoCHIgktrial11
Concentration of CHI (mM)	0.3
Concentration of HA (mM)	0.75
pH value	4.00 ± 0.05
Concentration of NaCl (M)	0.15

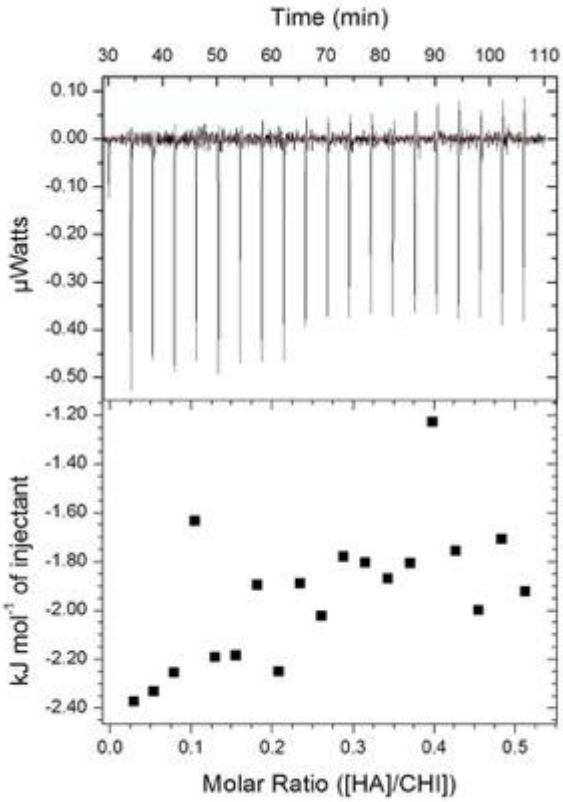

Figure A.11. Final figure of experiment #11 (top: graph of the power difference between cells versus time (i.e. raw data), bottom: graph of the energy change per mole of injectant (HA) versus on mole ratio (i.e., thermogram)).

Table A.12. Parameters of experiment #12 done using the ITC instrument.

Name of the experiment's file	HAtoCHIgktrial12
Concentration of CHI (mM)	0.6
Concentration of HA (mM)	1.5
pH value	6.25 ± 0.05
Concentration of NaCl (M)	0.2

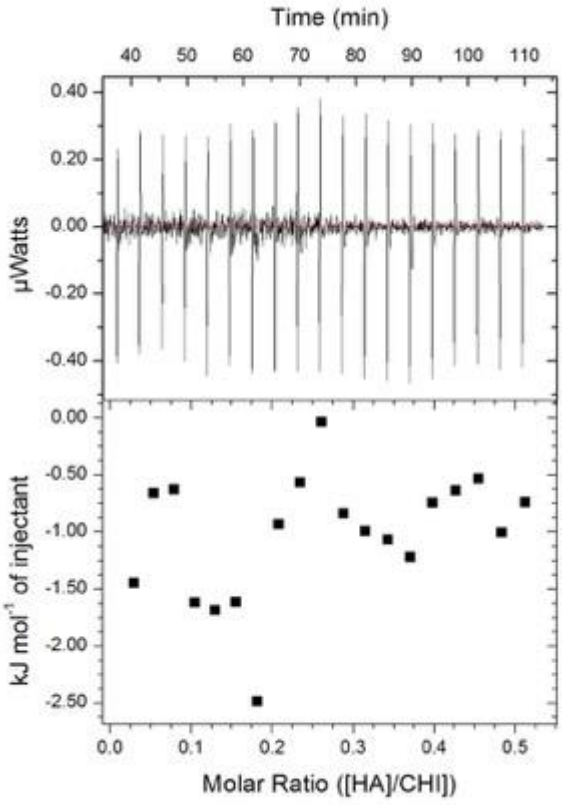

Figure A.12. Final figure of experiment #12 (top: graph of the power difference between cells versus time (i.e. raw data), bottom: graph of the energy change per mole of injectant (HA) versus on mole ratio (i.e., thermogram)).

Table A.13. Parameters of experiment #13 done using the ITC instrument.

Name of the experiment's file	HAtoCHIgktrial13
Concentration of CHI (mM)	0.3
Concentration of HA (mM)	1.0
pH value	6.25 ± 0.05
Concentration of NaCl (M)	0.2

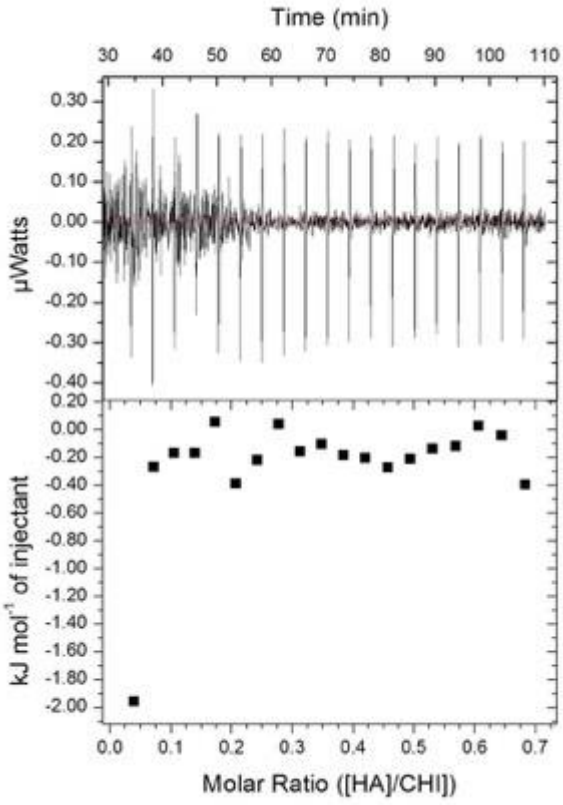

Figure A.13. Final figure of experiment #13 (top: graph of the power difference between cells versus time (i.e. raw data), bottom: graph of the energy change per mole of injectant (HA) versus on mole ratio (i.e., thermogram)).

Table A.14. Parameters of experiment #14 done using the ITC instrument.

Name of the experiment's file	HAtoCHIgktrial14
Concentration of CHI (mM)	0.6
Concentration of HA (mM)	1.0
pH value	6.25 ± 0.05
Concentration of NaCl (M)	0.2

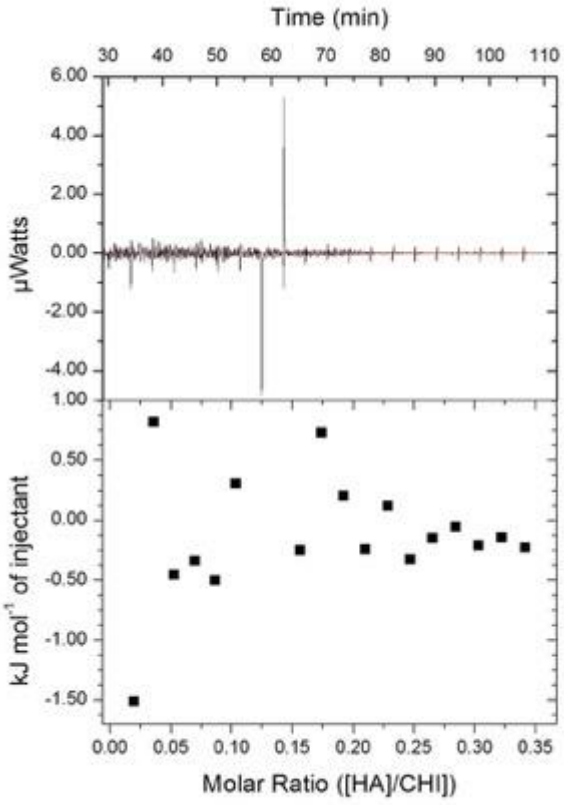

Figure A.14. Final figure of experiment #14 (top: graph of the power difference between cells versus time (i.e. raw data), bottom: graph of the energy change per mole of injectant (HA) versus on mole ratio (i.e., thermogram)).

Table A.15. Parameters of experiment #15 done using the ITC instrument.

Name of the experiment's file	HAtoCHIgktrial15
Concentration of CHI (mM)	0.3
Concentration of HA (mM)	1.0
pH value	3.00 ± 0.05
Concentration of NaCl (M)	0.2

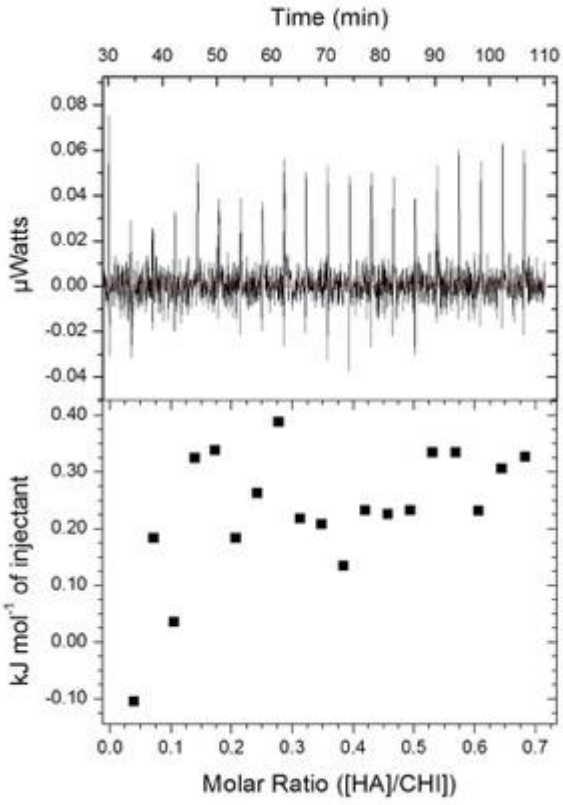

Figure A.15. Final figure of experiment #15 (top: graph of the power difference between cells versus time (i.e. raw data), bottom: graph of the energy change per mole of injectant (HA) versus on mole ratio (i.e., thermogram)).

Table A.16. Parameters of experiment #16 done using the ITC instrument.

Name of the experiment's file	HAtoCHIgktrial16
Concentration of CHI (mM)	0.3
Concentration of HA (mM)	1.0
pH value	4.00 ± 0.05
Concentration of NaCl (M)	0.2

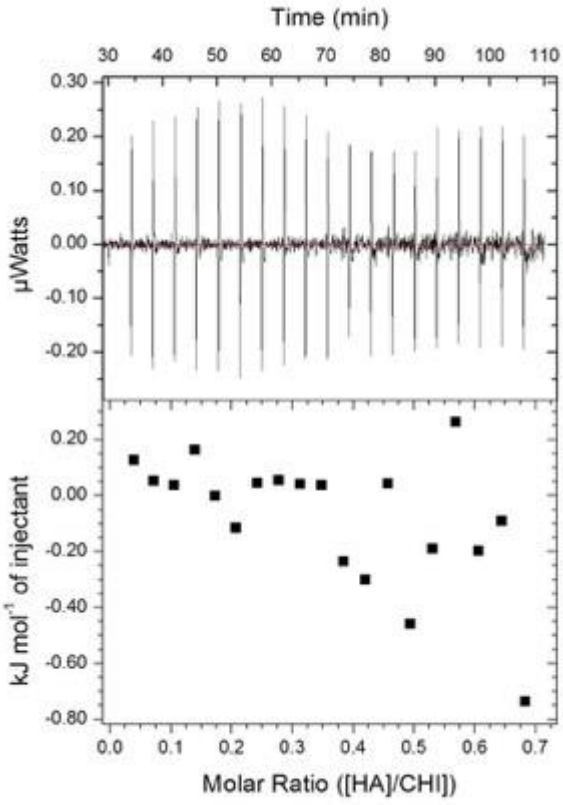

Figure A.16. Final figure of experiment #16 (top: graph of the power difference between cells versus time (i.e. raw data), bottom: graph of the energy change per mole of injectant (HA) versus on mole ratio (i.e., thermogram)).

Table A.17. Parameters of experiment #17 done using the ITC instrument.

Name of the experiment's file	HAtoCHIgktrial17
Concentration of CHI (mM)	0.3
Concentration of HA (mM)	0.75
pH value	4.00 ± 0.05
Concentration of NaCl (M)	0.2

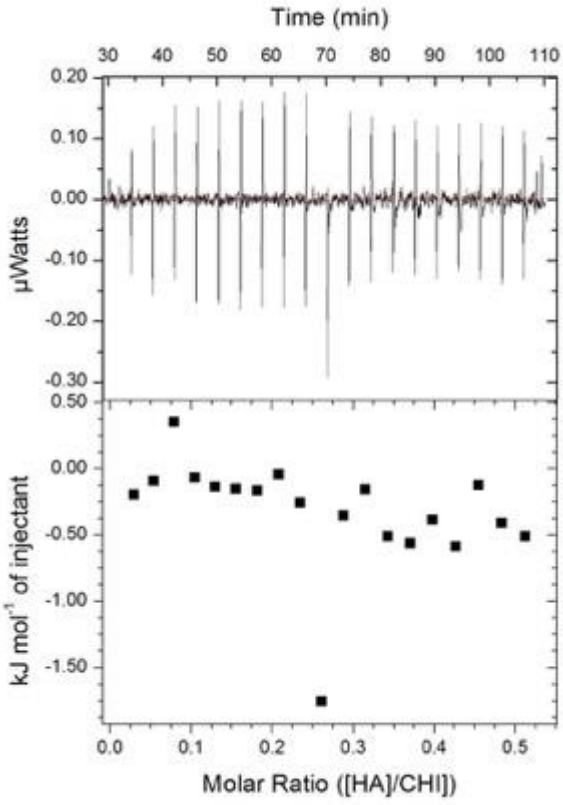

Figure A.17. Final figure of experiment #17 (top: graph of the power difference between cells versus time (i.e. raw data), bottom: graph of the energy change per mole of injectant (HA) versus on mole ratio (i.e., thermogram)).

Table A.18. Parameters of experiment #18 done using the ITC instrument.

Name of the experiment's file	HAtoCHIgktrial18
Concentration of CHI (mM)	0.3
Concentration of HA (mM)	0.5
pH value	6.25 ± 0.05
Concentration of NaCl (M)	0.2

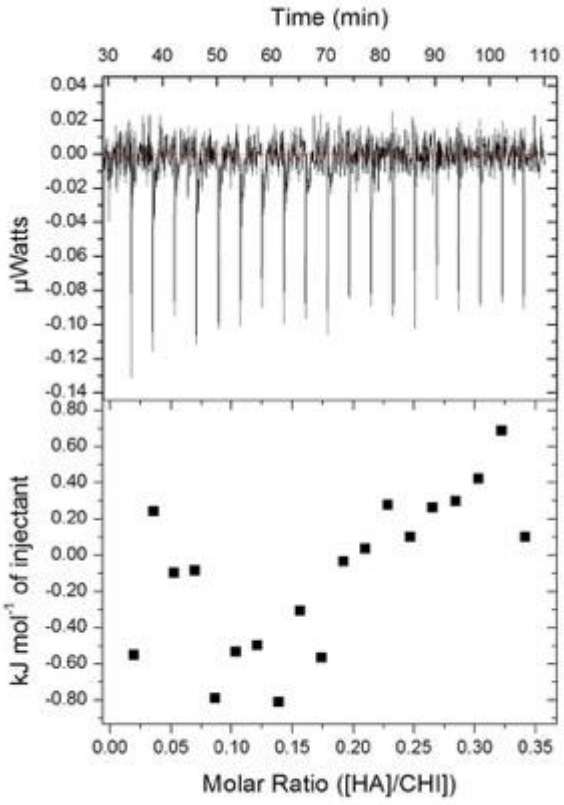

Figure A.18. Final figure of experiment #18 (top: graph of the power difference between cells versus time (i.e. raw data), bottom: graph of the energy change per mole of injectant (HA) versus on mole ratio (i.e., thermogram)).

Table A.19. Parameters of experiment #19 done using the ITC instrument.

Name of the experiment's file	HAtoCHIgktrial19
Concentration of CHI (mM)	0.3
Concentration of HA (mM)	0.4
pH value	6.25 ± 0.05
Concentration of NaCl (M)	0.2

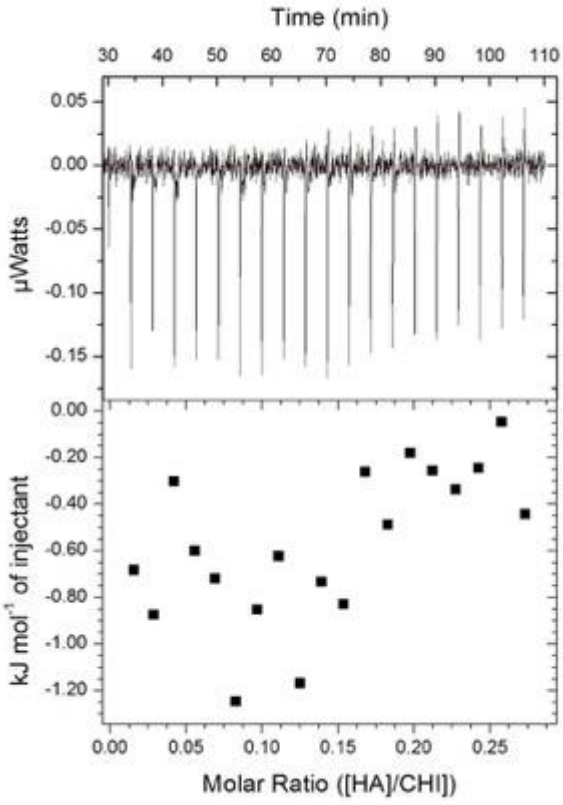

Figure A.19. Final figure of experiment #19 (top: graph of the power difference between cells versus time (i.e. raw data), bottom: graph of the energy change per mole of injectant (HA) versus on mole ratio (i.e., thermogram)).

Table A.20. Parameters of experiment #20 done using the ITC instrument.

Name of the experiment's file	HAtoCHIgktrial20
Concentration of CHI (mM)	0.6
Concentration of HA (mM)	0.6
pH value	6.25 ± 0.05
Concentration of NaCl (M)	0.2

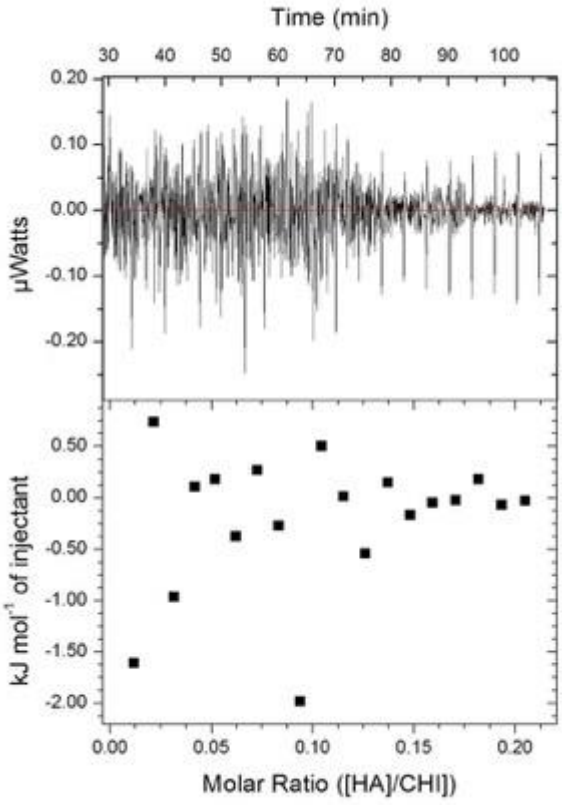

Figure A.20. Final figure of experiment #20 (top: graph of the power difference between cells versus time (i.e. raw data), bottom: graph of the energy change per mole of injectant (HA) versus on mole ratio (i.e., thermogram)).

Table A.21. Parameters of experiment #21 done using the ITC instrument.

Name of the experiment's file	HAtoCHIgktrial21
Concentration of CHI (mM)	0.5
Concentration of HA (mM)	0.6
pH value	6.25 ± 0.05
Concentration of NaCl (M)	0.2

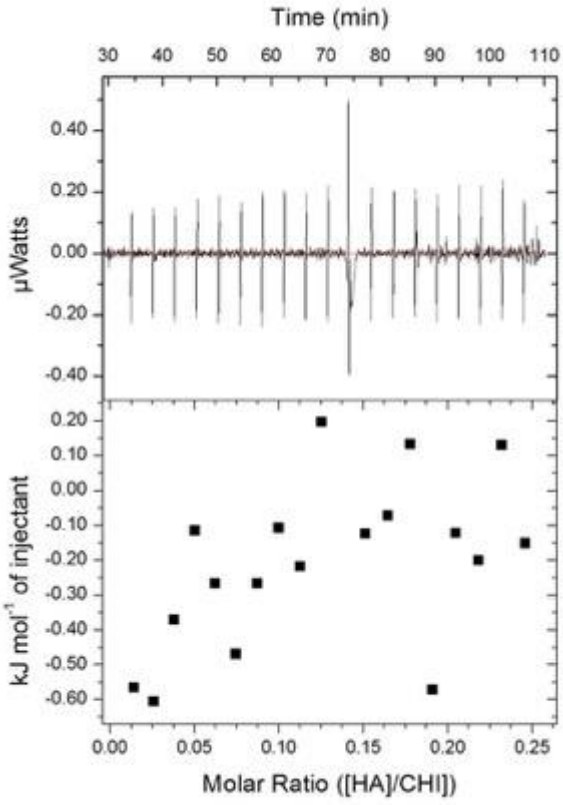

Figure A.21. Final figure of experiment #21 (top: graph of the power difference between cells versus time (i.e. raw data), bottom: graph of the energy change per mole of injectant (HA) versus on mole ratio (i.e., thermogram)).

Table A.22. Parameters of experiment #22 done using the ITC instrument.

Name of the experiment's file	HAtoCHIgktrial22
Concentration of CHI (mM)	0.4
Concentration of HA (mM)	0.6
pH value	6.25 ± 0.05
Concentration of NaCl (M)	0.2

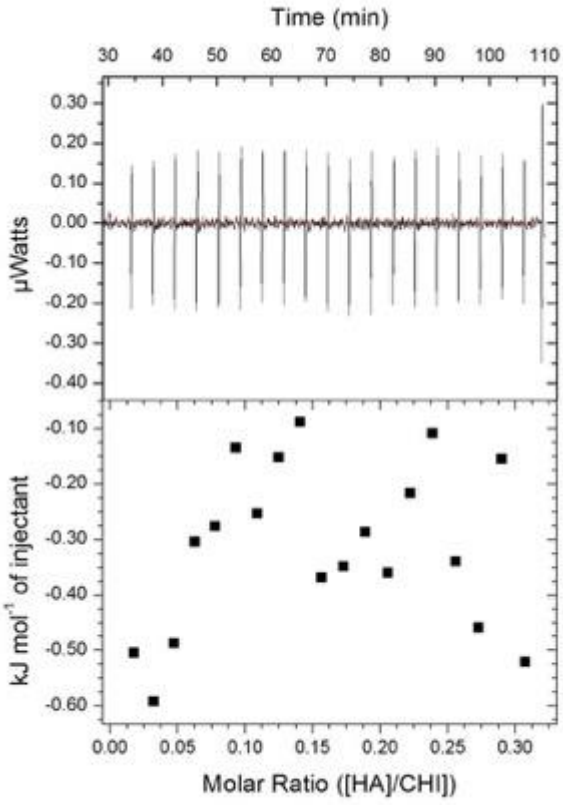

Figure A.22. Final figure of experiment #22 (top: graph of the power difference between cells versus time (i.e. raw data), bottom: graph of the energy change per mole of injectant (HA) versus on mole ratio (i.e., thermogram)).

Table A.23. Parameters of experiment #23 done using the ITC instrument.

Name of the experiment's file	HAtoCHIgktrial23
Concentration of CHI (mM)	0.9
Concentration of HA (mM)	0.6
pH value	6.25 ± 0.05
Concentration of NaCl (M)	0.2

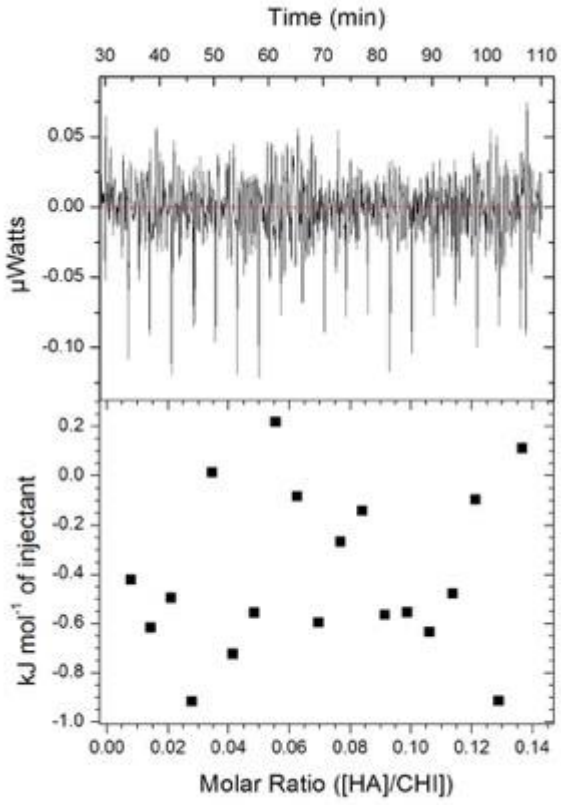

Figure A.23. Final figure of experiment #23 (top: graph of the power difference between cells versus time (i.e. raw data), bottom: graph of the energy change per mole of injectant (HA) versus on mole ratio (i.e., thermogram)).

Table A.24. Parameters of experiment #24 done using the ITC instrument.

Name of the experiment's file	HAtoCHIgktrial24
Concentration of CHI (mM)	0.3
Concentration of HA (mM)	0.4
pH value	6.25 ± 0.05
Concentration of NaCl (M)	0.15

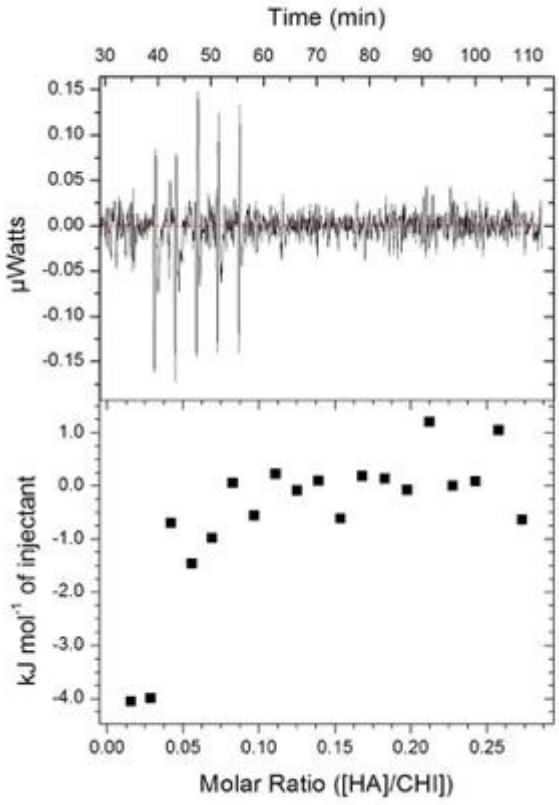

Figure A.24. Final figure of experiment #24 (top: graph of the power difference between cells versus time (i.e. raw data), bottom: graph of the energy change per mole of injectant (HA) versus on mole ratio (i.e., thermogram)).

Table A.25. Parameters of experiment #25 done using the ITC instrument.

Name of the experiment's file	HAtoCHIgktrial25
Concentration of CHI (mM)	1.5
Concentration of HA (mM)	3.0
pH value	6.25 ± 0.05
Concentration of NaCl (M)	0.2

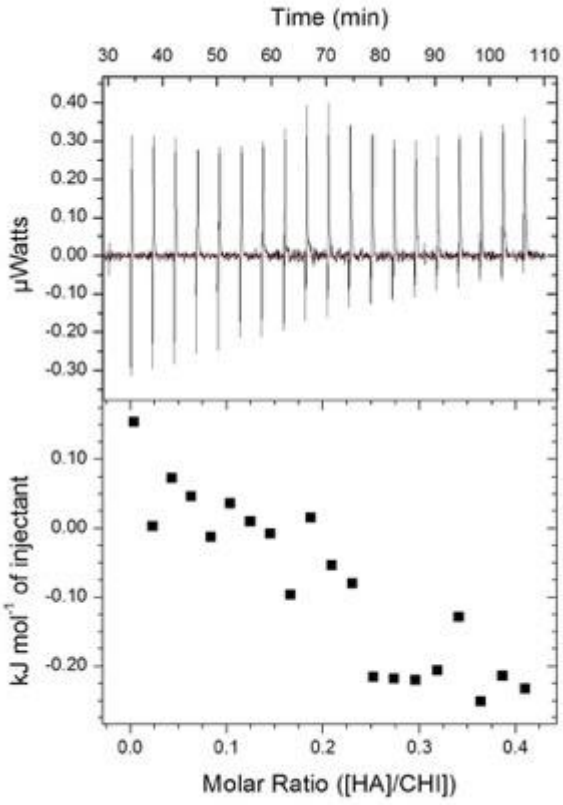

Figure A.25. Final figure of experiment #25 (top: graph of the power difference between cells versus time (i.e. raw data), bottom: graph of the energy change per mole of injectant (HA) versus on mole ratio (i.e., thermogram)).

Table A.26. Parameters of experiment #26 done using the ITC instrument.

Name of the experiment's file	HAtoCHIgktrial26
Concentration of CHI (mM)	0.3
Concentration of HA (mM)	6.0
pH value	6.25 ± 0.05
Concentration of NaCl (M)	0.2

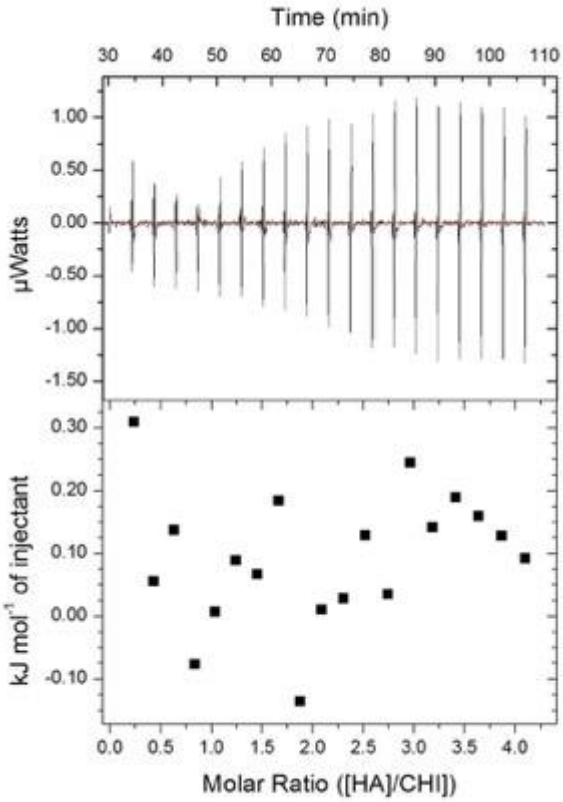

Figure A.26. Final figure of experiment #26 (top: graph of the power difference between cells versus time (i.e. raw data), bottom: graph of the energy change per mole of injectant (HA) versus on mole ratio (i.e., thermogram)).

Table A.27. Parameters of experiment #27 done using the ITC instrument.

Name of the experiment's file	HAtoCHIgktrial27
Concentration of CHI (mM)	0.3
Concentration of HA (mM)	3.0
pH value	6.25 ± 0.05
Concentration of NaCl (M)	0.2

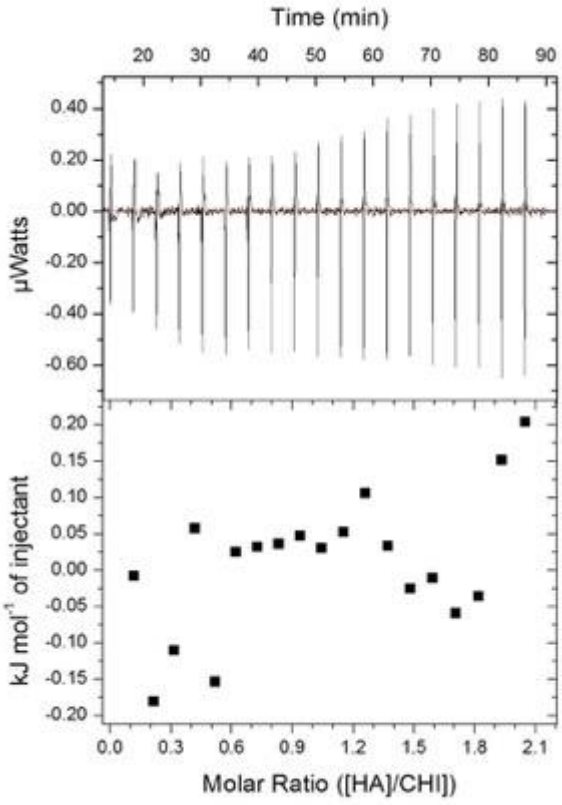

Figure A.27. Final figure of experiment #27 (top: graph of the power difference between cells versus time (i.e. raw data), bottom: graph of the energy change per mole of injectant (HA) versus on mole ratio (i.e., thermogram)).

Table A.28. Parameters of experiment #28 done using the ITC instrument.

Name of the experiment's file	HAtoCHIgktrial28HA199kDa
Concentration of CHI (mM)	0.3
Concentration of HA (mM)	6.0
pH value	6.25 ± 0.05
Concentration of NaCl (M)	0.2

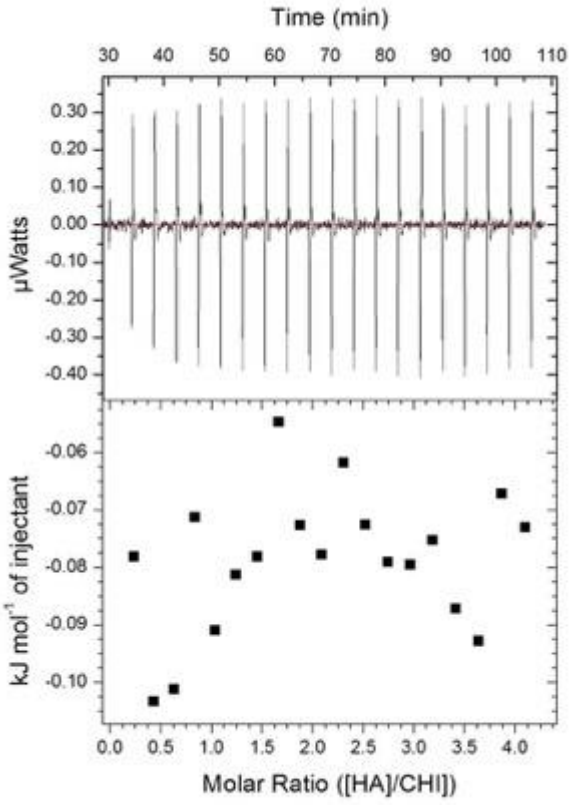

Figure A.28. Final figure of experiment #28 (top: graph of the power difference between cells versus time (i.e. raw data), bottom: graph of the energy change per mole of injectant (HA) versus on mole ratio (i.e., thermogram)).

Table A.29. Parameters of experiment #29 dosing the ITC instrument.

Name of the experiment's file	HAtoCHIgktrial29
Concentration of CHI (mM)	0.06
Concentration of HA (mM)	1.2
pH value	6.25 ± 0.05
Concentration of NaCl (M)	0.2

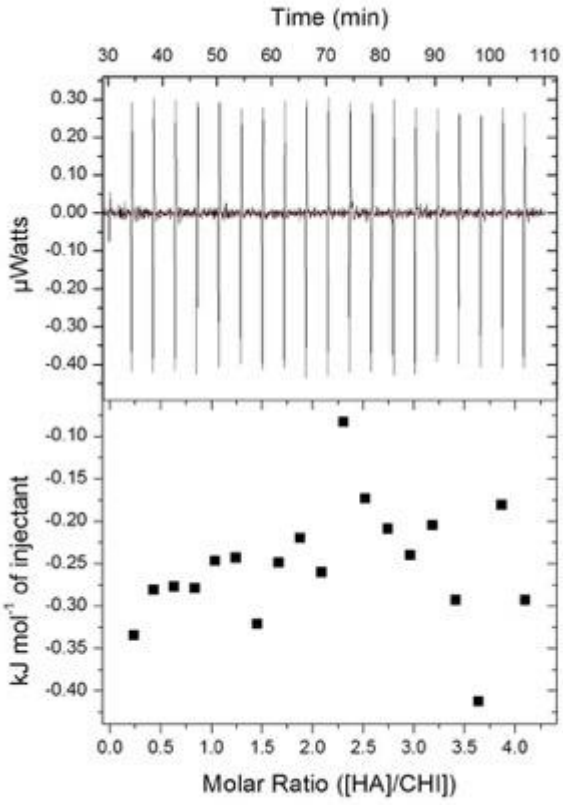

Figure A.29. Final figure of experiment #29 (top: graph of the power difference between cells versus time (i.e. raw data), bottom: graph of the energy change per mole of injectant (HA) versus on mole ratio (i.e., thermogram)).

Table A.30. Parameters of experiment #30 dosing the ITC instrument.

Name of the experiment's file	HAtoCHIgktrial30HA199kDa
Concentration of CHI (mM)	0.6
Concentration of HA (mM)	0.6
pH value	6.25 ± 0.05
Concentration of NaCl (M)	0.2

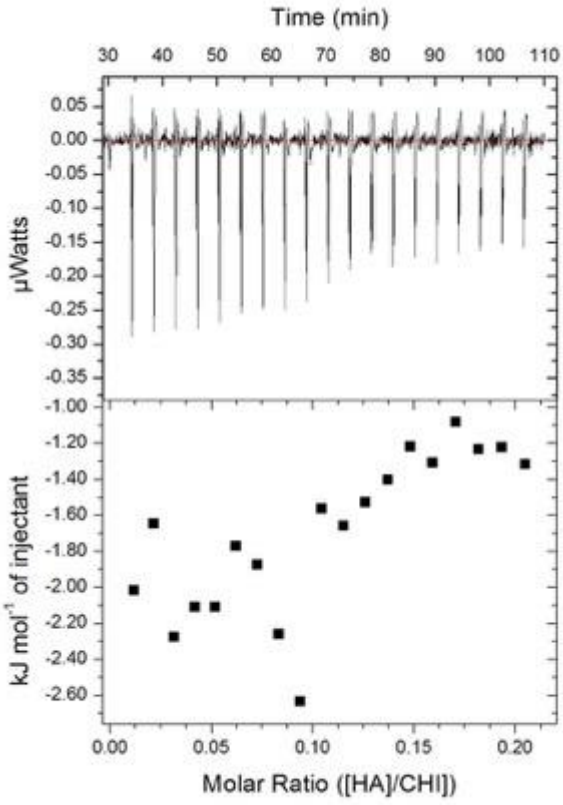

Figure A.30. Final figure of experiment #30 (top: graph of the power difference between cells versus time (i.e. raw data), bottom: graph of the energy change per mole of injectant (HA) versus on mole ratio (i.e., thermogram)).

Table A.31. Parameters of experiment #31 done using ITC instrument.

Name of the experiment's file	HAtoCHIgktrial31HA199kDa
Concentration of CHI (mM)	0.5
Concentration of HA (mM)	0.6
pH value	6.25 ± 0.05
Concentration of NaCl (M)	0.2

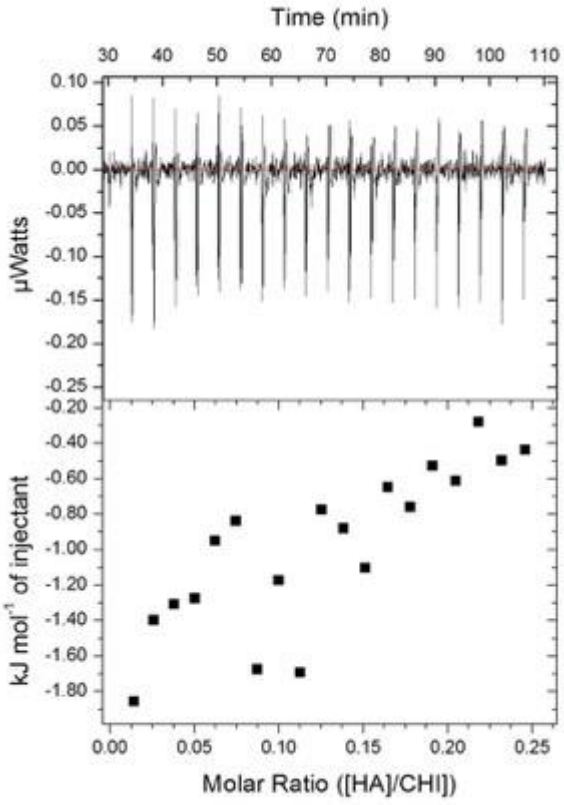

Figure A.31. Final figure of experiment #31 (top: graph of the power difference between cells versus time (i.e. raw data), bottom: graph of the energy change per mole of injectant (HA) versus on mole ratio (i.e., thermogram)).

Table A.32. Parameters of experiment #32 done using the ITC instrument.

Name of the experiment's file	HAtoCHIgktrial32HA199kDa
Concentration of CHI (mM)	0.6
Concentration of HA (mM)	6.0
pH value	6.25 ± 0.05
Concentration of NaCl (M)	0.2

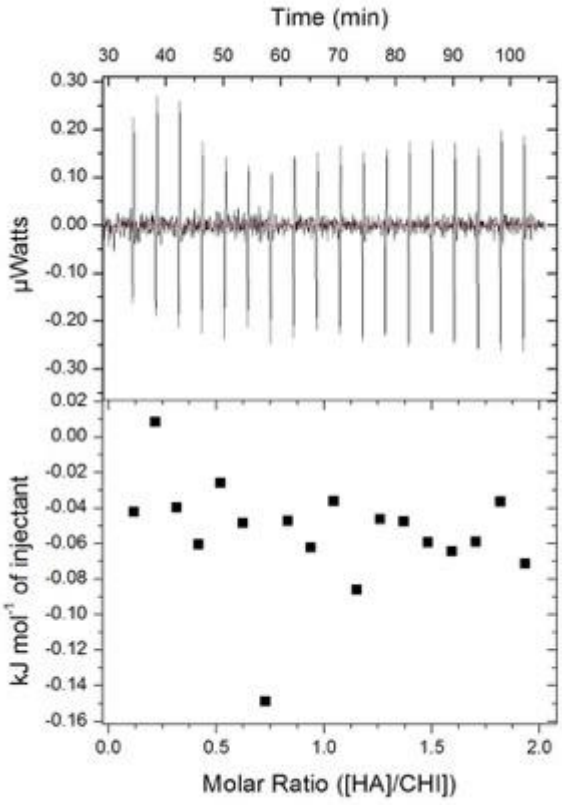

Figure A.32. Final figure of experiment #32 (top: graph of the power difference between cells versus time (i.e. raw data), bottom: graph of the energy change per mole of injectant (HA) versus on mole ratio (i.e., thermogram)).

APPENDIX B: RESULTS OF THE SEM-EDS EXPERIMENTS

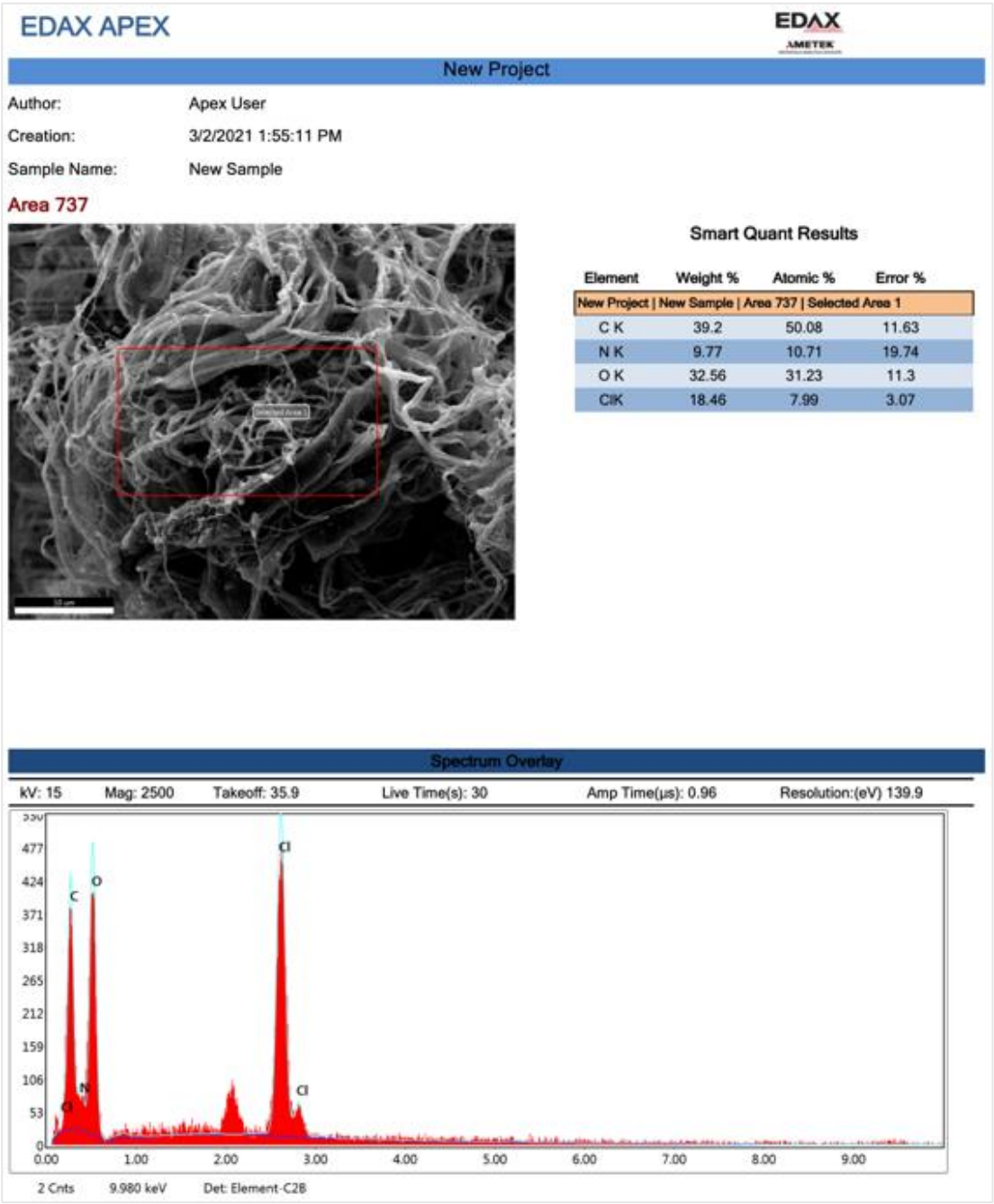

Figure B.1. Result of the SEM-EDS experiment done for the original CHI.

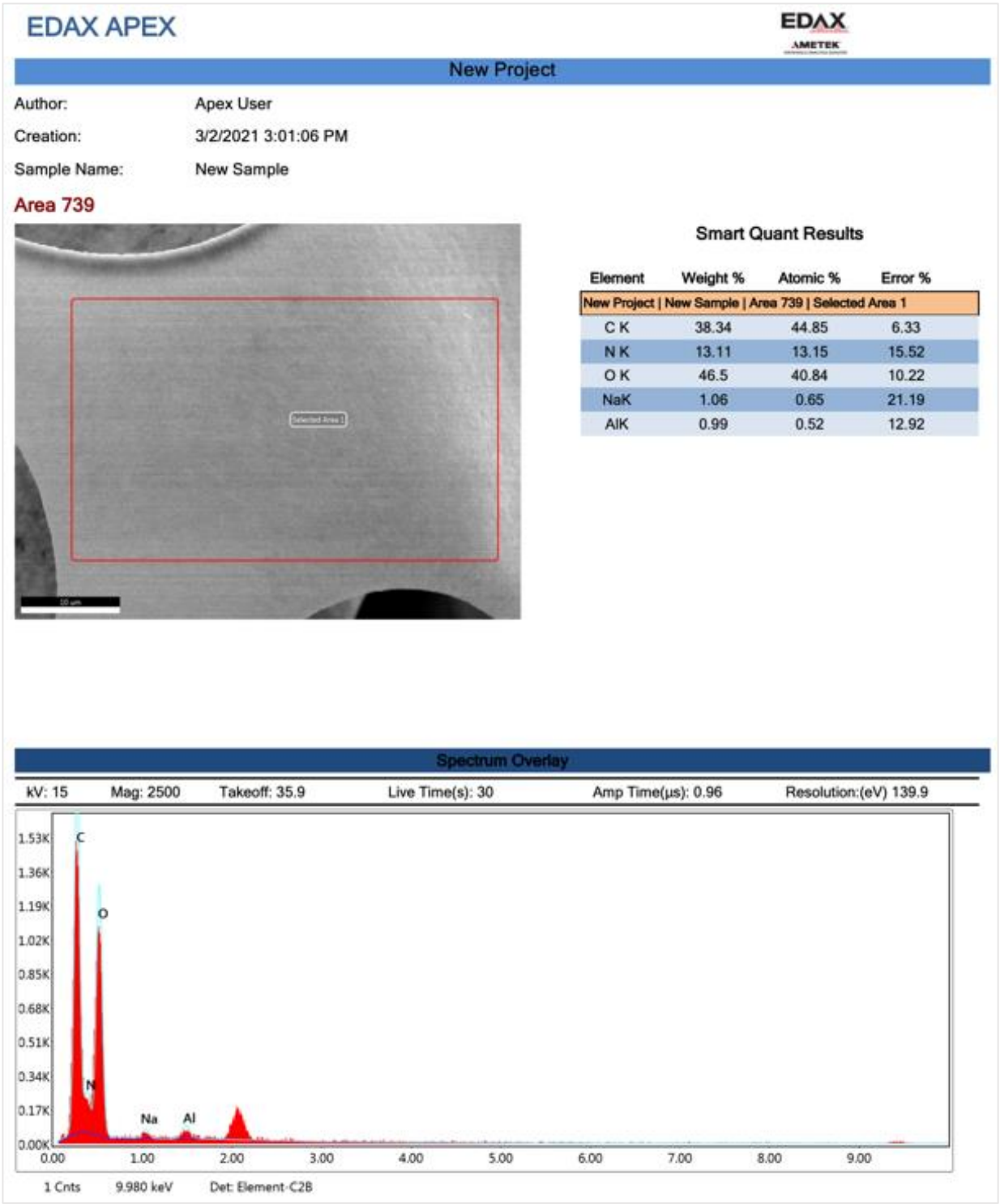

Figure B.2. Result of the SEM-EDS experiment done for the counterion exchanged CHI with replacement of Cl^- with OAc^-.

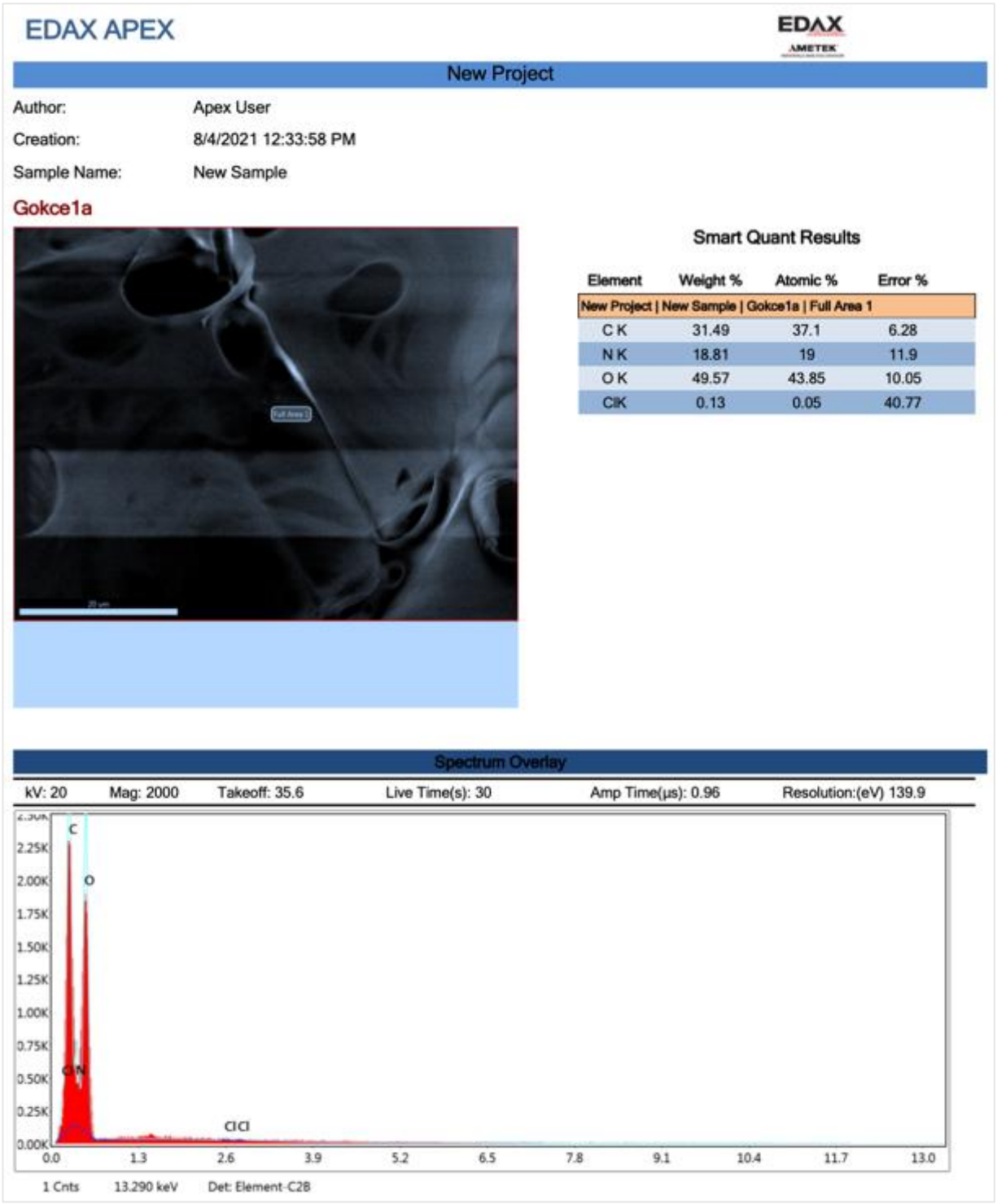

Figure B.3. Result of the SEM-EDS experiment done for the counterion exchanged CHI with replacement of Cl^- with NO_3^-.

EDAX APEX

EDAX AMETEK

New Project

Author: Apex User

Creation: 3/2/2021 12:49:26 PM

Sample Name: New Sample

BasakKyt

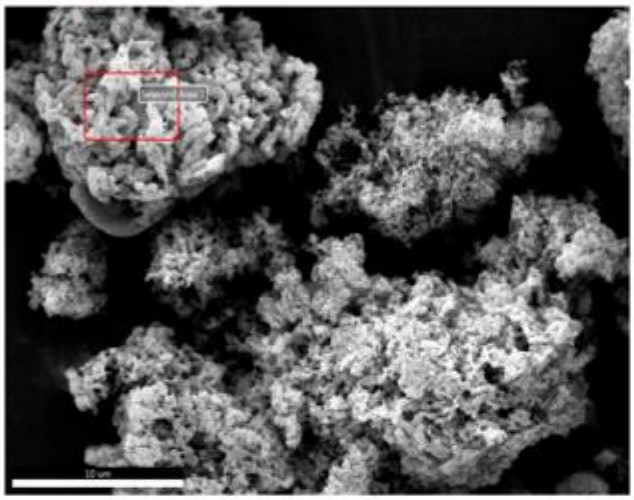

Smart Quant Results

Element	Weight %	Atomic %	Error %
C K	41.47	51.66	7.51
O K	43.02	40.24	9.46
NaK	11.74	7.64	8.33
P K	0	0	99.99
PtM	3.19	0.24	17.95
CaK	0.58	0.22	44.39

Selected Area 1

kV: 15 Mag: 3500 Takeoff: 35.9 Live Time(s): 30 Amp Time(µs): 0.96 Resolution:(eV) 139.9

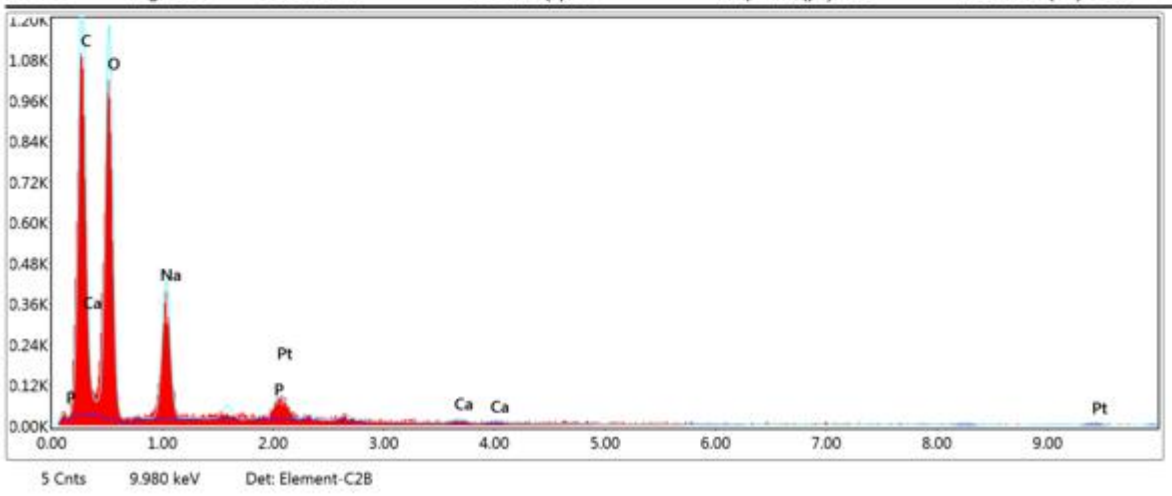

Figure B.5. Result of the SEM-EDS experiment done for the original HA.

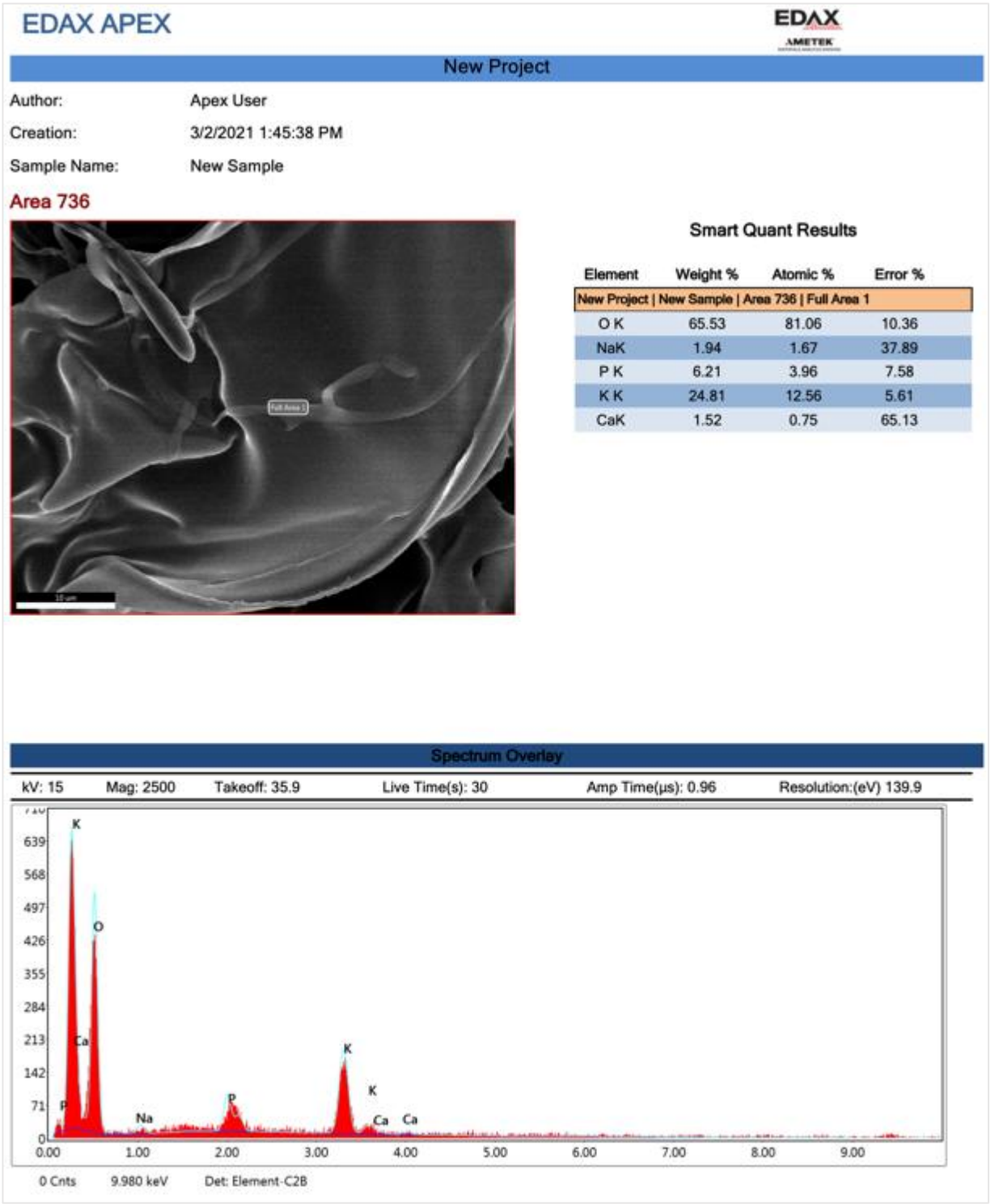

Figure B.6. Result of the SEM-EDS experiment done for the counterion exchanged HA with replacement of Na^+ with K^+.

EDAX APEX

EDAX AMETEK

New Project

Author: Apex User

Creation: 8/4/2021 1:38:36 PM

Sample Name: New Sample

Gokce4a

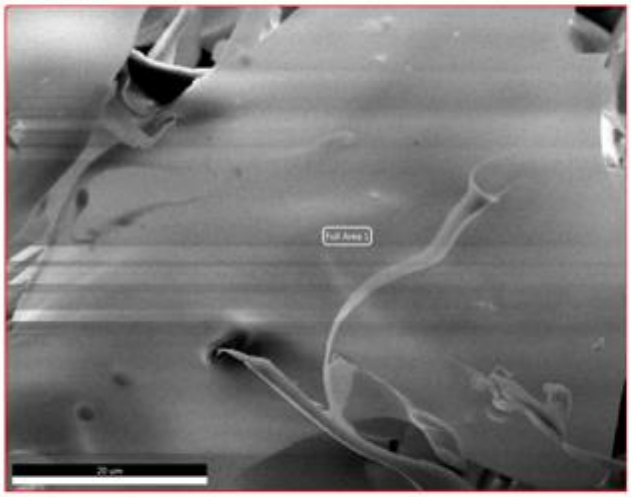

Smart Quant Results

Element	Weight %	Atomic %	Error %
New Project | New Sample | Gokce4a | Full Area 1			
C K	41.07	49.62	8.86
O K	51.1	46.35	10.19
NaK	0.34	0.22	83.76
MgK	3.94	2.35	8.98
P K	0.39	0.19	24.85
ClK	2.66	1.09	6.7
CaK	0.51	0.18	37.36

Spectrum Overlay

kV: 20 Mag: 2000 Takeoff: 35.6 Live Time(s): 30 Amp Time(µs): 0.96 Resolution:(eV) 139.9

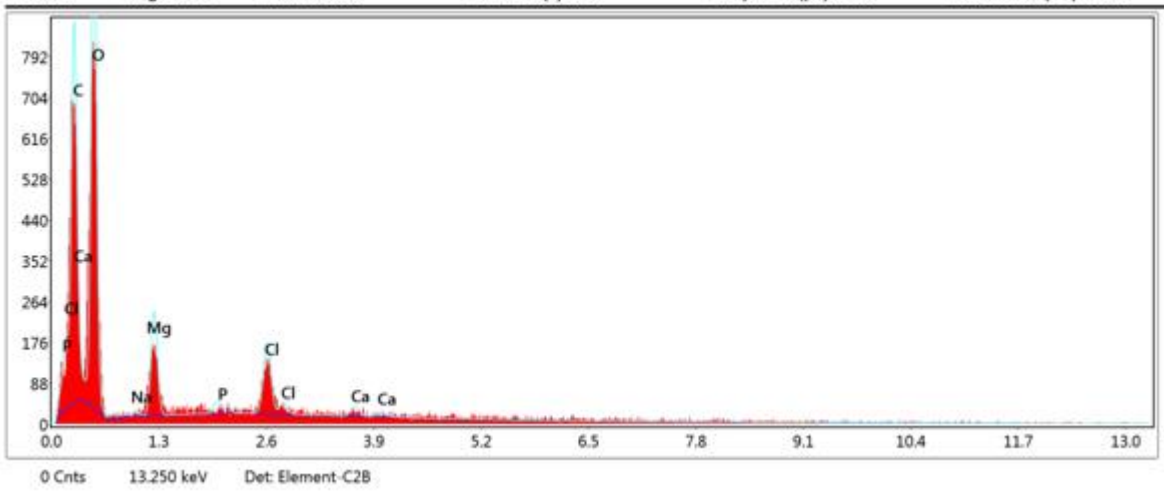

Figure B.6. Result of the SEM-EDS experiment done for the counterion exchanged HA with replacement of Na^{+} with Mg^{+2}.

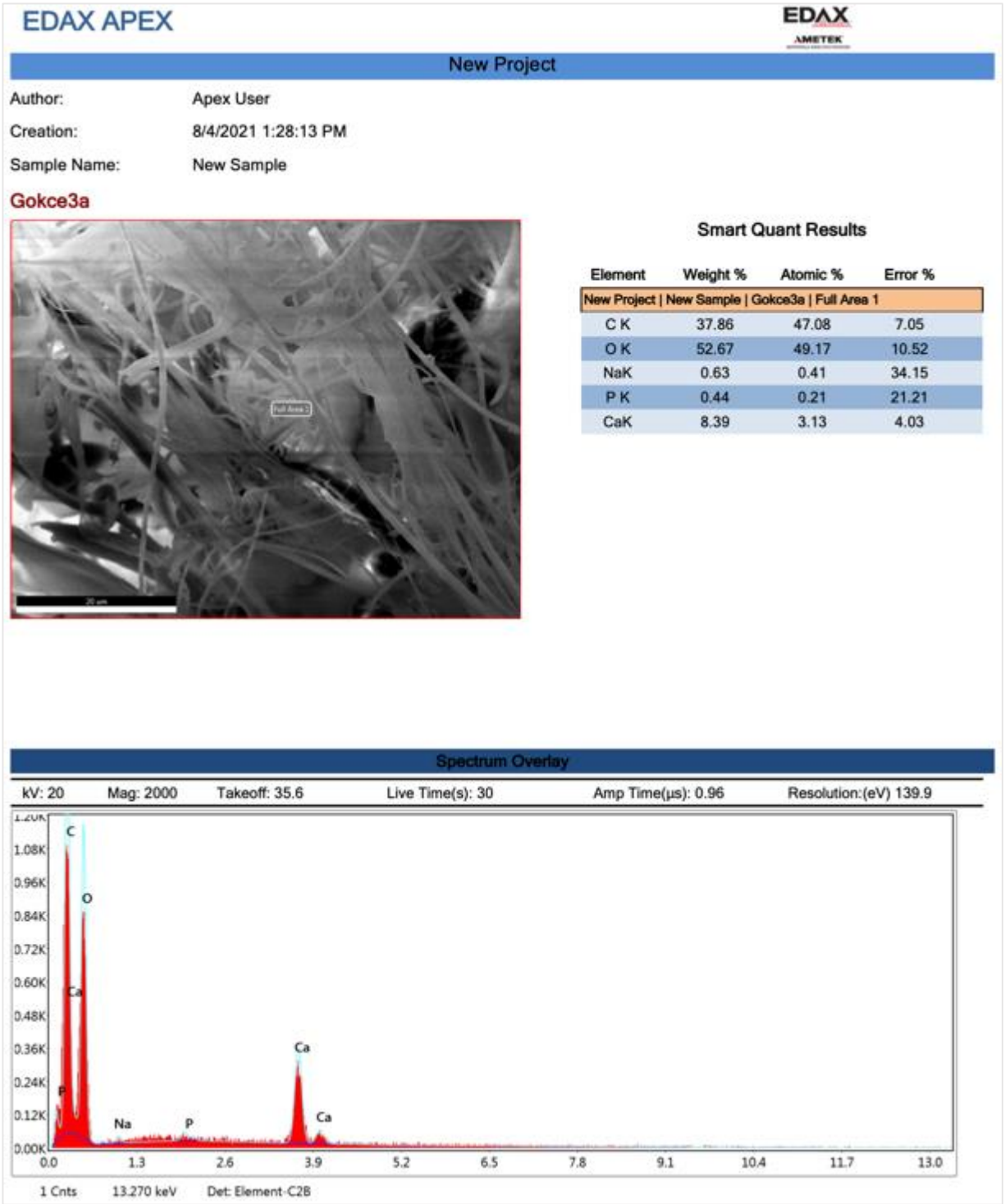

Figure B.6. Result of the SEM-EDS experiment done for the counterion exchanged HA with replacement of Na^{+} with Ca^{+2}.